ENHANCED VISCOELASTIC MODELING OF HOT MIX ASPHALT

by

TITO P. NYAMUHOKYA

Presented to the Faculty of the Graduate School of

The University of Texas at Arlington in Partial Fulfillment

of the Requirements

for the Degree of

DOCTOR OF PHILOSOPHY

THE UNIVERSITY OF TEXAS AT ARLINGTON

August 2015

Acknowledgements

I would like to offer deepest thanks to my supervising professor, Dr. Stefan A. Romanoschi for his guidance and unconditional support throughout the course of this research. None of the work herein would have been possible without his help and encouragement.

Thanks are also extended to the other members of my PhD dissertation committee, Dr. Sahadat Hossain, Dr. Xinbao Yu, and Dr. Dragos S Dancila for their valuable advice and review of this manuscript.

I would like to convey many thanks to my special friends, Dr. Mbaki Onyango, Regina Waweru and Dr. Said Selemani for their material and moral support. Thanks are also extended to Alireza Sayah, Ali Abdullah, Reza saeedzadeh, Dr. Oleh Kinashi, and all friends and students at UTA.

Most of all, I would like to give special thanks to my wife, Hilda, and daughter, Rose, for their uncountable love, encouragement, and great support. I also convey enormous thanks to my special father (the late Peter Nyamuhokya) and mother, Maria, brothers, sisters and the whole family in Africa and all over the world.

Lastly, I would like to thank families of Mr. Chacha, Dr. Otieno, Mr. & Jackson, Mr. & Mrs. Ngwenya , Mr. & Mrs. Hebron and others in America who helped me to go through hard times during my studies.

May 6, 2015

Abstract

ENHANCED VISCOELASTIC MODELING OF HOT MIX ASPHALT

Tito P. Nyamuhokya, PhD

The University of Texas at Arlington, 2015

Supervising Professor: Stefan A. Romanoschi

The primary objective of this research is to investigate the relationships between Compressive (CDM) and Tensile Dynamic Moduli (TDM) of Hot Mix Asphalt (HMA) and develop a material model that predicts tensile dynamic modulus from known compressive dynamic modulus. Moreover, the research develops an enhanced visco-hyper-elastic Finite element model that incorporates both CDM and computed TDM to predict the structural response of a perpetual pavement structure subjected to wheel loading.

In the laboratory, the Compressive and Tensile Dynamic Modulus parallel to the direction of compaction and Tensile dynamic modulus perpendicular to the direction of compaction were determined at different temperature and frequencies. The results of the experiments were used to develop relationships between Compressive and Tensile dynamic modulus at 10^{o}C, 20^{o}C, 30^{o}C, 35^{o}C and all

temperature combined. The research found that the data correlation at each temperature levels increased with temperature from fair to good (R^2 = 0.5-0.85) whereas the correlation at all temperature combined was strong (R^2 = 0.91). The model corresponding to the highest R^2 was evaluated for accuracy and rationality. This research incorporated both Compressive and computed Tensile Dynamic Moduli (based on the best model) into a visco-hyper-elastic FE model to predict strain responses of the Kansas US75 perpetual pavement sections.

This research developed mathematical models that may be used by engineers and researchers to estimate tensile dynamic modulus from known compressive dynamic modulus. In addition, the research demonstrated that the enhanced visco-hyper-elastic finite element model that incorporates both Compressive and Tensile moduli can predict HMA pavement responses.

Table of Contents

List of Figures

List of Tables

Chapter 1

Introduction

1.1 Introduction

In a simple form, asphalt concrete can be characterized as linear elastic material (Burmister D.M., 1943). The linear elastic behavior may be a close representation of asphalt concrete layers behavior at low temperature and high loading frequency where stresses and strains are low (Liao Y. 2007, Burmister D.M., 1943). However, when stresses and strains are relatively high, asphalt materials exhibits both viscous and elastic behavior (viscoelastic behavior).

The first application of viscoelastic properties to asphalt pavement was in 1960s by Sector and Monismith. However, the extensive application of viscoelastic models begun in late 1990s when mechanistic pavement design methods emerged. Since then the viscoelastic constitutive models have been frequently used to model mechanistic response of asphaltic pavements. The model closely represents the temperature-time dependency nature of asphalt concrete (Wang H., 2011).

When analyzing viscoelastic materials, laboratory measured dynamic modulus parameters are typically used to define the temperature-time dependency behavior of the materials. The protocol for determining dynamic modulus was originally developed by Coffman and Pagen at Ohio State University in the

1960's. The protocol was adopted by ASTM test in the early 1970s and AASHTO later on. According to the protocol, the dynamic modulus is defined as the ratio of the amplitude of the sinusoidal stress at any given time and the loading frequency and the amplitude of the sinusoidal strain at the same time and frequency. The test may be applied in compression or tension (Charles E. Dougan 2003). However, most of the results obtained over the past 45 to 50 years are based on compression tests.

In this research, the relationship between Compressive and Tensile dynamic modulus of HMA is investigated. Typically, the compressive dynamic modulus is performed under uniaxial cyclic loading tests whereas the tensile dynamic modulus is determined through indirect tensile tests such as IDT (indirect tension test) (Kim et. al. 2004, King et. al. 2005). However, for better comparison, this research measures both the Compressive and Tensile dynamic moduli under direct uniaxial loading and derives the relationships between them to enhance a Finite element viscoelastic model of HMA. The applicability of the model to HMA was validated using field responses from the Kansas US 75 perpetual pavement project.

1.2 Problem statement

The dynamic modulus used for the characterization of HMA pavements is typically determined from Compressive dynamic modulus test. Currently,

engineers and researchers use the Compressive dynamic modulus to characterize both compressive and tensile behavior of Hot Mix Asphalt (HMA) with an assumption that HMA behave the same in compression and tension (Kim et al. 2005). Nevertheless, previous research suggested that the Compressive and Tensile strength of HMA are different. A few of these studies showed the difference exists also for the HMA dynamic modulus. This research expects the difference to be more pronounced for tensile dynamic modulus performed on samples extracted perpendicular to the pavement direction of compaction. The difference in stiffness between aggregates and mastic (mix of fine particles and asphalt binder) may be a major reason for this phenomenon. During HMA compaction, aggregates reorient and lock to offer to HMA, additional stiffness in the direction of compaction (compressive direction) than the parallel or perpendicular (tension direction) direction. The stiffness in parallel and perpendicular to the direction of compaction depends significantly on the HMA mastic (mix of asphalt and fines) stiffness, which is several orders of magnitude less than aggregates stiffness.

Since HMA behave differently in compression and tension, this research believe the material may be characterized better if both compression and tension stiffness of the material are considered. Therefore, a viscoelastic constitutive material model that combines compressive and tensile behaviors is needed.

1.3 Objectives

The main objectives of research are:

i. Determine cyclic dynamic moduli of HMA in compression and tension, parallel and perpendicular to the direction of compaction.

ii. Determine a relationship between compressive and tensile dynamic moduli.

iii. Develop a viscoelastic material model for asphalt concrete that incorporate the behavior in tension and compression.

iv. Validate the model by computing strains at the bottom of asphalt concrete layer subjected to moving loads and compare them with measured strains.

Chapter 2

Background

2.1 Flexible pavements

More than 93 percent of the 2.6 million miles of paved roads and highways in the United States are flexible pavements. This represents about 63 percent of all roads (paved and unpaved) (HAPI, 2014). These pavements are sometimes called blacktop pavements to refer to the existence of black hot mix asphalt (HMA) on the surface layer of the pavement. But to most people, especially in civil engineering community they are known as asphalt or flexible pavements.

As the name implies, flexible pavements are pavements designed to flex without failure under applied traffic loads. Typically the pavements are constructed with strong layers at the top surface to resist the effects of direct contact with traffic and other environmental forces. The materials towards subgrade (foundation) are relatively of inferior quality and cheaper compared to the surface layer, to reflect the diminishing loads magnitude at the bottom of the pavement structure (Figure 2-1).

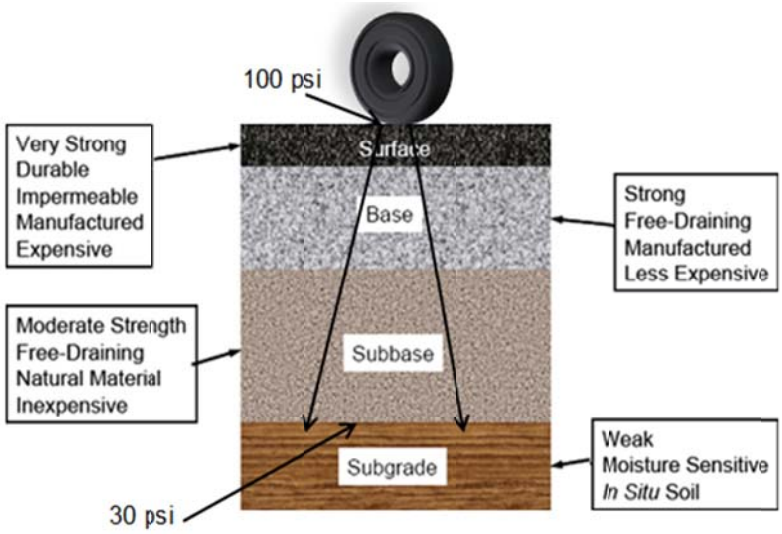

Figure 2-1 A typical asphalt pavement structure

In terms of structural construction of the layers, asphalt pavements may be categorized into two major types: conventional asphalt concrete and full-depth asphalt pavements. The conventional asphalt concrete pavement consists of an asphaltic surface layer on top of granular base and sub-base laying on natural or compacted sub-grade. Full-depth asphalt pavement on the other hand, consists of a thick layer of asphalt concrete subdivided into layers (surface, intermediate and base) of different mix designs to limit the occurrence of distresses only to the top layer .

2.1.1 Conventional Asphalt Concrete pavement structural layers

In order to control traffic and environmental effects at reasonable costs, conventional asphalt concrete pavements are generally designed to comprise layers of carefully selected materials with the following functions:

- Surface course

This is the contact layer between vehicles wheels and the pavement and normally is the most expensive layer because of its high quality materials. The layer is made up of mixture of selected aggregated and bituminous materials properly compacted to reach the desirable density. The layer provides characteristics such as friction, smoothness, rut resistance and noise control. In additional, this layer prevents ingress of water to the underlying materials. If the layer is too thick, it may be subdivided into wearing and binder course and its function may extend to distribution of loads over a larger area. During construction, a paver is typically used to uniformly spread the HMA over a prepared base (Figure 2-2).

Figure 2-2 Flexible pavement wearing course construction (courtesy of RODTEC)

- Base course

The base course is the layer found directly under the surface course layer of flexible pavement. The base course must consist of strong aggregate and enough thickness for it to fulfill the following functions: uniformly distribute the applied traffic load to the sub-base and/or subgrade below, withstand the stresses produced in the base itself and resist the vertical pressures that tend to produce consolidation and result in distortion of the surface course. Additionally, the materials for the base layer may be stabilized with bitumen or Portland cement to improve resistance to volume changes due to frost action and moisture movement within the layer. Figure 2-3 shows a pavement constructed up to a base course level.

Figure 2-3 Asphalt pavement base construction (Photo by NCAT)

- Subbase course

Subbase course is one of the structural layers of flexible pavement laying between the subgrade and the base course. Subbase course is important when frost action and unstable clay soils exists at the depth where the pavement is going to be placed. The layer is constructed using weaker materials than in base and surface course to respond to lower stresses that develop at this depth under the passing wheel loads. Granular materials are preferred for this layer because they improve drainage (Figure 2-4). The subbase's primary function is to offer support to the base course. However, with stabilized or well-compacted granular materials, the layer can also offer the following:

- Minimize the intrusion of fines into the pavement structure.
- Improve drainage.
- Minimize frost action damage
- Provide a working platform for construction of the upper layers.

Figure 2-4 Asphalt pavement granular sub-base course

- Subgrade course

This is a well compacted natural soil that constitutes the foundation of the pavement system. Since load stresses decrease with depth, subgrade layer is always subjected to lower stresses than the surface, base, and subbase courses. In addition, it is typical to build the subbase, base, and wearing surface layers with a combined thickness enough to reduce the stresses occurring in the subgrade to values that will not cause excessive distortion or displacement of the subgrade soil layer. Typical equipment used for the construction of this layer includes graders and roller compactors. For compaction of soft subgrade soil, sheep foot roller is preferred (Figure 2-5).

Figure 2-5 Subgrade Construction

2.1.2 Perpetual Pavements

Asphaltic pavements designed to endure the present and forecasted high traffic volumes for many years (more than 50 years) without structural failure are

known as perpetual pavements. The superior performance of this pavement structure depends on performance of materials and thicknesses to minimize pavement strains under applied loads. The pavements are constructed directly on top of stabilized subgrade soil, replacing the conventional granular base/ subbase with high quality HMA layers. The bottom layer of the pavement is flexible to resist tensile strains caused by traffic, and thus stops potential distresses (i.e. bottom up cracks) underneath the pavement (Figure 2-6).

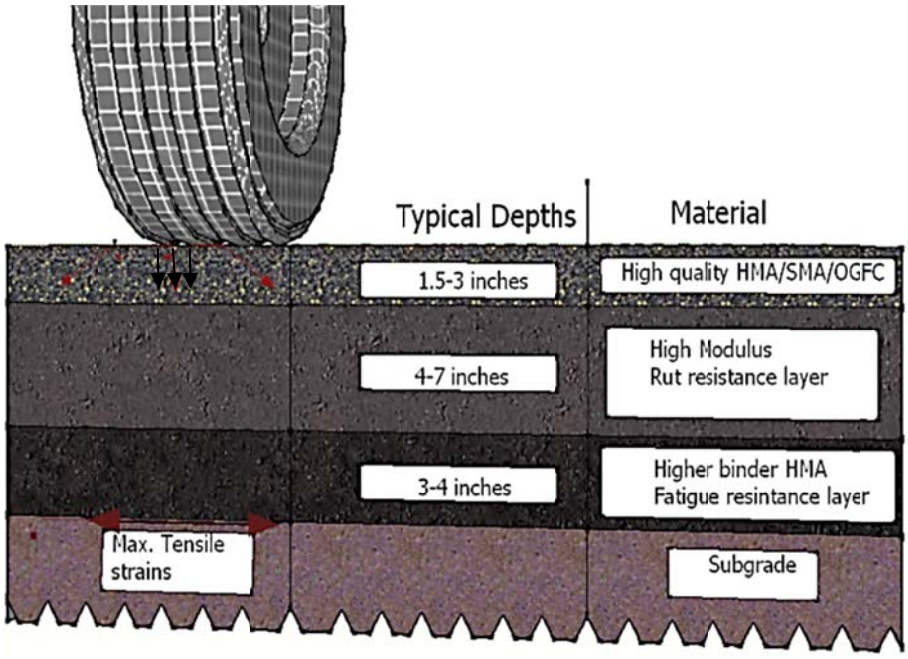

Figure 2-6 Typical Perpetual pavement structure

2.1.2.1 Origin of Perpetual Pavements

Among the early evidence of perpetual pavements are the two sections of I-40 in downtown Oklahoma City. The sections were built in 1967 and still are

performing as intended. The pavement that include these sections carries average daily traffic (ADT) of over 100,000 vehicles with approximately 30 percent heavy trucks. The total thickness of the pavement was 14 inch of well-selected asphaltic materials in three layers: surface, intermediate and base layer. The total thickness of the layers is great enough to eliminate fatigue cracking and rutting at base and intermediate layers (MAPA, 2012, APA, 2014). As such, the pavement met the requirement for Perpetual Pavement design which was introduced three decade later to respond to the ever increasing traffic volume and loads in the US pavements.

The Perpetual Pavement concept was first introduced by Huddleston, et al. (2001) in an Asphalt Pavement Alliance (APA) publication called "Perpetual Pavements". In this publication, Huddleston, et al. (2001) defined Perpetual Pavement as:

> An asphalt pavement designed and built to last longer than 50 years without requiring major structural rehabilitation or reconstruction, and needing only periodic surface renewal in response to distresses confined to the top of the pavement" (APA, 2010).

2.1.2.2 Advantages of Perpetual Pavements

According to APA, the U.S Department of Transportation (DOT) and other pavement engineering researchers, perpetual pavements offer the following to the pavement industry.

- *High structural capacity.* Well-designed asphaltic subsurface layers of perpetual pavements are structurally stronger than the granular base and sub base of the conventional asphalt pavements.
- *Low life-cycle cost*. Because of the thicker HMA layers of the perpetual pavements, the short term costs like construction surpass that of the conventional HMA pavement by about 10 percent. Nevertheless, in a long run, the perpetual pavement are considered cost effective as it needs only a few maintenance for a very long life (Walubita L, 2010).
- *Less user-delay cost*. Since maintenance is limited only to the surface layer, the longer delays associated with the construction of sub-surface structural will no longer exists and thus money and time will be saved (MAPA, 2012).
- *Less environmental effects*. The use of recycled and less materials over the life span of perpetual pavements reduces the impact to the environment. Also, the less maintenance activities throughout the pavement's life contribute in energy saving (APA, 2010).

- *Competitive option to rigid pavements*. Before perpetual pavements, the pavements that were known to live for a long time under heavy loads were rigid pavements. The superiority of the rigid pavements (in terms of design life) remained so till APA officially introduced the concept of perpetual pavements. Perpetual pavements not only competed in performance but also cost wise. In 2004, Sargand S. reported that the construction costs per mile of perpetual pavement were 8.5 percent lower than that of the rigid pavement for the same performance (Sargand S., 2004). The report is based on one Ohio Department of Transportation bid for perpetual pavements construction that included rigid pavement for comparison purposes.

2.1.2.3 Perpetual Pavement concept implementation

Two main approaches are recommended for the implementation of the perpetual pavement concept. In the first approach, the bottom lift of the base layer should have a softer binder grade and/or higher binder content to allow the layer to stretch and accommodate excess strains that normally would cause bottom-up cracks to conversional mixes. The second approach requires to increase the total thickness and stiffness of the asphalt layers so that no fatigue damage would develop at the bottom of the asphalt layer (Button J. W., 2001).

Monismith et al. (1970), Carpenter et al. (2003) and other researchers have proven through laboratory experiments that if the asphalt concrete material is

subjected to a minimum limiting strain, it will never fail under repeated loads. The limiting strain concept, which is also called fatigue endurance limit (FEL), is the major design criteria in the mechanistic-empirical design of Perpetual Pavements. The thickness of the Perpetual PPavement structure is deemed to be acceptable if meets the following set of criteria designed to limit structural rutting (vertical strains) and bottom-up cracking (horizontal strains) to occur (Timm, D.H. et. al. (2006) and Walubita L, (2010)).

- Horizontal strains at the bottom of the pavement must be kept below 70 micro-strains (or 100 micro-strains as suggested by some researchers) to limit the existence of fatigue bottom up cracking
- Vertical compressive strains at the top subgrade must be kept at or below 200 micro-strains to limit structural rutting.

2.1.2.4 Perpetual Pavement layers structure

A well designed Perpetual Pavement may consist of the following structural layers:

- Wearing Surface Layer

The mix design of this layer varies depending on the traffic conditions, environment, local experience and economy to satisfy performance requirements such as resistance to rutting and surface cracking to the upper pavement layer (about 4 inches). Because of high vertical compressive stresses from truck tires, it is advisable to use crushed aggregate for both medium and high traffic conditions,

while a limited amount of gravel might be used in the mix for low volume roads. For the same reason, a polymer modified asphalt should be used as the binder for high-volume roads (Newcomb, D.E. and K.R. Hansen. 2006). If the pavement project is located in a wet zone, Open-Graded Frictional Courses (OGFC) mix may be selected to assure long term performance (Figure 2.7). The OGFC mix is designed to have 18-22% air voids to drain water from the surface and therefore improve wet-weather-friction. Fibers may also be included in the OGFC to prevent asphalt drain down (Huber, G. 2000)

Figure 2.7 Close-up view of Perpetual Pavement wearing course with OGF mix

- Intermediate Layers

As was for the wearing course, this layer (especially the top four inches) is also vulnerable to rutting due to high stresses from heavy traffic loading. Therefore, the materials used for this layer must offer resistance to shear failure (which equals to resistance to surface rutting) and have good stability and durability (APA, 2010). Large nominal maximum aggregate size crushed stones or gravel may be used to improve internal friction (to resist shear failure), whereas improvement to stability may be achieved by adding appropriate high-temperature

grading binder (Kandhal, P.S.,1990). Small aggregates may also be used for this layer as long as the stone-on-stone contact is maintained (APA, 2010).

The asphalt binder grade used for this layer may be selected using the LTTBind software to determine the proper high and low service temperatures (APA, 2010). In order to avoid rutting distresses, the upper requirement of the binder temperature grade may be the same as of the surface layer. However, the low temperature requirements may be one level below the surface temperature, since the low temperature in this layer is normally less severe than the temperature in the surface layer (Asphalt Institute,1996a).

- HMA Base Layer

This is a layer where potential bottom up fatigue cracking may develop due to heavy vehicles repeated loading . For a pavement to be called "perpetual," must have a base layer that can overcome repeated traffic induced tensile strains for a very long design life (i.e. more than 50 years). Since the early beginning of this century, several studies aimed to characterize the mechanics of asphalt materials that may be used for this layer. Some of these studies concluded that for the HMA base to function as intended, it needs to be designed with mixes of high binder content and less in place air void. The high binder content allows the layer to be densely compacted, durable, resistant to moisture penetration and offers high fatigue life by improving the stretching ability under repeated forces (Figure 2.8) (APA, 2010, Kassem et.al., 2008, Timm, D., 2004)

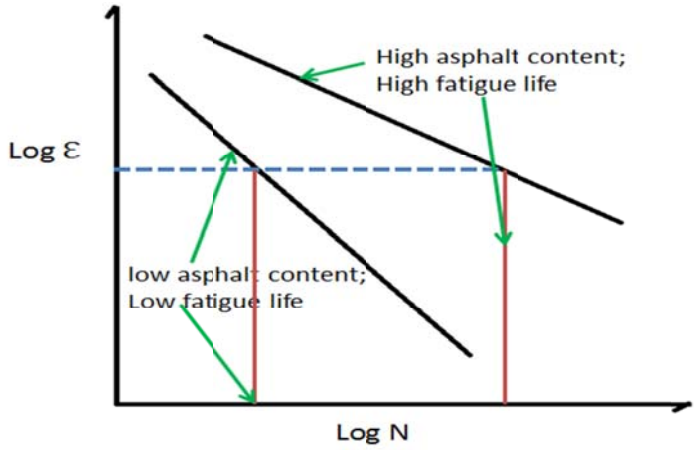

Figure 2-8: Improving Fatigue life with addition asphalt content

Another way obtaining a well performing HMA base is by designing a thick layer that reduces the strains at the bottom of the asphalt base layer (Figure 2-9). In order to lower the cost by using a few inches thinner base layers, some researchers have suggests the use of a single mix for both base and intermediate layers (APA, 2010, Corte, J-F. 2001).

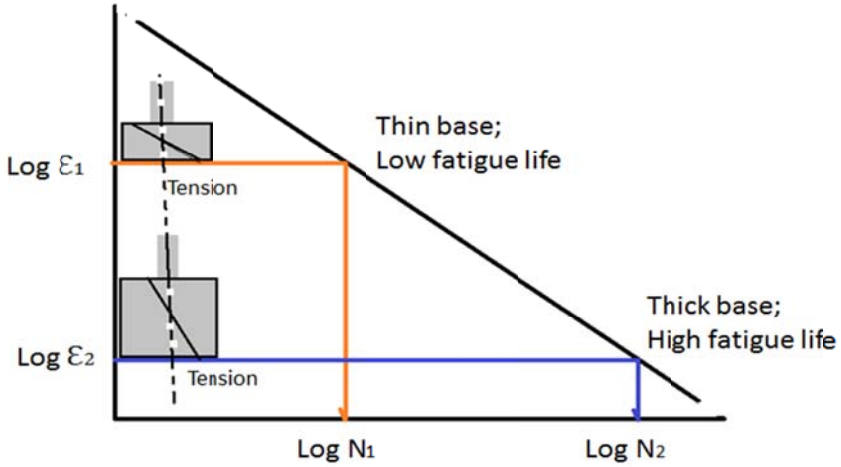

Figure 2-9: Reducing Tensile strains with thick pavement

A research by Molenaar et. al. (2008) reported that a based layer thickness reduction of about of 40% met the necessary design criteria when a modified binder (6-7% SBS polymer) was used instead of a conventional, unmodified binder.

- Subgrade

The strength and other characteristics of sub-grade soil layer has a great role in the determination of the thickness of the perpetual pavement layers. A weak subgrade requires thick pavement layers to reduce the effect the traffic loads cause at its surface. However, too thick layers may become expensive and impractical to construct. Therefore, the subgrade material must be stabilized to improve its strength. The strengthened subgrade is not only reducing the pavement thickness but is also acting as a stable platform for vehicles and equipment during construction.

In light of the minimum stability requirements for virgin subgrade soil, Von Quintus (2001) suggested a minimum subgrade soil resilient modulus of 25,000psi to be available for perpetual pavement construction. Illinois DOT requires that the soil must have a minimum California Bearing Ratio (CBR) of at about 8 to qualify for a Perpetual Pavement construction.

Nunn et al. (1997) proposed a more detailed criteria to improve the subgrade soil. He proposed the use of varying thickness of granular capping and

sub-base materials depending upon the CBR of the existing soil layer, as shown in Table 2-1.

Table 2-1 Subgrade improvement proposed by Nunn et. al.

Foundation Soil CBR	**2**	**2-5**	**>5**
Subbase thickness	150	150	225
Capping thickness	**350**	**600**	**N/A**

2.2 Basic Mechanical Behavior of HMA Pavements

When a vehicle passes or stands on the surface of a HMA pavement, it generate stresses to the surface and subsequent layers below. As the stresses develop within the layers, they generate shear strains at the surface layer, tensile strains at the bottom of the asphaltic layers and vertical stresses and strains at the top of subgrade and other various layers (Pavement Interactive, 2008). The magnitude of the generated strains and stresses depends upon the pavement thickness and stiffness of the layers. Thick pavements with layers possessing high modulus, high tensile strength and high shear strength are less susceptible to damages due to the stresses generated by traffic loads.

2.2.1 HMA Modulus

Mathematically, the modulus of HMA may be defined as a ratio between applied stresses over resulting strains. There are two types of tests commonly used to determine the modulus of HMA: Resilient Modulus and Dynamic

Modulus. While resilient modulus tests apply the same load several thousand times at the same frequency, dynamic modulus tests apply a load over a range of frequencies (25Hz, 10Hz, 5Hz, 1Hz and 0.5Hz).

2.2.1.1 Resilient Modulus

AASHTO 1993 Design Guide uses the Resilient Modulus of HMA in the design of flexible pavement structures. The Modulus is used to estimate the structural coefficient (a_i) for the HMA. The structural layer coefficient is a measure of relative ability of a unit thickness of a given material to function as a structural component of the pavement. Figure 2-10 shows how Resilient Modulus is converted into structural coefficient in accordance with AASHTO 1993 Design Guide.

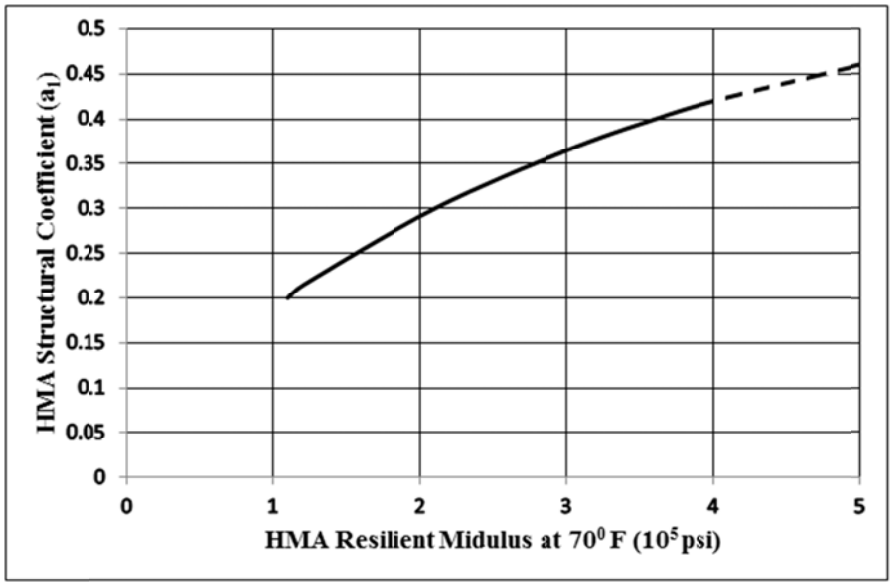

Figure 2-10 Chart for estimating HMA layer coefficient based on HMA Resilient Modulus

The resilient modulus of HMA can be determined using a repeated-load indirect tension test (Figure 2-11). Typically, three laboratory fabricated specimens or field cores are recommended for the determination of the resilient modulus of an asphalt mix. Each of the specimens is tested two times to produce six measured resilient modulus values (ASTM D 7369-11).

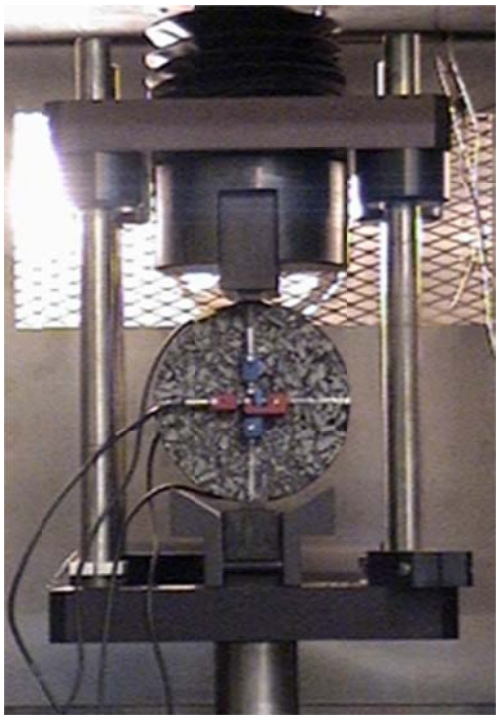

Figure 2-11 HMA indirect tensile test (courtesy of CAIT)

According to ASTM D 7369-11, the repeated-load indirect tension resilient modulus test of bituminous mixtures is conducted through repetitive applications of compressive loads in a haversine waveform. The compressive load is applied along a vertical diametral plane of a cylindrical specimen of asphalt concrete. The resulting horizontal and vertical deformations of the specimen are

measured. Values of resilient Poisson's ratio are calculated using recoverable vertical and horizontal deformations. The resilient modulus values are subsequently calculated using the calculated Poisson's ratio and the applied cyclic load.

$$M_R = \frac{P_{cyclic}}{\delta_h t}(0.2329 + 0.7801\mu) \quad \text{.....2.1}$$

where

M_R = instantaneous or total resilient modulus, psi,

δ_h = recoverable horizontal deformation, inches

$P_{cyclic} = P_{max} - P_{contact}$ = cyclic load applied to specimen, lbs.,

P_{max} = maximum applied load, lbs.

$P_{contact}$ = contact load, lbs.,

$\mu = \frac{-1.0695 - 0.2339\frac{\delta v}{\delta h}}{0.3074 + 0.7801\frac{\delta v}{\delta h}}$ = instantaneous or total Poisson's ratio

δ_v = recoverable vertical deformation, inches

2.2.1.2 Dynamic modulus

The Dynamic Modulus is the parameter used to characterize the behavior of HMA in the Mechanistic Empirical Pavement Design Guide (MEPDG) and most advanced finite element software for modeling the viscoelastic behavior of materials (AASHTO, 2004). Dynamic modulus is defined as any modulus that has been obtained from repetitive non-static test loading. For asphalt viscoelastic response, dynamic modulus, |E*|, (also known as complex modulus) may be

computed based on a sinusoidal or haversine loading test performed under a given frequency domain and temperature. The modulus is the ratio between the maximum stresses and the maximum strain recorded in a cyclic uni-axial tension or compression test. Due to the viscoelastic behavior of asphalt concrete, the sinusoidal stress and strain do not occur at the same time (Yoder, E.J., and Witczak, M.W., 1975). The time lag between the stress and strain cycles can be converted into aphase angle (φ) and may be combined with the other test parameters to determine dynamic modulus |E| of HMA (Figure 2-12).

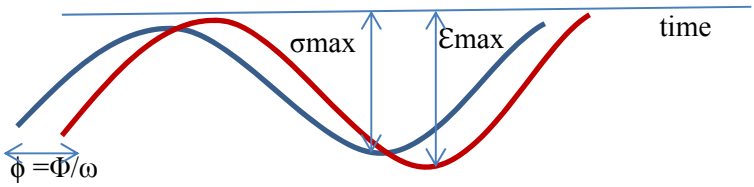

Figure 2-12 Typical Dynamic modulus response curves

Due to the time lag between the stress and strain waves, the dynamic modulus |E*|, is normally represented as Complex number, in exponential or Cartesian form.

- *Dynamic modulus in exponential form*

$$|E^*| = \frac{\sigma_{max} e^{i\omega t}}{\varepsilon_{max} e^{i(\omega t - \varphi)}} \quad \text{.....2.2a}$$

Where

σ_{max} = peak stress

ε_{max} = peak strain

ω = angular velocity

φ = phase angle

t = time

- *Dynamic modulus in Cartesian form*

E* = E'+ iE"……..……2.2b

Where

E* = complex modulus,

E' = storage modulus (elastic component),

E" = modulus (viscous component),

The components of Equation 2-2b may also be presented in graphical form, as shown in Figure 2-12.

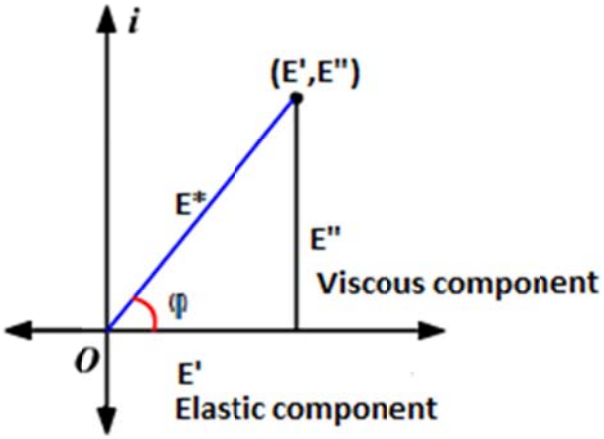

Figure 2-13 Graphical representation of a complex modulus

2.2.2 Tensile strength

An HMA mix with high tensile strength can tolerate higher strains before developing cracks. MEPDG uses the tensile strength to predict the low-temperature cracking of flexible pavement. In laboratory, the tensile strength is typically determined from diametral indirect tensile test (IDT) as was for the resilient modulus test of HMA (Figure 2-12). However, the failure load and dimensions of the specimen are the only parameters needed in this test for calculating the tensile strength.

$$S_t = \frac{2 \times P}{\pi \times D \times b} \quad \text{.....2.3}$$

Where:

S_t = Tensile strength

P = Failure load

D = sample diameter

b = Sample thickness

2.2.3 Shear Strength

The shear strength of HMA is one of the properties that may be used to predict the rutting susceptibility of HMA mixes. Researchers that worked on the relationship between rutting and shear strength of HMA mixes have found that mixes with less shear strength are more likely to develop rutting damage (K. Su et al. 2009). Shear strength of HMA may be measured on SST machine (Superpave Shear Tester). The SST is a servo hydraulic machine that can apply both axial and

shear loads at constant temperatures using closed-loop control. The machine is expensive. As a result, its use is not widespread. To characterize the rutting potential of HMA mixes, simulative tests such as Humburg wheel rut test, are used instead. The Humburg wheel rut test measures the rutting resistance of the HMA by rolling a loaded wheel device repeatedly on top of a prepared HMA specimen (Figure 2-14) (Brown, E. R. et. al., 2001b).

Figure 2-14 Hamburg Wheel rut tracking

2.3 Laboratory test set up methods for characterizing HMA behavior

In the laboratory, HMA tests may be performed in compressive, tensile or compressive-tensile mode to determine the parameters for characterizing the behavior of HMA. In this section, the relationship between the compressive and tensile test set up and resulting behavior of HMA are discussed.

While compressive tests are simple and more widely used, tensile tests may offer results which best relate to the field performance of HMA, especially concerning fatigue cracking. The tensile tests can be performed direct (axial tests) or indirect (e.g. Indirect Tensile test (IDT)). The indirect tests are relatively easier to perform and thus more used than axial tensile tests. The axial tensile tests on the other hand are time consuming and difficult to perform. These tests require samples to be uniform and strongly attached to the testing plates with glue. But most of glues that offer strong bonds require hours or even days to achieve maximum capacity. Because of these complexities, most researchers tend to derive material characteristics from compressive tests in order to analyze both compressive and tensile behavior of HMA. By doing so, the differences between compressive and tensile properties of HMA are neglected.

Literature dated back to 1960's has shown that compressive and tensile behavior of HMA may be different. In early 1960's Monismith et. al. and Harget et. al. were among the first researchers to suggest that HMA compressive and tensile behavior are different.

When analyzing the tensile and compressive strains developed during bending creep test, Secor and Monismith (1965) observed that at temperatures above 25^{o}C, tensile strains were about two times the compressive strains. A few years earlier, a research by Hargett and Johnsons (1961) observed higher

difference between HMA compressive and tensile strengths. They reported HMA tensile strength 10 times lower than the compressive strength.

Kallas (1970) used uniaxial loading in tension, compression and tension-compression to determine the dynamic modulus. At low frequency (1 HZ) and high temperatures (20^{o}C and above) Kallas found that dynamic modulus in tension was a half to two-third of the dynamic modulus in compression. This investigation caught the attention of Witczak and Root (1974) who suggested that HMA pavements may be best analyzed if using test results consistent with field loading

Von Quintas et. al. (1982) conducted resilient modulus tests in compression and indirect tension and found that the modulus in compression was higher than that in tension. The difference was more pronounced at higher temperatures. Lytton et al. (1993), performed uniaxial dynamic modulus in both tension and compression under the same end condition (glued ends) and found at a temperature of 25^{o}C, tensile strains were about 10 times higher than compressive strains.

Shatnawi et al. (1994) developed a device that fits into Superpave Shear Tester to determine stiffness and repeated load behavior of asphalt concrete based on repeated direct tension test. The research used the equipment to determine the number of cycles to fail an HMA prism with dimensions of 200mm tall x 50 mm x 63 mm. To accompany this test, the typical dynamic modulus test in

compression mode at 20^{o}C was also conducted for comparison and verification purposes. The comparison results indicated that there was no difference between compression and tension stiffness, at all frequencies.

Another research that compares tension and compression properties of HMA is by Romanoschi et al. (2006). The research compared stiffness of HMA determined from flexural bending beam (indirect tensile) and dynamic modulus tests (in compression) and found that HMA dynamic modulus is more than twice the corresponding bending stiffness.

Wu et al. (2011) compared compressive and tensile properties of HMA based on four mixes commonly used in Tennessee. The research found that, at high temperature (40^{o}C) and frequency between 0.1 Hz to 25Hz, the dynamic modulus in tension was about half of the dynamic modulus in compression. At low temperatures (10^{o}C) the behavior flipped; the tensile dynamic modulus was found to be about 20% more than the compressive dynamic modulus. The results at low temperature differ from earlier studies where the same dynamic modulus is suggested.

Ebrahimi et al. (2013) conducted a research to compare HMA dynamic moduli derived from Indirect Tensile test (IDT) and uniaxial compression dynamic modulus test. The research used mixes commonly used in New Zealand. Five HMA mixes were tested at different temperatures and frequencies for both

IDT and compressive dynamic modulus test. The research concluded that no difference exist between compressive and tensile dynamic modulus.

2.4 Development of analysis theories for HMA responses

2.4.1 Elastic theories

The early elastic analysis theories of pavement structures were introduced by Boussinesq (1885) and Burmister in 1943 and 1945. While Boussinesq's (1885) theory assumed the pavement as homogeneous infinite half space, Burmister theories considered pavement to be comprised of two to three layers of different characteristics (Elastic Modulus, Poisson's ratio and thickness).

2.4.1.1 Boussinesq Theory

The analysis and design of asphalt pavements during the first half of the 20th century were based on Boussinesq theories. Under this theory, the pavement structure is modelled as a semi-infinite half-space made of a linear elastic, isotropic and uniform material (Chrishao Han. H. 1973, Huang, 2004). The simplified model required material modulus of elasticity, Poisson's ratio and pressure load applied over a circular area to determine the stresses and strains in the pavement structure. To simply the application of this theory, Foster and Ahlvin (1954) created surface deflection and stress development charts based on this theory (Huang 2004).

2.4.1.2 Burmister Theory

As the road network expanded during the early 20th century, a need for a design technique that closely considers the actual state of the pavement became essential. In 1943 and 1945 Burmister developed solutions for a two-and three-layer pavement system . The Burmister solution was difficult to use at first, but with improved computer technology, the theory was extended to multilayer pavement system (Huang 1967, Huang 2004). Pavement analysis programs such as BISAR, KENLAYER, ELSYM, EVERSTRESS, WESLEA, and JULEA were originally designed based on Burmister theories (Huang 1993, Chen Y. G, 2009).

Burmister assumes a pavement is a multi-layer structure with superior materials on top of subgrade (Figure 2-15). Other assumptions to be satisfied by Burmister theory are:

1. The materials/soils of each layer are homogeneous, isotropic and linear elastic.
2. The layers are weightless
3. The top layers have finite thickness “h” and are infinite in horizontal direction
4. The subgrade has infinite thickness
5. A uniform Pressure, q, is applied on the pavement surface over a circular area of radius a.

6. Continuity conditions of stress and displacements are satisfied across interfaces, meaning that vertical stresses, shear stresses, vertical displacement and radial displacement are the same at layers interfaces.

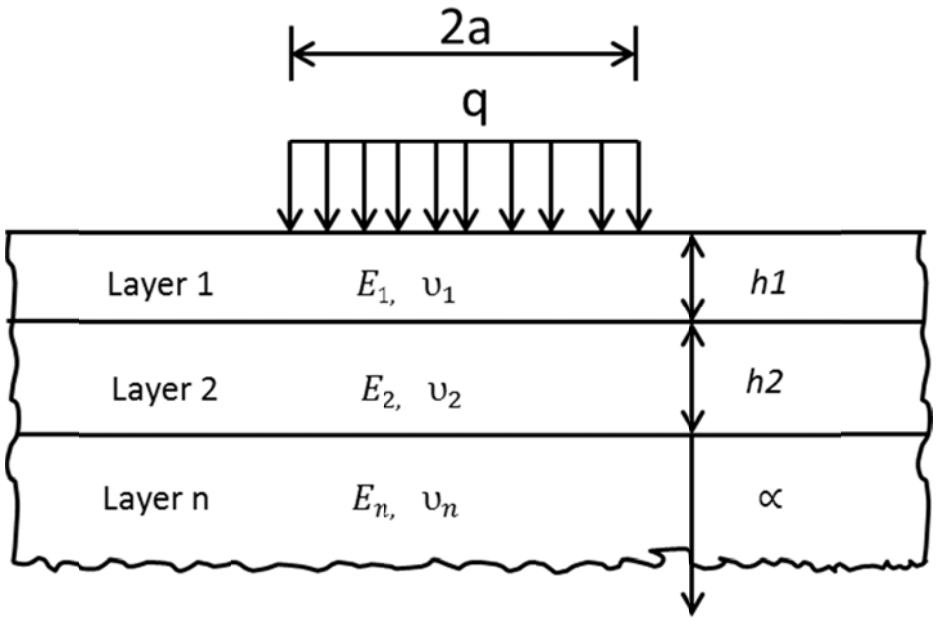

Figure 2-15 A multi-layer system subjected to a circular load

2.4.2 Viscoelastic solutions

HMA is a viscoelastic material whose behavior depends on the time of loading, so it is natural to apply the theory of viscoelasticity to the analysis of Asphalt pavement layers. Viscoelastic materials (including asphalt mixes) are those with viscous and elastic behavior. There are two ways of characterizing viscoelastic materials: by using mechanical models or creep compliance curves.

Both techniques rely on the following basic assumptions pioneered by physicists such as Boltzman, Kelvin and Maxwel in the early twentieth century:

- for a constant strain, the stress decreases with time (relaxation);
- for a constant stress, the strain increases with time (creep);
- the modulus of the material varies depending upon the application rate of the load.

- 2.4.2.1 Viscoelastic Materials Mechanical models

The basic mechanical model of viscoelastic materials normally presented in simple combination of springs and dashpots either in series (Maxwel model) or in parallel (Kelvin model). Though easy to work with, the simple models cannot independently simulate some properties associated with viscoelastic behavior. For instance, the Maxwel model does not simulate creep behavior accurately, while the Kevin model does not simulate relaxation. Because of these deficiencies, complex mechanical models use combination of the simple models to more closely define the viscoelastic materials .

Maxwell Model. Maxwell model is comprised of a circuit of springs and dashpots arranged in series, as shown in Figure 2-16. Under a known elapsed time and constant stress, Maxwell model can predict the total strain using Equation 2.8 (Huang, 2004).

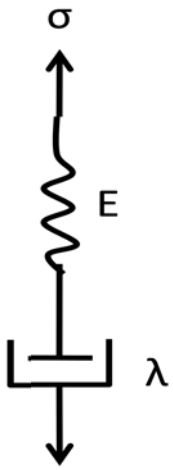

Figure 2-16: Maxwell Model

$$Strain, \varepsilon = \frac{\sigma}{E} + \frac{\sigma \times t}{\lambda} = \frac{\sigma}{E}\left(1 + \frac{t}{T}\right) \quad \text{.....2.4}$$

Where:

σ = stress

E = elastic modulus

λ = viscosity

t = time

T= $\frac{\lambda}{E}$ = Relaxation time

Under the Maxwell equation, the strain increase linearly with the increase in loading time. But in reality, for asphaltic materials the rate of change of strain reduces with time. So, when it comes to materials creep modeling, one can at best assume that the model can predict strains at low stresses.

Kelvin Model. Kelvin model or Kelvin-Voigt as sometimes called, is formed by a combination of a Newtonian damper (dashpot) and Hookean elastic spring connected in parallel, as shown in Figure 2-17.

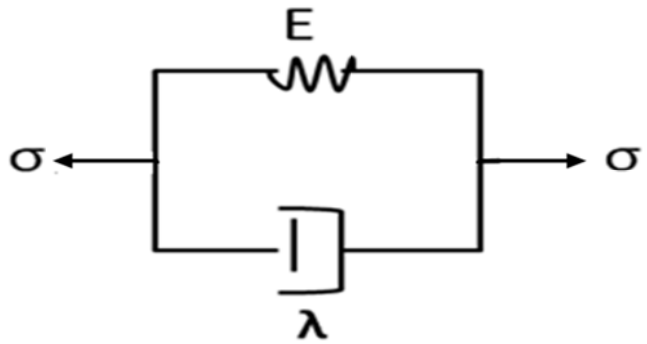

Figure 2-17 Kelvin-Voigt Model

In this model the total stress in the system is determined by a combination of two stresses derived from the spring and the dashpot. The derived stress is shown in equation 2.5 (Huang, 2004).

$$\sigma(t) = E\varepsilon(t) + \lambda\frac{d\varepsilon(t)}{d(t)} \quad \text{.....2.5}$$

When a constant stress is applied to the system, Equation 2.5 is rearranged and integrated from 0 to Ɛ and from 0 to t to get:

$$\varepsilon = \frac{\sigma}{E}\left[1 - e^{-\frac{t}{T}}\right] \quad \text{.....2.6}$$

Burgers Model. Burgers model is a result of combining Maxwell and Kelvin model in series as shown in Figure 2-18.

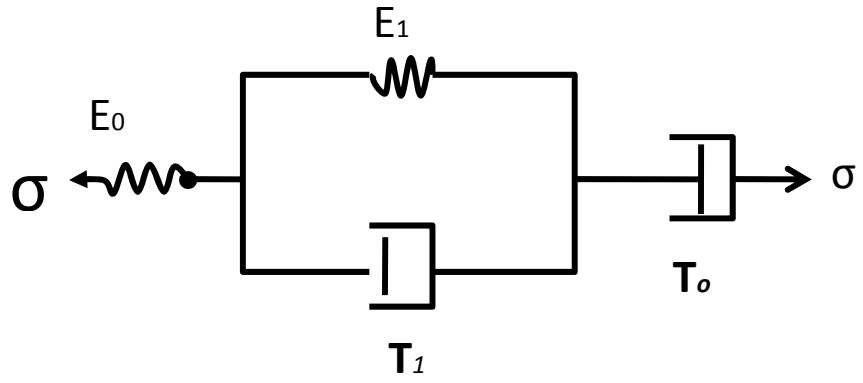

Figure 2-18 Burgers model

The mathematical equation (eq. 2.7) of Burgers model compensates deficiencies that limit the use of Kelvin equations in problems which involve retarded strains (Huang, 2004):

$$\varepsilon = \frac{\sigma}{E_o}\left(1+\frac{t}{T_o}\right)+\frac{\sigma}{E_1}\left[1-e^{-\frac{t}{T_1}}\right] \quad \text{..... 2.7}$$

The subscript o in E_o and $T_o(=\lambda/E_o)$ is used to represent Maxwell model, whereas subscript "1"in E_1 and T_1 $(=\lambda/E_1)$ represents Kelvin model.

Generalized model. Figure 2-19 show a generalized model that combines a Maxwell model and a number of Kevin models in series (subscripts 1 to *n*) to characterize any viscoelastic material (Huang 2004).

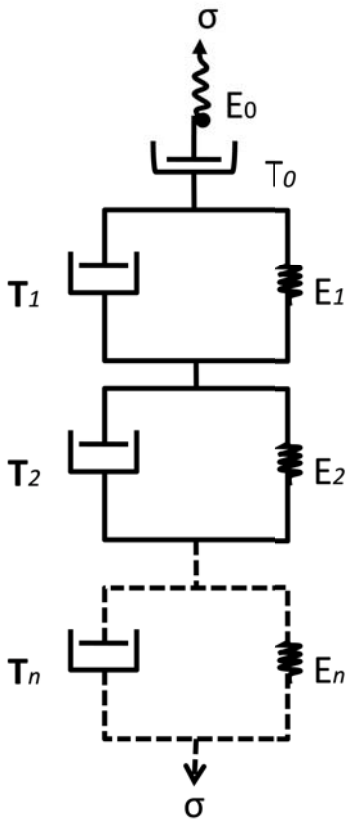

Figure 2-19 A generalized model

Under Constant stress, a generalized model can be used to determine strain based on equation 2.12; the parameter "n" represent the number of Kelvin models in the circuit.

$$\varepsilon = \frac{\sigma}{E_o}\left(1+\frac{t}{T_o}\right)+\sum_{i=1}^{n}\frac{\sigma}{E_i}\left[1-e^{-\frac{t}{T_i}}\right] \quad \text{.....2.8}$$

- 2.4.2.2 Viscoelastic Materials Creep compliance Model

Another way of characterizing viscoelastic materials (e.g. HMA) is by adopting creep compliance models. The key behavior of the materials to be characterized by creep models is that when subjected to constant step stress, the materials respond with a time dependent increase in strain (Figure 2-20).

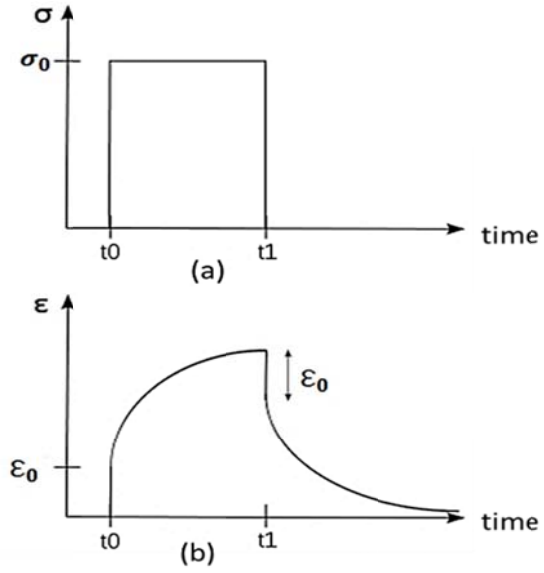

Figure 2-20: Creep compliance phenomenon. (a) Applied constant stress, (b) Strain response curve

At its simplest state, creep compliance, D(t), may mathematically be defined as follows:

$$D(t) = \frac{\varepsilon(t)}{\sigma} = \frac{1}{E(t)} \quad \text{.....2.9}$$

Where

Ɛ (t) = Time dependent strain

σ = Constant stress

E(t) = Young's Modulus at various times

For a Generalized model creep compliance can be determined through the following relationship (Huang 2004).

$$D(t) = \frac{1}{E_o}\left(1 + \frac{t}{T_o}\right) + \sum_{i=1}^{n} \frac{1}{E_i}\left\{1 - e^{\left(-\frac{t}{T_i}\right)}\right\} \quad \text{.....2.10}$$

Where, E_o, T_o, E_i and T_i are viscoelastic constants.

2.5 Finite Element Modeling methods for Flexible Pavements

The finite element method (FEM) is a computerized analytical method that closely predicts performance of pavements and other structures under forces such as traffic loading, vibrations, and heat. The power of Finite elements modeling has enabled engineers to properly address issues such a materials inelastic behavior, and geometry irregularities of flexible pavements and analyze the effect of dynamic loads. Depending upon the shape of analyzed structure, computer memory available and computational time, one of the following modeling techniques is typically employed to solve problems with FE programs: Axisymmetric analysis, Two-Dimensional Finite element analysis, and Three-Dimensional Finite element analysis.

2.5.1 Axisymmetric Analysis

Axisymmetric analysis is used to solve FE engineering problem when a geometric part is a solid revolution and radially loaded with a constant axial force along any diameter on the surface. This analysis method allows the user to create a section plane FE models on one side of the rotational axis and hence dramatically reduce the size of the finite element mesh and the analysis time.

In pavement structure modeling, the axisymmetric analysis can be used only when a simple statically loaded pavement is to be analyzed. To do so, the pavement must be idealized as a cylindrical section with a static load applied in a circular area. For example, in Figure 2-21, only plane geometry ABCD, applied load "a" and support conditions are needed in the axisymmetric analysis for the determination of responses of the whole pavement section.

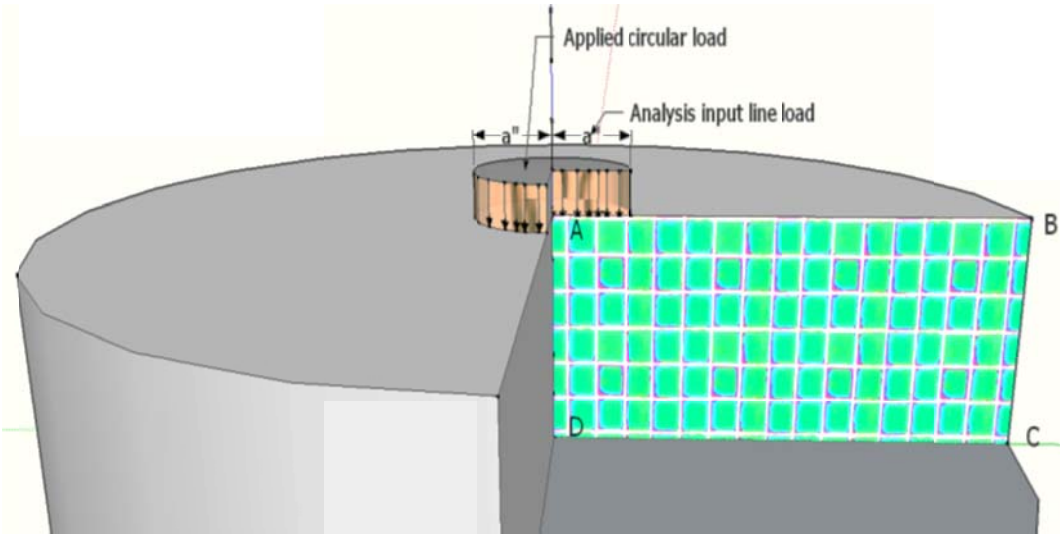

Figure 2-21 Typical Axisymmetric geometry for finite element analysis

2.5.2 Two-Dimensional Finite element analysis

This is another Finite element analysis method that uses relatively shorter time in solving engineering problems. In the field of pavements the 2-D analysis method is typically used to analyze simple statically loaded pavements. Since the geometry is planar, the traffic load at any section parallel to plane HIJK (Figure 2-22) is typically applied as a line pressure load "2a" (effective tire print width) perpendicular to the direction of movement. And because of the shape and nature of load application, the 2D analysis assumes the stresses and strains in the axis parallel to traffic movements are not of interest; only responses in the direction perpendicular to the direction of travel are computed (Kim et. al. 2010).

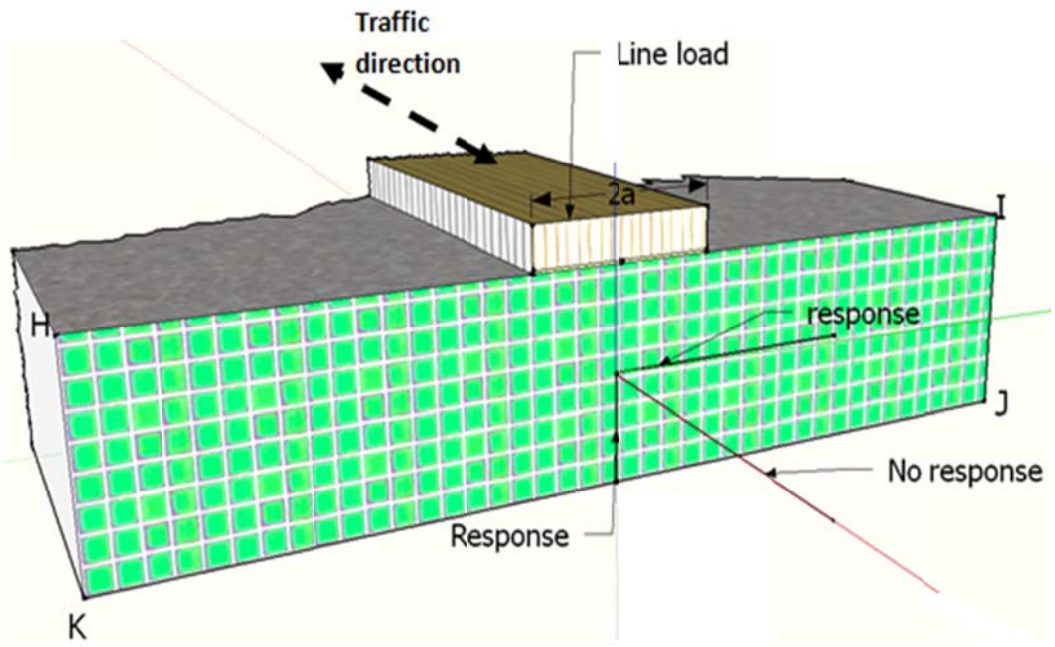

Figure 2-22 Typical 2-D planar geometry for finite element analysis

2.5.3 Three-Dimensional Finite element analysis

Advancements in the computational power and speed of modern computers have allowed 3-D finite element geometry models of complex engineering problems to be analyzed at relatively short time. When compared to the other aforementioned analysis methods, the 3-D analysis emerges to be the best technique for analyzing complex pavement structures that may include moving dynamic loading, pavement discontinuity, material non-linearity, and infinite ends and rigid foundation (Kim et. al. 2010). In 3-D analysis mode, the user can built geometric parts, load and perform analysis that yields responses in both x, y, and z-direction, as shown in Figure 2-23.

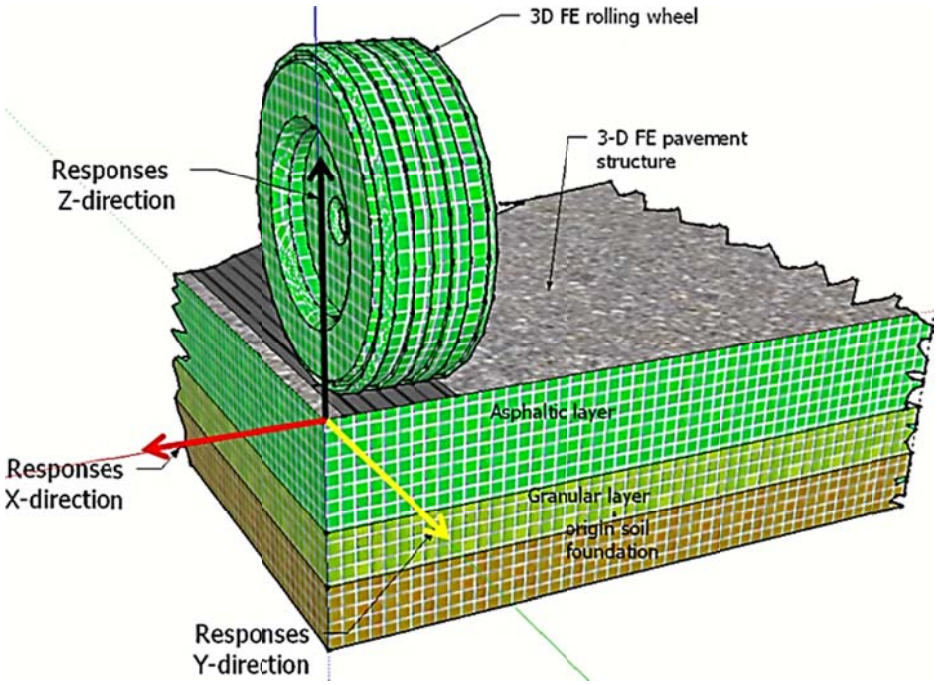

Figure 2-23 Typical 3-D Pavement geometry for generalized FE analysis

2.6 Application of viscoelastic theories to FE Asphalt pavement modeling

The application of viscoelastic theory in FE models is more difficult, but researchers who applied this theory found that it offers better result than the simple linear elastic theories. The FE analysis results by Elseifi et al. (2006) showed that the elastic FE model grossly under-estimated pavement stress and strains at intermediate and higher temperatures. But with linear viscoelastic FE model, the field results and the FE predicted responses were close.

Loulizi et al (2006), assumed linear elastic behavior of asphalt concrete when comparing field measurements and finite element simulations. The research employed axisymetric and 3D Finite Element analysis to determine responses of an instrumented section on Virginia Smart Road test. The results of this experiment concluded that linear elastic behavior overestimates stress and strains at low temperature. An overestimate of response was also observed by Portillio (2008) when comparing field results of an instrumented perpetual section on US 75 highways in Kansas. Portillo used the EVERSTRESS program with linear-elastic material behavior at 20^{o}C to compute strain responses at the bottom of the HMA layers. In general these two researchers show that linear elastic models poorly represent the field behavior of asphalt concrete.

Yoo et al (2006) investigated asphalt pavement responses under dynamic moving trapezoidal and continuous loading using the Abaqus finite element software. The asphalt concrete layers were considered viscoelastic with elastic

properties collected from the resilient modulus test and the viscoelastic properties obtained from the creep compliance test. After a series of testing and analysis, it was concluded that modeling of asphalt pavement with viscoelastic properties and continuous loading provides better results than the analysis when trapezoidal loading amplitude is used

Wang and Al-Qadi (2009) used FE viscoelastic analysis to compare the effect of uniform contact stresses to 3-D contact stresses measured in the field. The model used for the analysis represented a 254 mm deep perpetual pavement placed on 305 mm lime stabilized subgrade. Viscoelastic behavior of materials was assumed. After performing the finite element analysis at various load levels, it was observed that higher compressive and shear strains developed near the surface when the pavement subjected to the field measured 3-D tire contact stresses than when was under the uniform contact stresses. This suggests that the assumption of uniform contact stresses might underestimate the near-surface cracking potential and shear flow in the perpetual pavement. Furthermore, the difference in pavement responses for uniform contact stresses and 3-D contact stresses was more profound at higher wheel loads.

In 2005, Park et al. used an elastic-viscoplastic constitutive model in a 3-D finite element analysis of asphalt pavement to determine the effect of tire pressure distribution on pavement rutting. The research compared the permanent deformation (rutting) obtained from the 3-D FE analysis to the one directly

measured from WesTrack test sections. Two major results were obtained: the non-uniformity of tire pressure impacts the response of the pavement and the elastic-viscoplastic constitutive model can be used to compute asphalt pavement permanent deformation.

Panneerselvam (2005) used a multi-dimensional hyperelastic-viscoelastic-viscoplastic-damage model to capture the rutting and linked behaviors of asphalt concrete. Each component of the model was designed to capture different behavior of asphalt concrete during finite element modeling. A second order hyper-elastic model was used to define elastic behavior of asphalt concrete whereas a viscoelastic component was used to capture the time and temperature dependence of the material. The viscoplastic component was included to capture load rate dependent behavior of the asphalt concrete pavement. Anisotropic and isotropic damage in the material was also accounted for by the model. The constitutive model was verified against laboratory experiments and later was used in the Abaqus finite element program to compute strain responses of a pavement structure subjected to repeated wheel loading. There was a fairly good agreement between the FEM and lab experiments especially at low strains level (Figure 2-24 and 2-25).

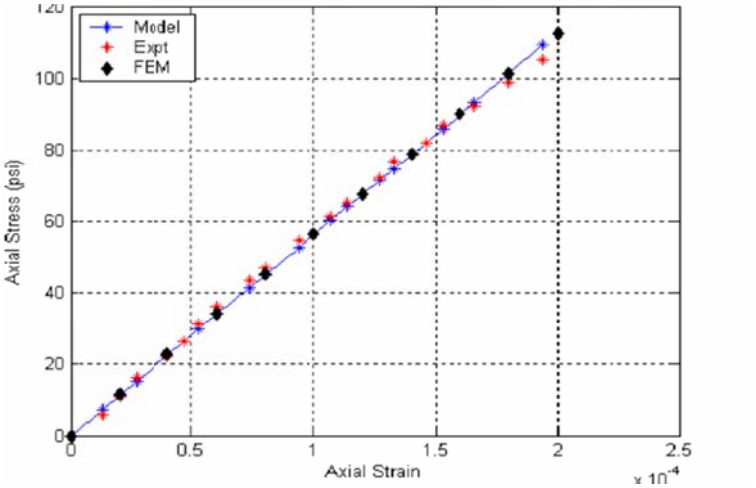

Figure 2-24 Comparison of Finite Element model with Experimental data: Axial Stress vs. Axial Strain (Panneerselvam (2005)

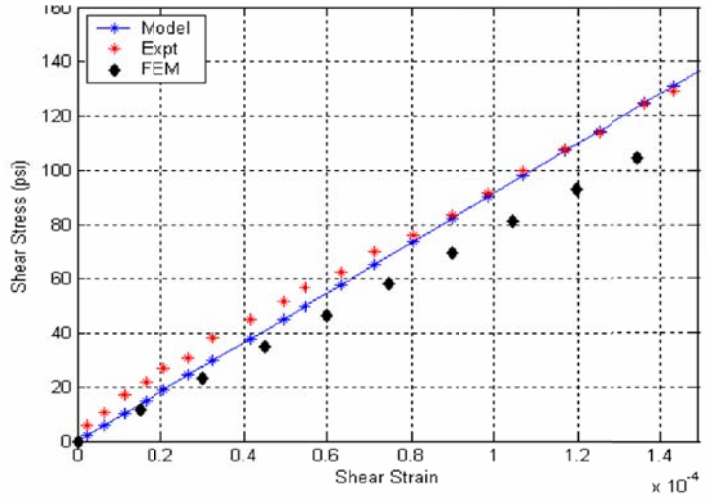

Figure 2-25 Comparison of Finite Element model with Experimental data:Shear Stress vs. Shear Strain (Panneerselvam 2005)

2.7 Summary

In the beginning of this chapter, the basic information that describe flexible pavement were introduced to the readers. Thereafter, results of

experimental investigations that searched for differences between Compressive and Tensile behavior of HMA were presented. In addition, the chapter covers the development of FE viscoelastic modeling for HMA pavements.

The literature reviewed show evidence that the Compressive and Tensile properties of HMA may be different as opposed to the long held idea that they are the same. Most of the literature suggest a compressive/tensile strength ratio greater than 1 (up to 10); varying depending upon type of test and temperature. However, for dynamic modulus tests, a compressive/tensile modulus ratio of one or even less was reported for tests conducted at low temperatures (Christensen et al. (2004), Kim et al. (2004)). Above all, this research found no publications with extensive experiments and statistical/analytical models that strongly relates compressive and tensile modulus. Such models could eliminate axial tensile tests which are more difficult to perform.

When it comes to the Finite element modeling of HMA materials, the literature showed that elastic models overestimate pavements' responses, whereas viscoelastic models predictions are closer to the field responses. In addition, some researchers have modified the original Finite element Viscoelastic models to capture specific HMA behavior. For example, a viscoelastic constitutive model coupled with viscoplastic was used by Panneerselvam (2005) to capture HMA loading rate dependence at higher temperatures and extreme loading.

Chapter 3

Field responses of Perpetual Pavements

3.1 Introduction

Unlike the old empirical design methods such as AASHTO design Guide, the concept of Perpetual Pavements, if well implemented, can create pavements which are economical and of high quality to withstand existing local conditions for many years. To achieve its goals, the concept requires thorough laboratory investigations to get the best materials and HMA mixes that can significantly improve the life of the pavement. Additionally, relatively expensive full-scale field performance or accelerated pavement tests (APT) may be used in states where the concept is fairly new and the best materials mix design is not known (Newcomb et al. 2001).

Since late 1990s, when perpetual pavement concept emerged, a number of field performance studies have been conducted including the Kansas US 75 Project. The Kansas US 75 perpetual pavement project will later be used in this research to validate through Finite Element program, a Compressive-Tensile material model of Hot Mix Asphalt (HMA). Kansas US 75 project and a few other field performance perpetual pavements researches are discussed in this chapter.

3.2 NCAT Perpetual Pavement Experiment

The National Center for Asphalt Technology (NCAT) at Auburn University was established in 1986 with a purpose of testing the performance of asphalt pavement materials and structure. So far, the center has played a great role to ensure through excellent research in the lab and field that HMA pavements meet real time challenges and have a promising future.

NCAT obtains pavement response data from its world well known 1.7 miles oval shaped test track. The track consists of 46 different 200-ft long research sections mostly sponsored by state Department of Transportation and their counterparts in three year cycles since the year 2000. The three year cycle was designed to simulate 10 million equivalent axle loads (ESALs) from controlled heavily loaded tractor-trailers. On a typical highway, one would have to wait about 10 to 15 years to collect pavement data equivalent to what is obtained within one full operating cycle of the test track. That is why the test track is also known as accelerated pavement testing facility (APT).

The pavement sections of the NCAT facility are built with temperature and moisture sensors sandwiched between layers of the pavement to record moisture and temperature of the pavement at the time of testing. An on-site automated weather station is also available to collect hourly temperatures of the track surroundings. Furthermore, the structural layers of the experimental sections are instrumented with strains gauges (in both longitudinal and transverse

directions), pressure cells, and vertical compression gauges at selected location along the wheel path. When these sensors respond to passing loads, generate important data that quantify the pavements' performance and validate material mix designs, layer thicknesses, and construction methodologies.

Apart from field performance experiments, the NCAT center has a well-equipped materials testing laboratory for determining experimental data, which are useful for state-of-the-art pavement analysis and design. Nevertheless, the linking of laboratory to field responses still is a challenge to engineers. Project local conditions and complex material behaviors are among the reasons. To lessen the problems, NCAT center imports materials for construction from the sponsoring states to replicate some local condition (Powel, B. R., 2001). However, weather and other local conditions that are not possible to replicate on an open facility may still affect the performance of the pavement if constructed elsewhere. The effects are more pronounced when the experimental pavement sections are built with thin layer (Willis, J. R. et al. 2009, West, and R. et al. 2012).

NCAT has dedicated a number of perpetual pavements sections on its track to test the performance of different material mixes and the designed structural layers. In the year 2000 the first test cycle (1 test cycle = 10 million ESALs in 3 years) begun. The perpetual pavement sections accommodated during this cycle were extremely thick (Figure 3-1). The extra thickness was mainly due

to the use of AASSHTO 1993 Design Guide, which is among conservative methods of pavement design.

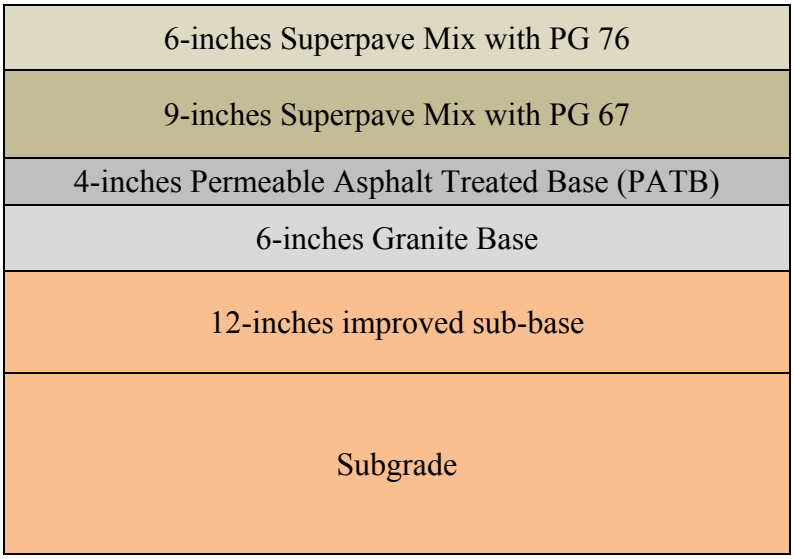

Figure 3-1 Perpetual Pavements at the 2000 Test Track. (Courtesy of NCAT)

The first test cycle, which ended in the year 2003, showed that the strains at the bottom of HMA were around 10 micro-strains, eight times below the typical value above which bottom crack can initiate. These sections were simply overly designed.

The second test cycle of experiments began in 2003; immediately after the first cycle. During this cycle, eight instrumented thinner sections were included to replace the thick sections constructed in the first test cycle. The target of the experiment was to evaluate the structural performance of differing pavement

thickness and materials stiffness. Out of the eight sections, two were 5 inches deep, another two were 9 inches deep and the rest were 7 inches deep. According to Willis J. R. et. al. (2009), thinner sections (5 and 7 inches thick) developed fatigue failure cracks before the end of test cycle (less than 10 million ESALs); de-bonding was considered the source of the failure for some of them. On the contrary, the 9 inches sections survived the 10 million ESALs without showingfatigue cracks even when the measured strains were higher than expected. More than 90 percent of the measured strains at the bottom of one of the survived sections were above 100 micro-strains. The other section had more than 85 percent of strains above 70 micro-strains. Based on this limited field strain measurements, the research concluded that for a 9 inches or more full depth asphalt pavement subjected to 10 million ESALs and above, an HMA can be design not to fail in fatigue even when the 70 (or 100) micro-strain threshold for the tensile strain is exceeded (West, R., and Timm D.H., 2012).

In addition to field performance tests of the 2003 track cycle, two asphalt base mixtures were tested in the laboratory using the bending beam fatigue test, (AASHTO T 321), to evaluate fatigue endurance limits of the materials. Attempts were made to directly relate the laboratory and field measure strains. However, no good correlation was found (Willis, J. R. et al. 2009).

The third cycle began in November 2006 with 11 perpetual pavements test sections. The test sections included two 9 inches and other three instrumented

sections were left in place from the previous cycle. In addition, six more instrumented sections were newly constructed. Among them; two were the 14.4 and 9.9 inches perpetual pavements sponsored by Oklahoma DOT.

The result of the 3rd cycle showed that the two 9 inches sections survived 10 million more ESALs (on top of the 10 million ESALs of phase 2) without bottom up fatigue cracks. A 14 inches section which was constructed during this phase also found to perform very well under fatigue loading. These three sections continued to perform very well in the following cycles, proving that perpetual pavements with right materials can be thinner and carry more than 30 million ESALs, an equivalence of more than 50 years of a normal highway traffic (West, R., and Timm D. H., 2012).

3.3 Perpetual Pavement Experiments in Ohio

In Ohio, the first perpetual pavement project research works begun in 2005 under the sponsorship of ODOT and supervision of Ohio University. The project consists of two instrumented sections (with sensors at the bottom of HMA layers), built on rural freeway U S 30 which carried about 18,000 ADT at that time (Sargand, S. M. et al. 2006).

A task force assigned to design the US 30 perpetual pavement sections, conducted design analyses using axle weights 20 percent more than stipulated in the guide of Ohio legal dimension and weight limits for highway vehicles. They designed the sections to include typical ODOT specified materials at the bottom

two layers and polymer-modified binder in the top two HMA layers. In total, the HMA thickness was 16.25 inches (Sargand S. M. et al., 2006, Liao Y., 2007).

During field-testing, the engineers used a truck weighing around 25KN on the steering axle and 22KN on its rear single axle to trigger sensors buried at the bottom of the HMA layers. The sensors were connected to a computer for collecting and reporting real-time responses (i.e. longitudinal and transverse strains). Liao Y. (2007) reports that the maximum tensile strain observed in this project, was about 80 micro-strains during summer and close to 35 micro-strains during winter. In all situations, no traces of bottom up cracking were observed (Sargand S. M. et al., 2006, Liao Y., 2007).

In addition to field perpetual pavement experiments, the Ohio State University runs an accelerated pavement testing (APT) facility. The facility consists of different types of pavement sections including perpetual pavements. In 2009, perpetual pavements sections of 16, 15, 14, and 13 inches thick were built at the APT facility. At an initial loading of 10,000 repetitions, strains less than 50 micro-strains were observed at the bottom of all sections (Hernandez J. A. 2010). By the end of 2012, three years after construction of the sections, the strains recorded were still below the design limit of 70 micro-strains.

3.4 Marquette Interchange

In continuing efforts to validate local materials and thickness designs for perpetual pavements, Wisconsin Department of Transportation sponsored a

research project of instrumented pavement section along I-43 to determine real time performance of perpetual pavements. The project, which in records is known as Marquette Interchange Instrumentation project, was built and completed before the end of the year 2008 under the supervision of the University of Wisconsin. The structure of the Perpetual Pavement section included 710mm foundation layers of different aggregate sizes followed by 330mm HMA layers on top (Table 3.1) (Hornyak, N. J. 2010).

Table 3.1 Marquette Perpetual Pavement thickness and materials breakdown

Description	Thickness (mm)	Nominal Max Aggregates. (mm)	Binder grade (PG)
SMA	50	12.5	70-28
E30	180	19	64-22
C2	100	19	64-22
Open graded aggregates.	100	N/A	N/A
Dense graded aggregates.	150	N/A	N/A
Selected crushed aggregates.	460	N/A	N/A

Immediately after construction, the University team of engineers began recording the pavement performance data and carry out associated analyses. The data collected includes strains at the bottom of HMA, earth pressure, pavement moisture, pavement temperature, traffic and other environmental data. Hornyak

N. J. (2010) reported that the field strains recorded during the first three years of testing never exceeded 16 micro-strains.

3.5 Kansas US 75 Perpetual Pavement Project

In 2005, Kansas Department of Transportation (KDOT) developed Perpetual Pavement designs for four sections that were constructed on US-75 highway near Sabetha, Kansas. The highway carried medium to high traffic volume at the time of construction. Moreover, it was estimated that at the end of 20 years of design life the pavement would accumulate 5.7 million ESALs per lane. The KDOT engineers adopted two different approaches to design the layers thicknesses of the sections. Sections 1, 2, and 3 were designed based on the Mechanistic ILLI-Pave algorithm. The algorithm assumes that during the lifetime of the pavement, flexural strain at the bottom of the pavement will never surpass 70 micro-strainsfatigue endurance limit as suggested by Monismith et al. (1972) and Carpenter et al. (2003). Section 4 was designed based on Empirical algorithms recommended in 1993 AASHTO Design Guide. The Empirical 1993 AASHTO Design Guide produced a relatively thicker HMA pavement than the Mechanistic ILLI-Pave algorithm (Table 3-2) (Portillo M., 2008).

Table 3-2 Perpetual Pavement sections designs

Section	1	2	3	4
Design Approach	ILLI-Pave algorithm			1993 AASHTO Design guide
Wearing Course	1.5 inches			
Binder Course	2.5 inches			
Base Course	9.0 inches	7.0 inches	9.0 inches	12.0 inches
Chemically Stabilized Embankment Soil	6.0 inches,			
Natural Sub-grade	High plasticity clay (A-7-6)		High plasticity clay (A-7-6)	

The Kansas US75 perpetual pavement project was design to meet the following objectives (Portillo, 2008):

- Validate the two Perpetual Pavement Concept approaches under local materials and environment. In this case, the strains developed at the bottom of *a much deeper section with a harder binder grade* (PG70-22) *at base layer* and strains developed at a *less deep sections with softer binder at base layer* (PG64-22) are checked against the fatigue endurance limit (FEL) recommended in literature.
- Use economic analysis to evaluate design alternatives. The sections costs and reliability are compared to determine the economic feasibility of the full-depth asphalt pavement design to the State of Kansas.

- Validate flexible pavement linear-elastic and viscoelastic models using field performance data. Horizontal strains at the bottom of the pavement developed due to known truck loading are measured and then compared to those computed with linear elastic and visco-elastic models for flexible pavement structures.

Out of the three objectives, the third goal required extensive laboratory investigations to determine material input parameters and to search for a model that better explain the behavior of flexible pavement materials. Initial attempts by Portillo (2008) showed that, Finite Element analyses with linear elastic models (e.g. Ever-stress) overestimated the computed strains, whereas the FE linear-visco-elastic models underestimated the strains.

3.5.1 Material characterization

Experiments to characterize materials for the Kansas US 75 perpetual pavement project were performed at Kansas State University Civil Engineering laboratory. Much of this work is reported in Portillo, M. (2008) master's thesis. In here, only relevant laboratory works are presented.

- Subgrade soil

Geotechnical engineers for the Kansas Department of Transportation (KDOT) identified two natural subgrade soils along the project location (labeled as soil A & B). The soils were both classified as high plasticity clay based on AASHTO soil classification and the Unified soil classification. Triaxial resilient

modulus tests were performed on the soils to determine their modulus. The results are given in Table 3.3.

Table 3-3: Subgrade Triaxial Resilient Modulus (MPa) Test Results

Relative Density (%)	Moisture Content (%)	Deviator Stress (kPa)				
		23.8	37.5	50.8	71.2	105.2
Soil A						
90	19	104.7	95.7	86.1	79.6	70.6
	21	100.6	89.4	81.2	71.2	70.2
	24	70.4	62.1	58.8	57.4	-
	27	80	64	50.1	45.7	-
95	19	128.2	115.3	109.1	103.6	93.6
	21	126.6	107.6	108.8	102	89.2
	24	127.2	116.5	101.3	88.9	68
	27	83.8	59.7	49.4	47.5	-
100	19	167.6	160	155.5	146.5	132.9
	21	155	140.5	130.8	114.2	92.4
	24	149.7	148.4	134.6	121.8	98.1
	27	93.3	78.7	58.5	45.9	-
Soil B						
90	17	113.7	107.1	97.2	88.8	69.3
	19	118.1	111.8	111.5	98.5	84.6
	22	94.9	88.8	77.7	66	54.3
	25	94.3	73.6	62.2	59.7	
95	17	206.2	167.1	163	143.5	121.8
	19	152.8	140.1	129.4	113.8	95.9
	22	141.6	122.8	105.7	92	70.8
	25	97.4	76.3	61.3	48.9	46.1
100	17	210.8	143.1	140.1	136.7	122.7
	19	149.1	143.1	128.9	116.2	101.1
	22	187	160.6	144.3	112	88.2
	25	94	70.6	58.5	46.5	48.5

- Lime stabilized subgrade

In order to avoid frost heaving and improve the strength of the weak plastic clay soil found on the project site, the KDOT Engineers proposed the lime stabilization of the top 6 inches of the existing subgrade soils. The soils were mixed in place with six percent lime. A portion of the lime-stabilized soils was

collected and properly packed to reserve the moisture before being transported to the Kansas State University laboratory for testing. In the lab, 6 inches tall by 3 inches diameter samples with density the same as in the field were prepared and placed in a moist room for curing.

After 7, 28, 60, and 90 days of curing, the samples were tested for Resilient Modulus using IPC UTM 25 machine. The average resilient modulus for soil A (7 samples) and B (6 samples) are presented in Table 3-4 and Figure 3-2. The soils show a reduction in modulus within two months of curing before rising up again as curing increased to 90 days. In the general, the stabilization process increased the subgrade modulus by two to three times.

Table 3-4 Resilient Modulus (MPa) of Lime Stabilized Soil

Curing Time (days)	Deviator Stress (kPa)	Mean resilient modulus (MPa)	
		Soil A	Soil B
7	23.8	330.7	265.2
	37.5	365.6	293.8
	50.8	400.6	326.1
	71.2	434.4	396.2
	105.2	468.5	443.5
28	23.8	233.8	215.2
	37.5	249.7	237.4
	50.8	264.4	260.3
	71.2	295.2	293.9
	105.2	343.2	334.2
60	23.8	191.8	162.8
	37.5	194.1	184.8
	50.8	194.5	186.3
	71.2	205.7	205.1
	105.2	225.2	230.4
90	23.8	243.7	206.3
	37.5	259.8	211.6
	50.8	318.6	220.9
	71.2	388.5	238.2
	105.2	539.9	251.1

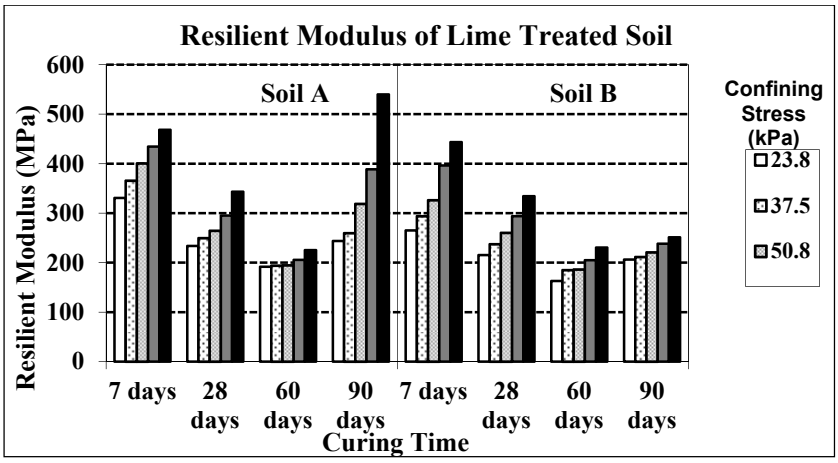

Figure 3-2 Average Resilient Modulus – Lime Treated Soils

- Hot Mix Asphalt

Figure 3-3 shows the HMA mixes placed on the four experimental sections. Five different mixes (denoted as S, M, 1, 3, and 4) designed to conform to Superpave Mix Design Guide were used.

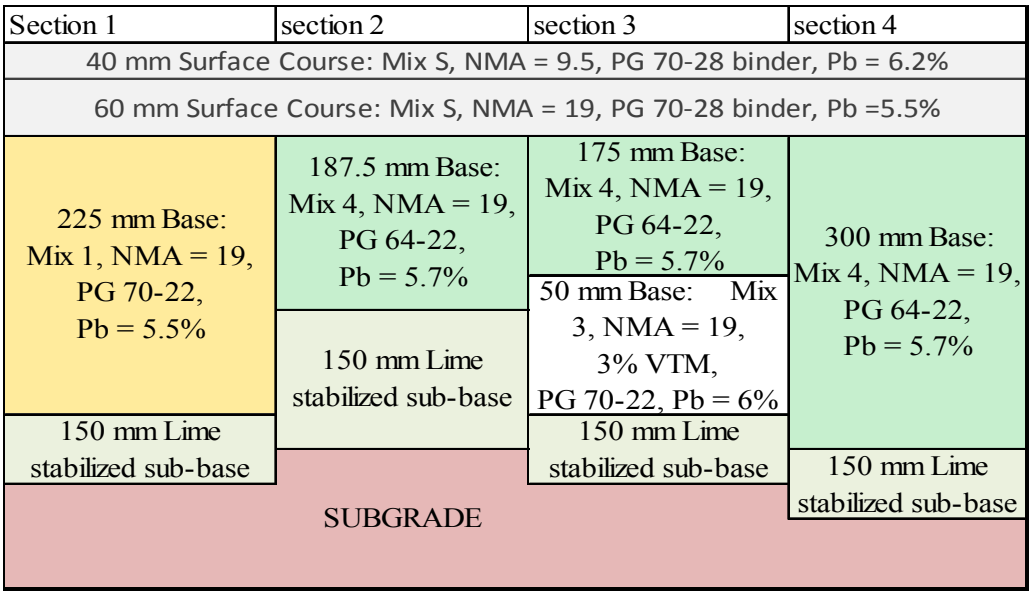

Figure 3-3 Configuration of Perpetual Pavements used in Kansas US 75 sections

The mixes were tested for dynamic modulus using IPC UTM 25 machine according to AASHTO TP 62 07. In this report, the dynamic moduli only for the mixes used in Section 1 are presented (Tables 3-5, 3-6 and 3-7). The rest of the dynamic modulus tests results are found in Portillo (2008).

Table 3-5 Dynamic Modulus Results for Mix S

Mix	Sample	Air Voids (%)	Temp. (°C)	Frequency					
				25	10	5	1	0.5	0.1
Dynamic Modulus (MPa)									
S	1	6.6	4	14,183	13,009	12,100	9,955	9,491	7,236
S	8	6.6	4	11,862	10,974	10,020	8,499	7,713	6,170
S	3	6.8	10	9,055	7,864	7,204	5,783	5,289	4,089
S	7	6.6	10	11,646	9,935	9,263	7,526	6,944	5,413
S	7	6.6	20	8,358	6,493	5,511	3,767	3,238	2,052
S	9	6.6	30	3,661	2,758	2,328	1,476	1,213	807
S	10	6.3	30	4,202	3,155	2,594	1,722	1,447	999
S	6	6.9	35	2,776	1,923	1,618	1,046	855	608
Phase Angle (degrees)									
S	1	6.6	4	5.35	5.88	9.96	12.05	15.5	17.9
S	8	6.6	4	5.88	7.75	9.64	12.82	16.39	18.84
S	3	6.8	10	8.38	11.21	13.3	16.86	21.33	27.37
S	7	6.6	10	9.19	8.99	11.93	15.22	18.92	23.64
S	5	6.7	20	16.53	19.66	22.52	25.97	31.7	32.51
S	7	6.6	20	14.69	16.45	19.97	24.4	29.97	33.28
S	9	6.6	30	19.51	21.71	24.75	28.13	34.45	33.84
S	10	6.3	30	21.16	23.56	26.14	28.95	35.63	34.33
S	6	6.9	35	23.56	24.8	26.73	27.91	33.27	30.45

Table 3-6 Dynamic Modulus Results for Mix M

Mix	Sample	Air Voids (%)	Temp. (°C)	Frequency					
				25	10	5	1	0.5	0.1
Dynamic Modulus (MPa)									
M	8	7.3	4	13,508	12,094	11,628	9,709	9,166	7,934
M	9	6.7	4	15,351	14,417	13,629	11,756	11,076	9,116
M	1	6.9	10	14,115	12,654	11,538	9,495	8,778	6,590
M	6	7.1	10	13,638	12,642	11,536	9,174	8,401	6,232
M	5	7	20	6,389	4,994	4,425	3,193	2,830	1,911
M	10	6.8	20	8,465	7,408	6,610	5,060	4,537	3,226
M	2	7.2	30	5,411	4,064	3,372	2,225	1,846	1,247
M	4	7.1	30	5,090	3,985	3,310	2,163	1,814	1,219
M	3	7.5	35	3,995	3,176	2,569	1,631	1,339	918
M	7	6.9	35	5,048	3,958	3,273	2,090	1,728	1,204

Table 3-6 continued

Mix	Sample	Air Voids (%)	Temp. (°C)	Frequency					
				25	10	5	1	0.5	0.1
Phase Angle (degrees)									
M	8	7.3	4	7.61	6.84	9.67	12.16	13.74	18.76
M	9	6.7	4	5.65	7.18	8.61	9.55	11.66	12.74
M	1	6.9	10	8.21	10.4	11.86	15.17	19.11	22
M	6	7.1	10	9.57	10.44	13.37	16.89	19.96	23.85
M	5	7	20	10.05	12.62	15.04	18.16	23.04	25.51
M	10	6.8	20	14.14	15.67	18.48	22.1	26.58	27.15
M	2	7.2	30	19.89	21.73	24.49	26.78	32.44	30.69
M	4	7.1	30	19.14	21.76	25.03	27.04	32.66	31.31
M	3	7.5	35	21.74	22.8	25.56	27.34	33.44	32.32
M	7	6.9	35	19.85	22.86	25.09	27.57	33.65	32.66

Table 3-7: Dynamic Modulus Results for Mix 1

Mix	Sample	Air Voids (%)	Temp. (°C)	Frequency					
				25	10	5	1	0.5	0.1
Dynamic Modulus (MPa)									
1	1	6.7	4	18,352	16,701	15,617	13,499	12,420	9,895
1	2	6.8	4	19,837	18,090	16,609	14,151	13,312	10,655
1	3	6.7	10	15,579	14,000	12,693	10,163	9,449	6,915
1	4	6.8	10	16,109	14,340	13,344	11,091	10,344	7,972
1	5	6.8	20	10,080	8,744	7,755	5,766	5,091	3,559
1	6	7.1	20	10,668	9,380	8,247	5,993	5,336	3,540
1	7	6.9	30	6,366	5,343	4,419	2,991	2,563	1,624
1	8	6.6	30	6,781	5,741	4,781	3,210	2,743	1,763
1	9	6.6	35	5,657	4,413	3,671	2,405	1,998	1,317
1	10	6.5	35	5,701	4,407	3,652	2,400	2,002	1,327
Phase Angle (degrees)									
1	1	6.7	4	5.8	6.12	8.19	12.24	13.61	16.32
1	2	6.8	4	6.2	6.78	9.43	12.03	13.77	16.58
1	3	6.7	10	7.2	9.91	13.2	15.54	19.83	23.44
1	4	6.8	10	6.5	9.06	10.99	14.01	16.68	20.22
1	5	6.8	20	12	14.01	16.75	21.7	27.29	33.42
1	6	7.1	20	13.7	15.85	18.38	23.09	28.11	34.4
1	7	6.9	30	16.8	20.34	23.91	27.72	35.01	37.33
1	8	6.6	30	16.99	20.44	23.67	28.1	35.15	37.71
1	9	6.6	35	19.85	22.32	25.37	29.07	36.14	36.54
1	10	6.5	35	19.79	22	24.5	27.27	33.48	32.39

This research is also reporting Master curves resulted from the dynamic modulus of materials used in Section 1(Figure 3-4, 3-5, 3-6). The Master curves

describe the time dependency of the mixes and are developed to obtain modulus of HMA at different levels of temperature and loading speed. They are constructed using the principle of time-temperature superposition, where dynamic modulus data obtained at different temperatures are shifted with respect to frequency until the curves merge into a single smooth function at reference temperature (Yin, 2007). The reference temperature used in this research is 20°C to reflect the temperature of the pavement during testing.

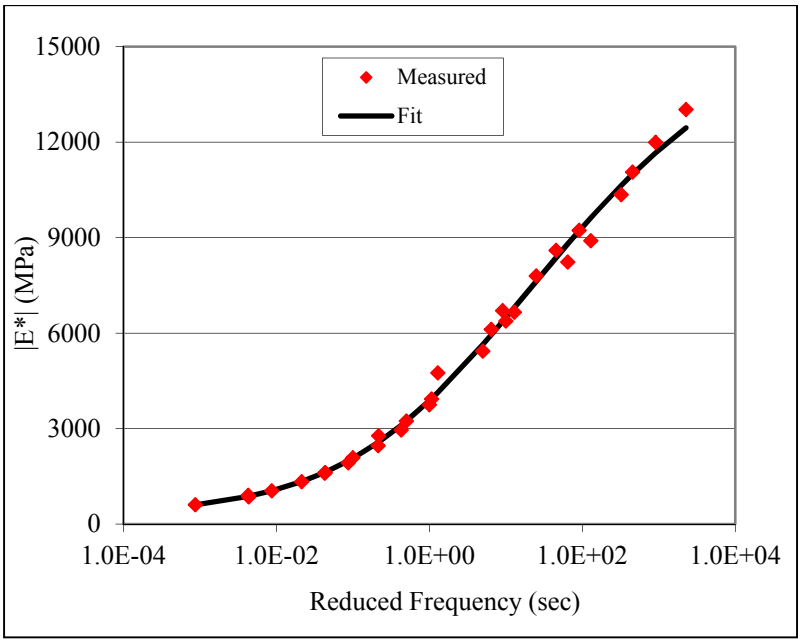

Figure 3-4 Dynamic Modulus Master Curve – Mix S

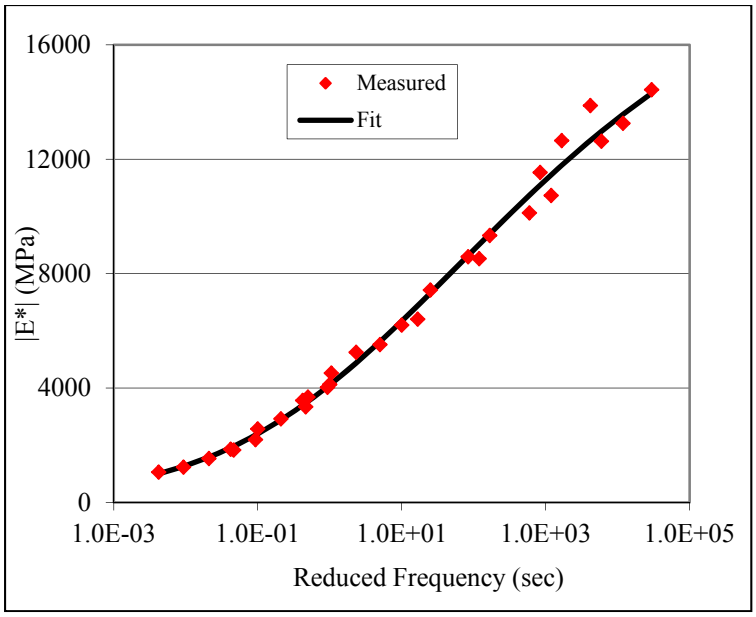

Figure 3-5 Dynamic Modulus Master Curve – Mix M

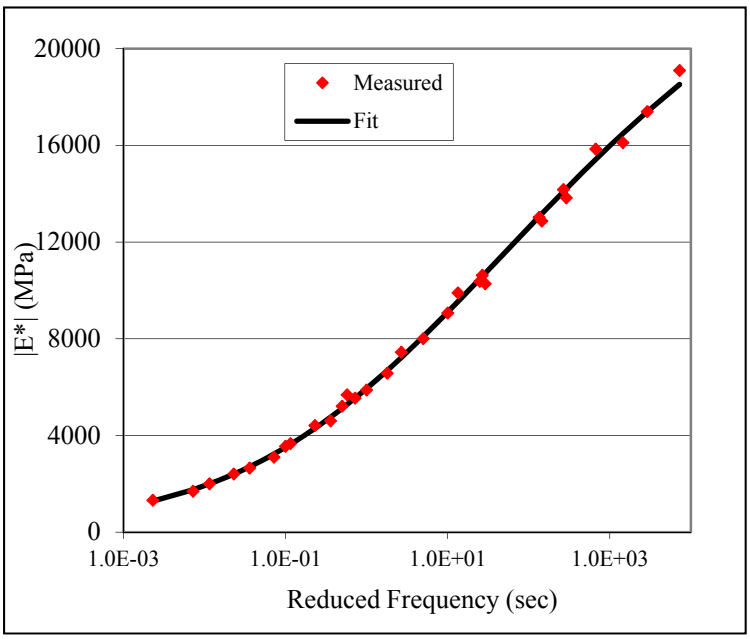

Figure 3-6 Dynamic Modulus Master Curve – Mix 1

3.5.2 Pavement section instrumentation

In order to record responses of the KS Perpetual Pavement sections, they were instrumented with gages at the bottom of the asphalt layers. A schematic diagram of the layout of the response measuring instrumentation is shown in Figure 3-7.

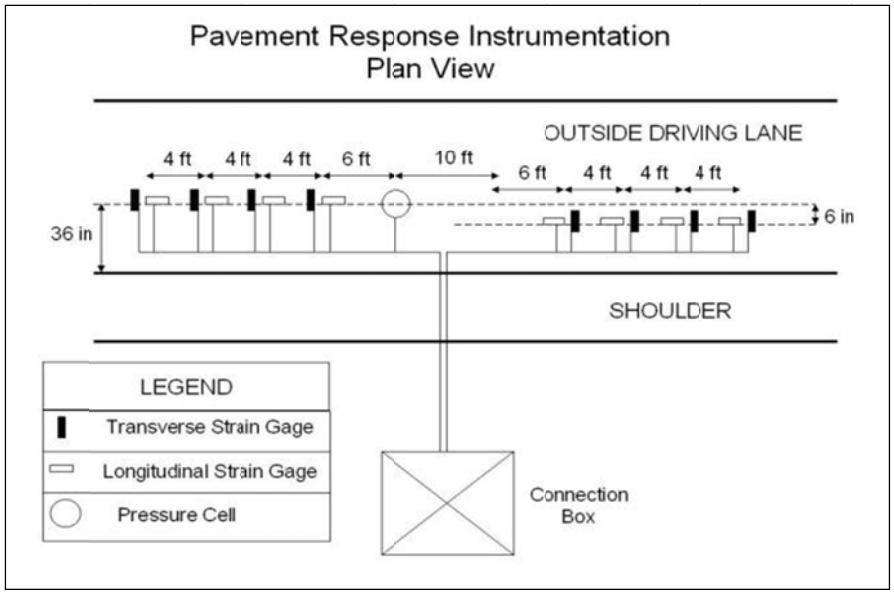

Figure 3-7 Plan view of instrumentation as installed in sections 1, 2, 4.

As seen in Figure 3-7, eight pairs of strain gages (model PML-120-2L) were placed to record strains developed at the bottom of the asphalt layers when a test truck passes on the experimental sections. Each pair consisted of two strain gages perpendicular to each other for recording transverse and longitudinal strains. Of the eight pairs of gages, four were placed in the outer wheel path while the remaining were placed 6 inches outside of the wheel path to record the strains

as a results of wheel wander. Aluminum bars were glued at each end of the gages to improve the bonding with the surrounding asphalt concrete (Figure 3-8).

Figure 3-8 Texas Measurement Gauges Model PML-120-2L

Figure 3-7 also shows the location of stress cell that used to record compressive stresses on top of the lime stabilized. As was for strain gages, the stress cell (Geokon type with stress range from 0-15 psi) was placed at the center of the estimated outside wheel path. A circular hole was dug on the surface of the compacted lime stabilized layer, and then filled with wet sand to offer a level and stable surface for laying the pressure cell perfectly flat (Figure 3-9).

Figure 3-9 Geokon Stress Cell

3.5.3 Testing vehicle

After the Perpetual Pavement sections were constructed, a dump truck with known dimensions and weight was brought to load the sections (Table 3-8). The truck driven over the sections at speeds of 20-25 mph, 40-45 mph, and 55-60 mph to investigate the effect of speed on the strains and stresses. For each speed, the truck drove five times on the sections to determine the variability in lateral position as result of wheel wander. In addition, two hoses connected to the acquisition system were placed on the pavement. The hoses were separated by a gap of 52.5 ft. (16m) to set an entry and exit position/time of the loading truck and thus estimate its speed.

Table 3-8 Dimensions and Weight of the Truck Tires (Miguel, 2008)

	Steering Front Left	Steering Front Right	Trailer Rear Left	Trailer Rear Right
Inflation pressure (psi)	90	96	101	97
Imprint Length (inches)	7.7	7.3	6	6
Imprint Width (inches)	8.25	8.25	8.9	8.9
Space between double tires (inches)	-	-	4.25	4.25
Wheel Load (lbs.)				
14-Jul-05	5,200	5,600	8,100	9,200
29-Sep-05	5,400	5,800	10,000	10,400
13-Apr-06	4,900	4,800	12,000	10,400
1-Aug-06	5,500	5,400	11,400	11,200
13-Oct-06	5,400	5,300	9,800	10,000
10-May-07	5,000	5,300	9,500	9,300
5-Oct-07	5,500	5,100	10,400	10,000

3.5.4 Field responses

Table 3.9 shows measured longitudinal and transverse strains developed at the bottom of Section 1. The pressure on top of the sub-base is also shown in the table. Temperatures corresponding to the date when field measurements were taken are presented in Table 3.10.

A general conclusion from Table 3.9 is that transverse response strains were significantly higher than longitudinal strains.

Table 3.9 Measured field-responses of section 1

Date	Nominal Speed (mph)	Long. Strain (μ-strain)		Trans. Strain (μ-strain)		Pressure (psi)	
		Min	Max	Min	Max	Min	Max
8/1/2006	20	37.00	75.40	71.00	106.80	3.62	4.21
	40	19.20	29.00	24.40	57.80	2.40	2.65
	60	18.40	26.80	29.00	58.00	2.03	2.10
10/13/2006	20	15.80	19.60	9.00	23.40	0.53	0.64
	40	8.20	10.40	12.00	17.60	0.41	0.44
	60	7.00	9.00	12.00	16.40	0.34	0.36
5/1/2007	20	21.00	30.20	18.00	42.80	2.16	2.29
	40	12.40	15.00	12.80	29.00	1.48	1.72
	60	12.60	14.20	16.40	30.40	1.25	1.42

Table 3.10 Section 1 - Pavement Layer Temperatures

Field Measurement Date	Temperature, ºC		
	Layer 1	Layer 2	Layer 3
08/01/2006	35.6	37.2	36.1
10/13/2006	16.1	13.3	10.6
05/01/2007	21.1	21.1	22.2

3.6 Summary

The projects reviewed in this chapter showed that typical strains under asphaltic layers of perpetual pavements are lower than 70 micro-strains, the endurance limit for asphalt concrete. However, well designed perpetual pavements can surpass this threshold and yet no bottom up cracks can occur (West, R., and Timm D.H., 2012). Furthermore, the chapter has presented an in-depth report on Kansas US 75 perpetual pavement to include layer characteristics, materials laboratory tests results, test truck characteristics (tires dimension and weight), and field responses. The parameters will be used in the verification of an FE-viscohyperelastic model to be developed in this research.

Chapter 4

Dynamic modulus tests

4.1 Introduction

This chapter presents laboratory-testing procedure for Hot Mix Asphalt (HMA) Compressive and Tensile dynamic moduli for specimen extracted parallel and perpendicular to the direction compaction. The tests were performed at the University of Texas-Arlington.

The Civil engineering laboratory at the University of Texas-Arlington (CELB) received cylindrical HMA specimens (4-inch. dia. x 6-inch deep) for dynamic modulus testing. The specimens were collected from several Asphalt plants in the state of New York. Table 4-1 shows the basic mix design information of the asphalt samples.

Table 4-1 HMA mix design information

Plant/Location	***Mix ID***	***Nominal Maximum Agregates (NMA)***	***RAP (%)***	***PG grade***	***Binder (%)***
BARRETT PAVING MATERIALS INC./ Richfield, NY.	0225	25	20	64-22	4.5
ROCHESTER ASPHALT MATERIAL / WalWorth, NY	0412	12.5	20	64-28	5.3
BLADES CONST. PRODUCTS/ Hornell, NY	0609	9.5	0	64-28	6.16
BLADES CONST. PRODUCTS/ Hornell, NY	0619	19	0	64-22	4.8
BARRETT PAVING MATERIALS INC./ Norwood, NY.	0712	12.5	20	64-22	5.2
COBLESKILL STONE PRODUCT/ Onetona, NY	0919	19	0	64-22	4.6
POSILICO MATERIALS/ Farmingdale, NY	1012	12.5	20	70-22	5.3
POSILICO MATERIALS/ Farmingdale, NY	1037	37.5	30	70-22	4.4
STAVOLA/ Old Bridge,NJ	1112	12.5	15	76-22	5.2

4.2 Sample preparation

Typical preparation of the 4-inch diameter dynamic modulus specimens follows the procedure stipulated in AASHTO TP 62-07. In summary, the preparation process is as follows.

- *Specimen compaction:* HMA Mixes are firstly heated in the oven at required temperatures then compacted with Super-pave Gyratory Compactor (SGC) to mold 6-inch diameter x 8-inch deep specimens (Figure 4-1).
- *Coring:* A 4-inch core is then extracted out of the 6-inch specimen.(Figure 4-2).
- *Sawing:* Lastly, the core ends are cut to get a 4-inch diameter x 6-inch deep specimen(Figure 4-3).

Figure 4-1 Compaction of HMA specimen using Super-pave Gyratory Compactor

Figure 4-2 Coring of HMA specimen

Figure 4-3 Trimming of HMA specimen ends using circular saw

The samples received from New York Asphalt plants were firstly tested for compressive and tensile dynamic modulus parallel to compaction. After the testing was completed, the samples were brought to a 2 inches coring cutter to extract samples perpendicular to the vertical axis (Figure 4-4a). The ends of the extracted samples were then cut square to form 2-inch diameter x 3-inch height

HMA cylindrical samples (Figure 4-4b). Figure 4-4c shows a finished 2-inch dia. x 3-inch height HMA specimens used in this research. These specimens were later used for measuring dynamic modulus perpendicular to the direction of compaction.

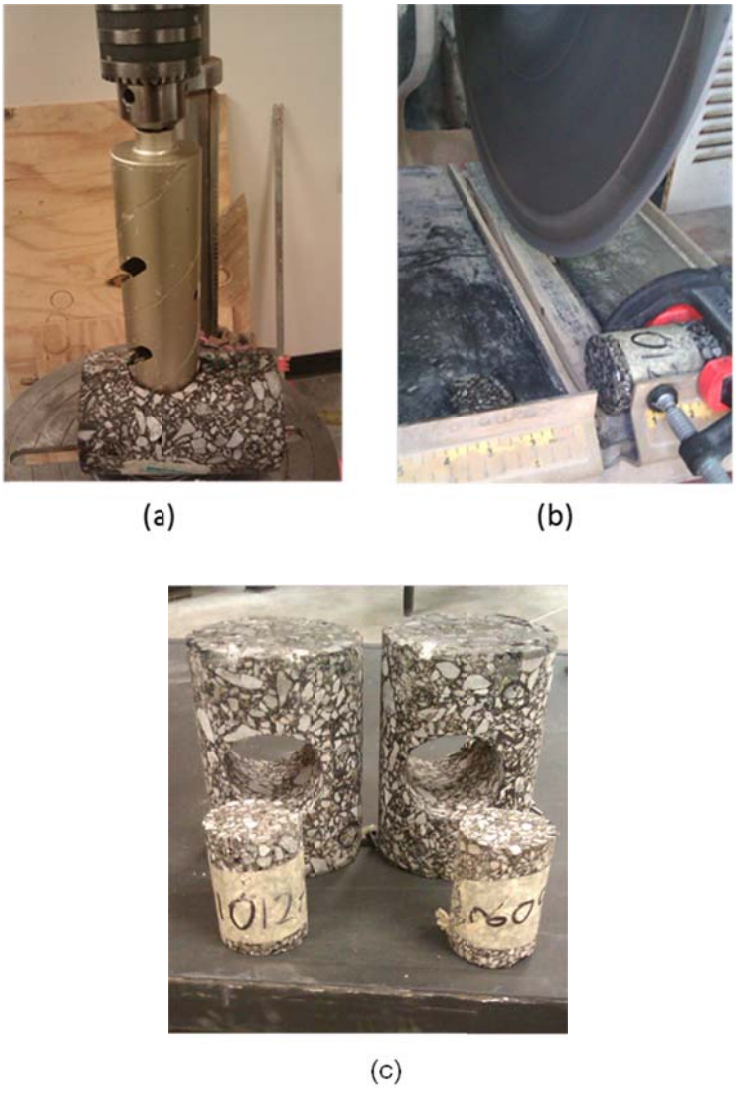

Figure 4-4 Preparation of 2-inch dia. x 3-inch deep HMA sample (a) coring by 2-inch dia. bit (b) cutting (c) extracted sample.

All samples tested required three lines of mounting screws (studs) spaced at 120^0 along the circumferential surface for fitting three LVDTs. Each line had two bolts glued with epoxy at a distance equal to designated gage length (4-inch for large sample and 2-inch for the small samples).The mounting screws together with L-shaped brackets and other hardware were used for holding three LVDT during testing (Figure 4-5).

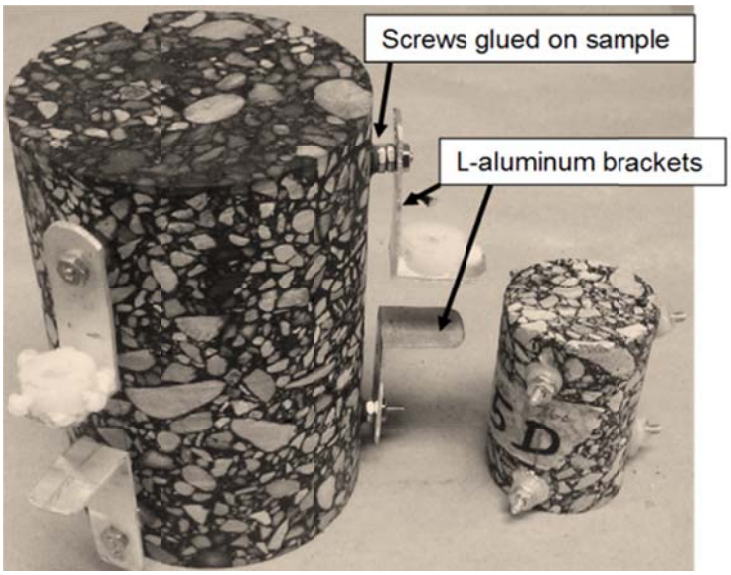

Figure 4-5 Attachments for LVDT mounting

4.3 Compressive Dynamic Modulus Test

The repeated compression dynamic modulus was performed in accordance with AASHTO TP 62-03 protocol. The test used the prepared 4-inch diameter HMA specimen placed in between two hardened steel disks. In between the steel disks and the sample, greased membranes were provided to reduce friction (Figure 4-6).

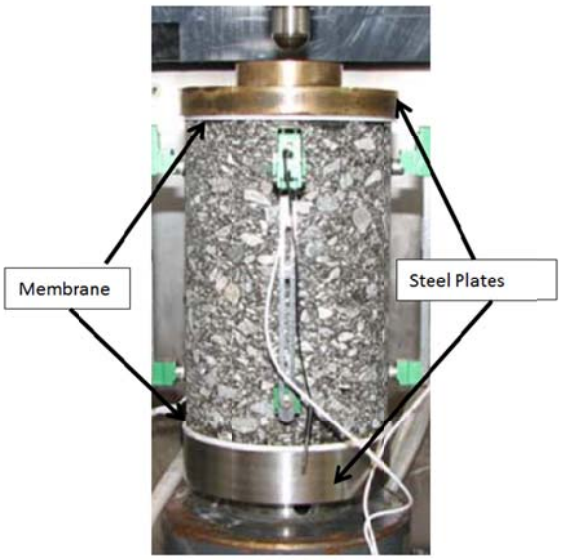

Figure 4-6 Specimen with top and bottom steel plate in position

4.3.1 Test set up

The test was set up on IPC UTM 25 hydraulic testing machine connected to a computer, which is equipped with easy-to-use software to run the dynamic modulus test. The machine is also equipped with a testing frame to conduct compressive dynamic modulus test.

Before placing a prepared sample onto the testing frame, the bottom base was adjusted to allow the loading actuator to work within its moving limits. Thereafter, a bottom disk was placed at the center of the frame followed by the sample and another disk on top. The setting up was complete when the LVDTs were in place and the actuator was lowered to touch the top disk. After the test was set up, sample dimensions and other identification information were inserted into the testing software.

The test was initiated a day after the sample reached the initial test temperature. This research performed the dynamic modulus test in compression at five different temperatures (4°, 10°, 20°, 30°, and 35°C) and six loading frequency (25, 10, 5, 1, 0.5 and 0.1Hz). The desired temperatures throughout the test were maintained by controlling the temperature in the environmental chamber (Figure 4-5). The loading was automatically controlled by the dynamic modulus software that runs the Control and Data Acquisition System (CDAS) and the hydraulic system (Figure 4-7).

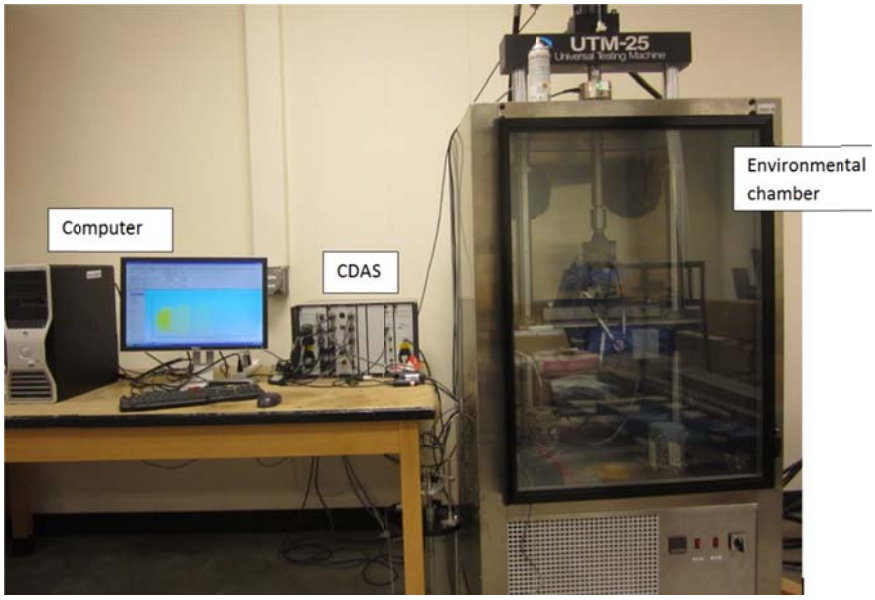

Figure 4-7 IPC UTM 25 Machine

According to AASHTO TP 62-03 protocol, the loading may be sinusoidal or haversine. This research used haversine loading with automatic 60 seconds rest period after every frequency (Figure 4.8). The resulting responses (dynamic

modulus, phase angle, stress, strains, etc.) calculated from the last 5 loading cycles were stored in the computer in the form ASCII text files which were further imported into Microsoft Excel for processing (Table 4.2).

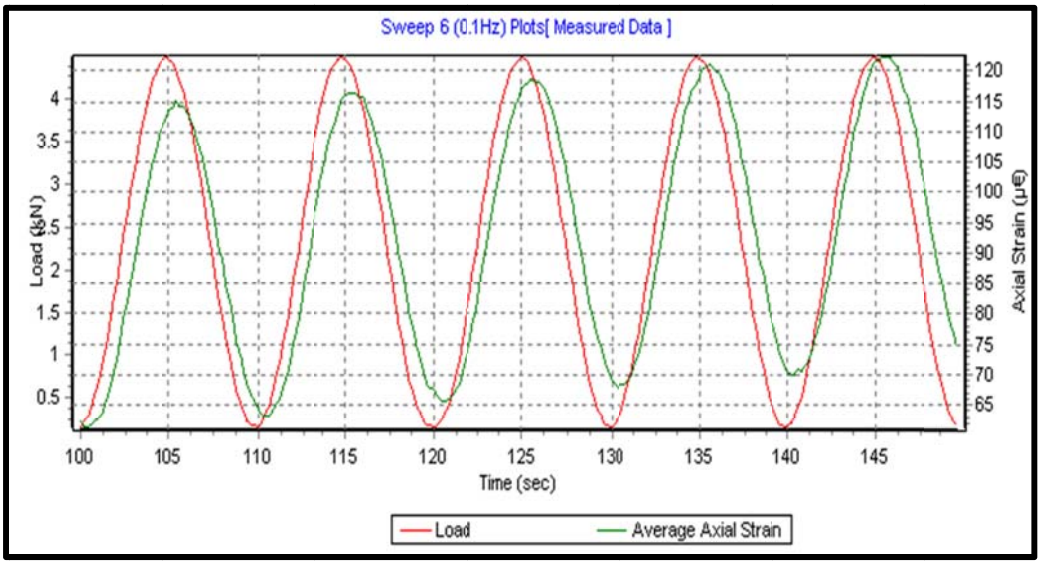

Figure 4-8 Samples of haversine load and corresponding strain waves

Table 4.2 Sample of responses from compression dynamic modulus test

	Pre-Cond	Sweep 1	Sweep 2	Sweep 3	Sweep 4	Sweep 5	Sweep 6
Frequency (Hz)	25	25	10	5	1	0.5	0.1
Cycle count	200	200	200	100	20	15	15
Dynamic modulus (MPa)	25888	24481	22363	20496	15941	14006	10264
Phase angle (Degrees)	23.38	17.66	17.27	17.64	20.18	17.47	14.84
Confinig pressure (kPa)	-0.5	0.1	0.1	-0.2	-0.4	-0.4	-0.4
Temperature (°C)	20.4	20.4	20.4	20.4	20.4	20.4	20.3
Stress magnitude (kPa)	202.9	235.4	294.8	303.9	284.6	288.7	269.7
Axial strain magnitude (με)	7.8	9.6	13.2	14.8	17.9	20.6	26.3
Permanent axial strain (με)	55.3	36	41.4	42.1	41.7	52.3	79.2
Stress standard error	5.6	6	5.1	5	4.1	3.9	3.7
Strain standard error	13.4	12.9	6.8	6.8	9.9	11.9	12.2
Strain uniformity coefficier	0	0	0	0	0	0	0
Phase uniformity coefficier	6.8	2.6	4.9	3.7	2.8	2.1	1.5

4.4 Tensile Dynamic Modulus Test (parallel to direction of compaction)

The Tensile Dynamic Modulus (parallel to the direction of compaction) was performed on the same IPC UTM 25 machine used for the compressive dynamic modulus test. However, user defined inputs and modifications on the testing frame were needed because there was no standardized protocol or designated software to run the test.

4.4.1Test set up

Since the test was performed in tension, additional components for holding the sample were required and modifications were done to the IPC UTM 25 testing frame (Figure 4-9). The components were attached to the sample by epoxy glue.

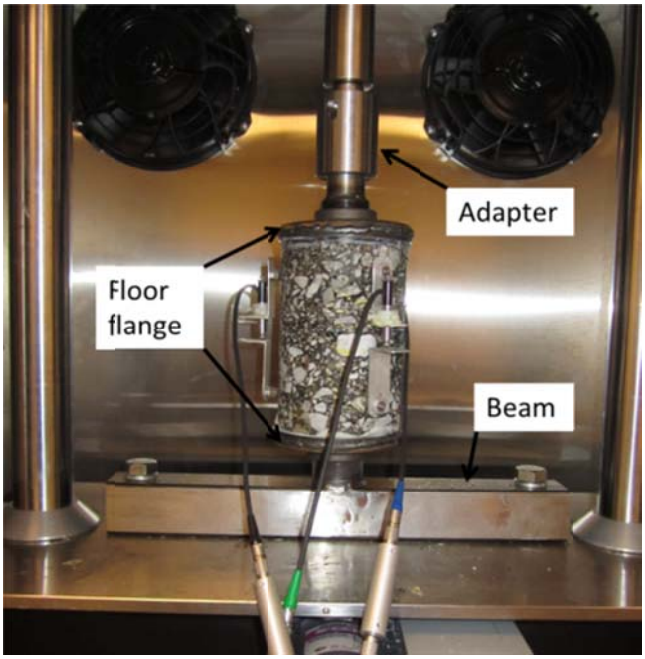

Figure 4.9 IPC UTM 25 testing frame with added components

i. Added components

The added components included a steel beam, a top and a bottom floor flange and steel connecting adopter. The following are the descriptions of each component.

- *2-inch x 2-inch x 15-inch bottom beam:* This was a tubular square steel beam with through holes at the two ends for securing it on the testing frame. The diameter of each hole was 1-inch, whereas the holding bolts were 5/8 inches to allow movements during centering of the test sample. At the center of the beam, an externally threaded short pipe was connected by welding (Figure 4-10) .

Figure 4-10 2-inch x 2-inch x 15-inch bottom beam

- *1-1/4-inch top and bottom floor flanges*: Floor flanges with steel disks welded on the surfaces were manufactured to uniformly distribute the load applied to the samples. The flanges came with internal thread on one end to offer easy connection with other parts of the frame (Figure 4-11).

Figure 4-11 1-1/4-inch Floor flange

- *Tension connecting adapter*: This was a solid steel piece with a dead hole on one end and a threaded rod extruding at the other opposite end. The hole at the end was deep and large enough to let the tip of the ram loosely fit. The function of this component was to connect the sample to the loading ram. (Figure 4-12).

Figure 4-12 Tension connecting adapter

ii. Gluing

In this research the samples tested in tension were connected to the testing frame components using a pretested two-part, high strength epoxy glue (Figure 4-13). The glue specifications are shown in Table 4-3.

Figure 4-13 High strength epoxy glue used in the tension test

Table 4-3: The epoxy glue specifications

Handling Time (Minutes)	Set Time	Cure time (Minutes)*	Strength (PSI)	Working Temp. Range (C)	Special Feature
5	10	60	2500	5^0– 93^0	blue dye indicator

**Curing time may vary depending upon the environment temperature. Lower temperatures require more curing time.*

Before applying glue, the specimen and floor flange surfaces were cleaned and dried to ensure good bonding. The glue was then applied uniformly on the surfaces using grooving tool (Figure 4-14).

Figure 4-14 Uniform spreading of epoxy glue on sample surface

Immediately after the application of glue, the specimens and the flanges were quickly put together and left to cure for about 20 hours. The glue joints, which were under-cured or perhaps not well cleaned could not withstand the extreme tension loads, hence de-bonded (Figure 4-15).

Figure 4-15: De-bonding due to improper gluing.

iii. Testing

Prior to applying cyclic loads to the samples, the environmental chamber was set to the desired temperature in accordance with AASHTO TP 62-03. The test was performed at four temperatures: 10°C, 20°C, 30°C and 35°C.

Immediately after attaining the desired temperature, the CDA and other components of the testing machine were switched on. Thereafter, a testing software was run to control the sinusoidal loading frequency and response strains of the samples during testing. This research used the "uniaxial stress-tension program to define the testing parameters, as there was no standardized tensile dynamic modulus program developed for the IPC UTM 25 machine. The uniaxial stress-tension test program has nine test blocks where user defined parameters can be specified. In this research, the following parameters were specified:

- *Loading wave shape*: The program has a library of different waveforms that can be. Typically, haversine and sinusoidal loading waves are preferred for dynamic modulus test. This research used sinusoidal waveform (see buffer 1) to apply loading cycles on the sample (Figure 4-16).

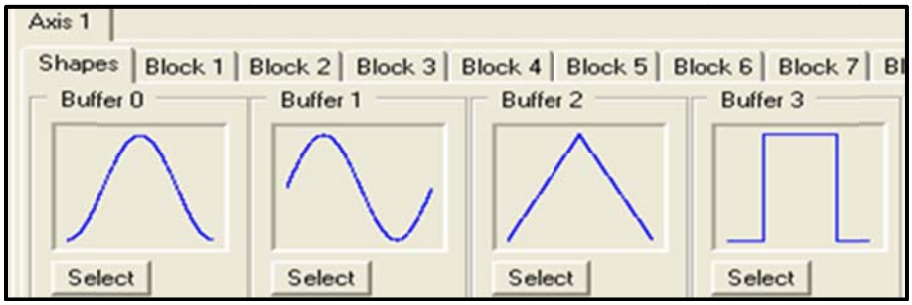

Figure 4-16 Sample of loading wave forms available in IPC stress-strain program.

- *Point of initial loading cycle*: Since this test was performed in tension only, an initial force that assures the specimen remained in tension throughout the loading cycles was established. Trial specimens were used to establish the base line for the applied loads while limiting strains below 1000 micro-strains (at strains ≥ 1500, the HMA specimen is considered to have failed). The magnitude of the applied load varied from 0.5kN to 2.5kN depending upon the stiffness of a sample. A ramp loading function was used to control the load from 0.0kN to the desired magnitude (i.e. -0.7kN) at a period of 1.0 second (Figure 4-17 and 4-18).

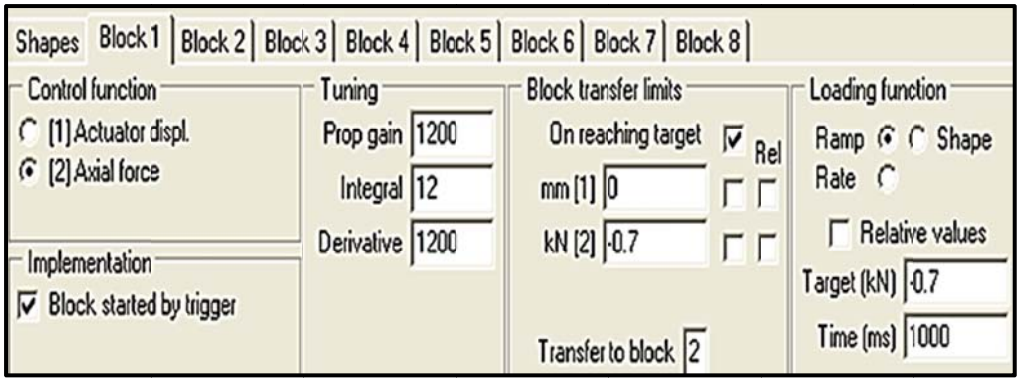

Figure 4-17: Setting up initial position of loading cycle

- *Frequency and number of cycles*: Loading times corresponding to frequencies of 25Hz, 10Hz, 5Hz and 1Hz were used in performing the tensile dynamic modulus test. The frequencies and associated parameters such as loading cycles, and amplitudes were inserted through block 2 to block 5 (Figure 4-15 and 4-16). In Figure 4-15 the loading time was entered in milliseconds.

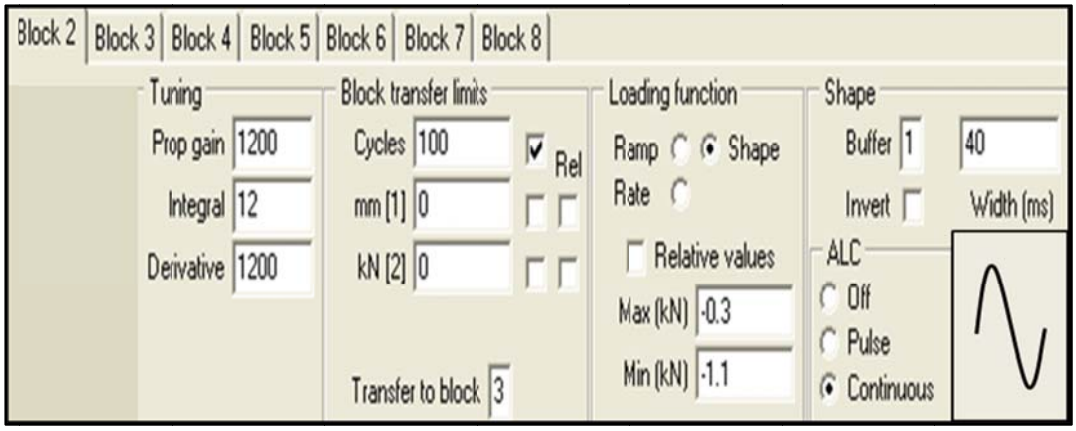

Figure 4-18 Setting up frequency and corresponding number of cycles

- *Ending of the test:* At the end of the loading cycle of the last frequency, the applied force was slowly reduced to zero (block 6) and the test was stopped (Figure 4-19).

During the testing process, proper operations were ensured by observing real time loading and strain response wave shapes on the computer screen. If unusual results were encountered during testing, the testing was immediately stopped and adjustment were made until good patterns were observed. Figure 4-16 shows an example of acceptable loading pattern where four loading frequencies can be clearly observed.

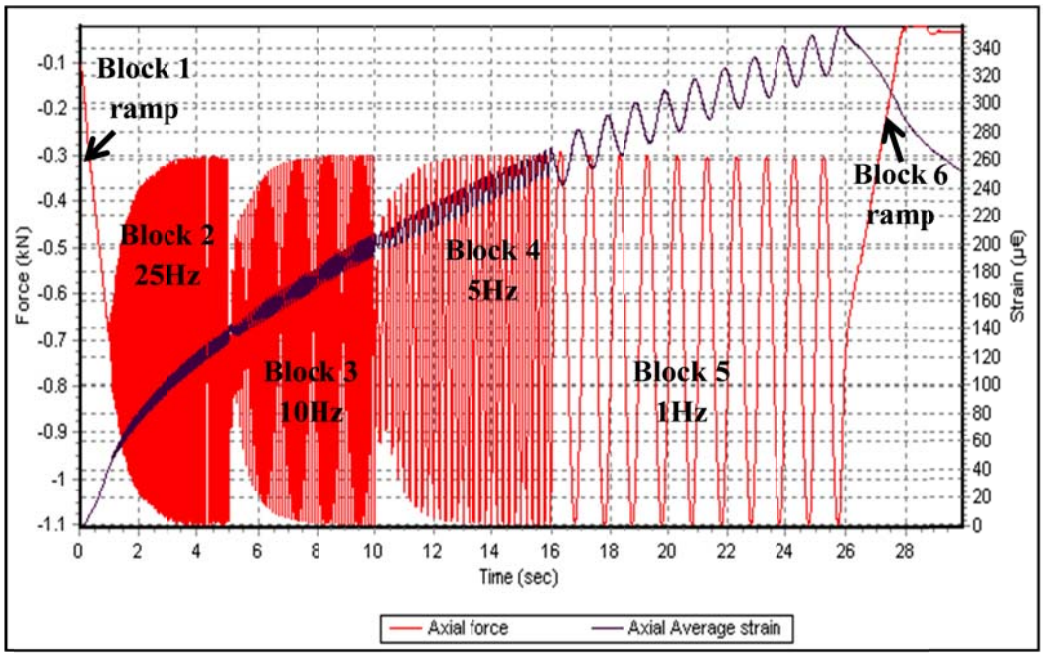

Figure 4-19 A sample plot showing implementation of continuously tensile dynamic loading on 4-inch HMA specimens

4.5 Tensile Dynamic Modulus Test-perpendicular to direction of compaction

Previous studies have shown that HMA materials behave differently in compression and tension. Moreover, flexible pavement experiences high tensile strains in the direction perpendicular to compaction. This research considered these facts by measuring the dynamic modulus of HMA in the direction perpendicular to the direction of compaction.

4.5.1 Test set up

As was for the previous test (section 4.3), additional components and high strength epoxy glue were used for connecting the sample to the UTM 25 testing frame. However, in this test, the components were smaller.

- *Bottom beam:* At first, the research planned to use a 1 inch x 2 inches tubular steel beam, but during preliminary testing the beam deflected too much. Though the deflection could not be seen by naked eyes, it was big enough to influence the measurements. In order to correct the errors, a 2.0 inch x 2 inch beam was used instead. This was the same beam used for the larger samples
- *Top and bottom floor flanges*: Two floor flanges of different sizes with proportional steel plates welded on them were used. A 1.25-inch floor flange was glued on top of the sample whereas a 0.25-inch floor flange was used at the top (Figure 4-20).

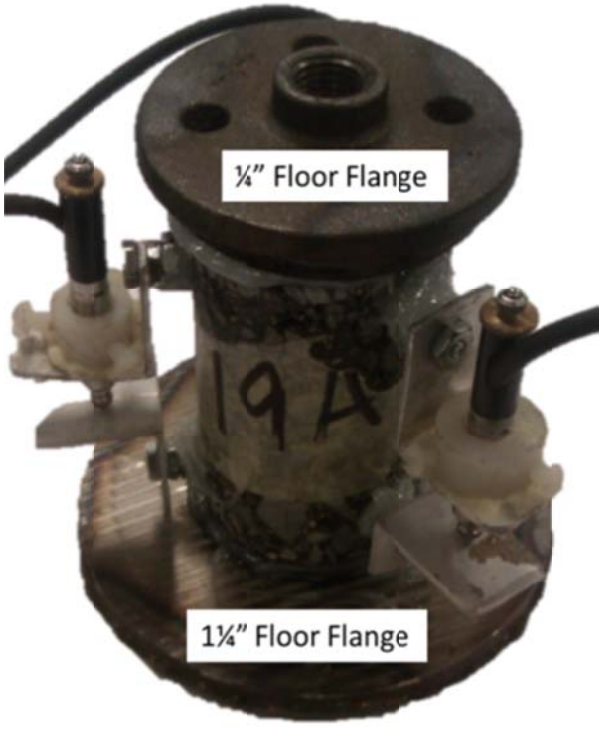

Figure 4-20 Small samples top and bottom floor flanges

- *Tension connecting adapter*: Except for the connecting bolt, the adapter used here had the shape similar to the one described in section 4.4. The connecting bolt was reduced to 1/4" diameter to fit into the 1/4" inch floor flange (Figure 4-21).

Figure 4-21 2-inch Tension connecting adapter

Each of the 2-inch HMA specimens was brought to the testing frame 20 hours after the flanges were glued on the surfaces. The specimen was placed at the center of loading actuator and fixed to it as straight as possible to reduce excessive stresses that would have occurred due to misalignment (Figure 4-22).

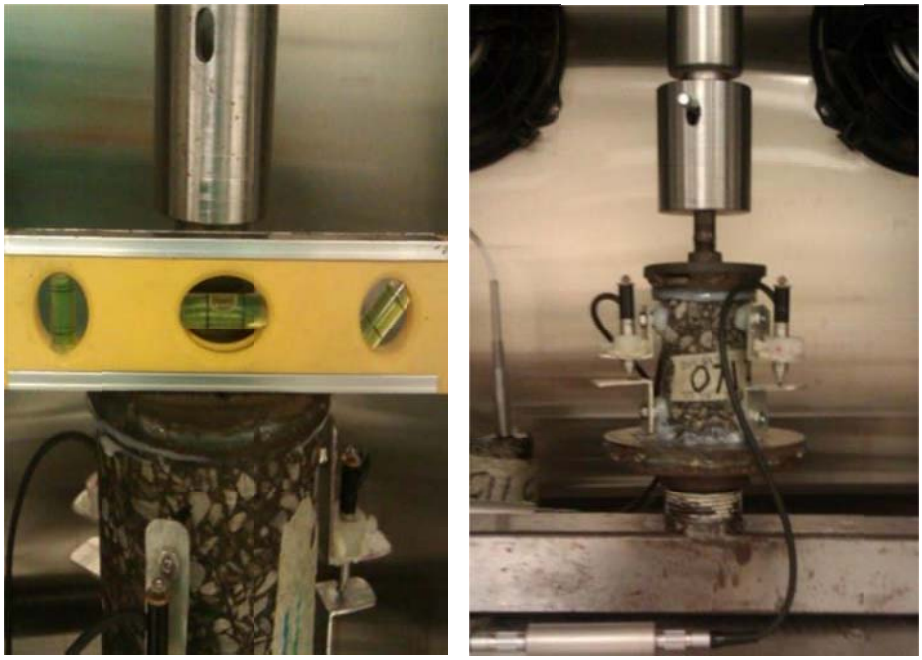

Figure 4-22: Fixing 2” HMA sample onto Testing frame

After properly setting the sample into the testing frame, the environmental chamber was turned on and set to the desired temperature. The dummy sample used in recording the core temperature was smaller to match up to the size of the tested samples.

The loading begun immediately after the set temperature as displayed by the computer reached the desired value. The stress-strain test software was used to control the tensile dynamic modulus test. Different blocks of the advanced load tab were used as the platform for defining the parameters of the dynamic modulus test; this time the applied dynamic force was significantly smaller. The applied maximum tension force ranged from -0.175kN to -0.5kN depending upon the stiffness of the sample and test temperature. Rest period of 5 minutes was applied

after every two loading frequencies. Typically long rest period like this are introduced between frequencies when the total cycles are above 200. At above 200 loading cycles , the sample may heat up and develop new characters that may affect the dynamic modulus. Total loading cycles for this test were less than 200; so technically there was no need for rest period. However, during preliminary testing it was determined that without rest period, small size samples could develop strains above the limit (1500 micro-strains) where results can still be meaningful. Therefore, the rest period was applied for this test. The rest period and other loading parameter applied for the test are shown in Table 4-4 and Figure 4-23.

Table 4-4 Loading parameters for tensile dynamic modulus of small samples

Loading Parameters			Description
Ramp Loading			Controls beginning and end of Test
	Block-1	Block-4	
Time (ms)	2000	2000	
Target (kN)	Range from -0.125 to -0.35	0	
Dynamic loading			1. Control loading waves for 25Hz and 10Hz frequencies 2. Amplitude magnitude depends on stiffness and temperature
	Block-2	Block-3	
Wave shape	Sinusoidal	Sinusoidal	
Frequency (Hz)	25	10	
Number of cycles	100	50	
Peak to peak amplitude (kN)	Range from 0.05 to 0.25	Range from 0.05 to 0.25	

Table 4-4 continued…..

Loading Parameters			Description
5 minutes Rest period and change parameters block 2 and 3			Healing period; stop test for 5 minutes (no enough blocks to implement auto rest).
Dynamic loading			1. Control loading waves for 5Hz and 1Hz frequencies 2. Amplitude magnitude depends on stiffness and temperature
Block	2	3	
Wave shape	Sinusoidal	Sinusoidal	
Frequency (Hz)	5	1	
Number of cycles	30	10	
Peak to peak amplitude (kN)	vary (0.05 to 0.25)	vary (0.05 to 0.25)	

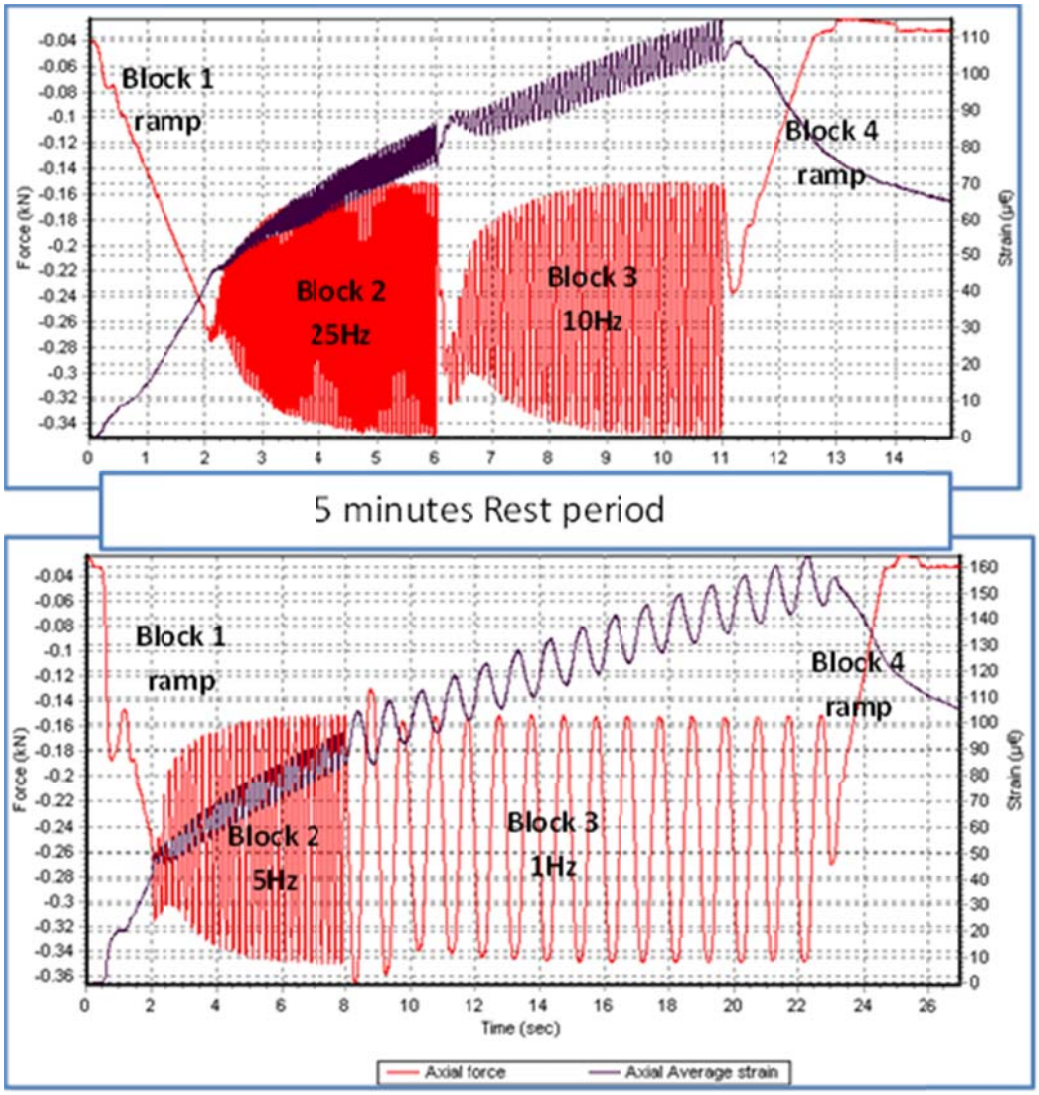

Figure 4-23: A sample plot showing implementation of tensile dynamic loading on small specimens

Chapter 5

Dynamic Modulus Tests Results and Comparison

5.1 Dynamic Modulus tests results

As expected, this research observed higher dynamic modulus at low temperatures and at higher loading frequencies in all of the three dynamic modulus tests performed (Compressive and Tensile Dynamic Modulus, parallel and perpendicular to the direction of compaction). This chapter presents the results from the three dynamic modulus tests. For each mix, at least two replicates specimens were tested.

5.1.1 Compressive dynamic Modulus (CDM)

The results of compressive dynamic modulus (CDM) are presented in Table 5-1. The table contains CDMs for individual samples and their averages to represent each of the mix tested. The CDM tests presents were performed at temperatures 10^{o}C, 20^{o}C, 30^{o}C and 35^{o}C.

Table 5-1: Compressive Dynamic Modulus

		Compressive Dynamic Modulus (Mpa)													
		Mix ID			Mix ID			Mix ID			Mix ID				
Freq. (Hz)	Temp. ^{0}C	0719A	0719B	Average	0225C	0225-D	Average	0419-A	0419-D	Average	1112A	1112B	1112C	1112D	Average
25	10	14,653	19,834	17,244	17,506	19,221	18,364	19,741	22,539	21,140	20,147	16,605	20,144	19,525	19,105
10	10	14,379	19,279	16,829	17,937	17,676	17,807	19,232	19,755	19,494	18,685	17,807	18,118	17,743	18,088
5	10	13,251	16,338	14,795	14,674	15,231	14,953	17,346	18,341	17,844	17,846	16,090	16,536	16,223	16,674
1	10	10,828	12,855	11,842	11,216	12,227	11,722	12,982	13,954	13,468	13,268	12,231	12,705	12,676	12,720
0.5	10	9,518	11,279	10,399	9,660	10,802	10,231	11,292	12,269	11,781	11,627	10,963	11,251	11,178	11,255
0.1	10	7,361	8,416	7,889	6,868	7,956	7,412	8,187	8,369	8,278	8,290	8,322	7,910	8,076	8,150
25	20	12,961	13,112	13,037	12,688	11,176	11,932	13,012	13,973	13,493	10,463	12,092	9,101	11,403	10,765
10	20	11,804	12,795	12,300	11,416	10,204	10,810	12,579	13,388	12,984	10,588	11,525	8,842	11,455	10,603
5	20	10,428	11,323	10,876	10,515	8,925	9,720	10,998	11,229	11,114	8,866	9,682	7,780	10,098	9,107
1	20	6,763	7,407	7,085	6,794	5,566	6,180	6,861	6,775	6,818	5,831	5,964	4,903	6,397	5,774
0.5	20	5,440	6,072	5,756	5,614	4,400	5,007	5,441	5,341	5,391	4,679	4,690	3,952	5,192	4,628
0.1	20	3,419	3,878	3,649	3,590	2,805	3,198	3,374	3,185	3,280	2,910	2,844	2,529	3,262	2,886
25	30	8,077	8,483	8,280	6,613	7,054	6,834	6,316	6,761	6,539	6,329	6,235	5,660	6,787	6,253
10	30	6,412	6,483	6,448	6,131	6,251	6,191	5,318	6,378	5,848	5,222	6,031	5,368	5,599	5,555
5	30	5,107	5,172	5,140	4,758	5,168	4,963	3,866	5,102	4,484	3,857	4,880	4,271	4,506	4,379
1	30	3,034	3,016	3,025	2,584	2,989	2,787	2,145	2,862	2,504	2,145	2,667	2,402	2,534	2,437
0.5	30	2,239	2,318	2,279	1,997	2,247	2,122	1,615	2,070	1,843	1,617	2,051	1,873	1,926	1,867
0.1	30	1,386	1,400	1,393	1,238	1,449	1,344	977	1,248	1,113	961	1,212	1,158	1,107	1,110
25	35	4,266	4,746	4,506	3,995	4,494	4,245	3,967	3,687	3,827	4,262	4,016	3,976	4,469	4,181
10	35	3,798	4,576	4,187	3,708	3,548	3,628	3,590	3,396	3,493	3,828	3,803	3,965	4,164	3,940
5	35	2,926	3,694	3,310	2,920	2,783	2,852	2,778	2,734	2,756	2,927	2,916	2,883	3,280	3,002
1	35	1,633	2,052	1,843	1,647	1,533	1,590	1,527	1,488	1,508	1,663	1,579	1,605	1,765	1,653
0.5	35	1,147	1,474	1,311	1,181	1,166	1,174	1,084	1,054	1,069	1,199	1,194	1,198	1,276	1,217
0.1	35	717	902	810	776	748	762	676	651	664	737	715	730	762	736

Table 5-1: Continued.

		Compressive Dynamic Modulus (Mpa)													
		Mix ID			Mix ID			Mix ID				Mix ID			
Freq. (Hz)	Temp. ^{0}C	0412-C	0412-D	Average	0619-A	0619-D	Average	1037-A	1037-C	1037-D	Average	0919-A	0919-B	0919-D	Average
25	10	20,933	17,550	19,242	15,050	14,099	14,575	28,081	30,472	17,600	25,384	16,123	19,948	18,404	18,158
10	10	20,898	17,778	19,338	14,504	13,313	13,909	28,736	33,705	17,374	26,605	15,982	17,955	19,068	17,668
5	10	18,659	15,963	17,311	13,987	12,488	13,238	27,198	32,025	16,706	25,310	14,848	16,404	17,534	16,262
1	10	14,767	12,769	13,768	11,204	9,634	10,419	23,177	27,461	14,925	21,854	11,919	12,782	12,883	12,528
0.5	10	13,036	11,398	12,217	9,871	8,545	9,208	21,340	25,558	14,038	20,312	10,692	11,489	11,093	11,091
0.1	10	9,617	8,663	9,140	7,586	6,604	7,095	17,147	20,434	11,941	16,507	8,189	8,680	7,993	8,287
25	20	11,101	11,688	11,395	15,069	11,680	13,375	21,677	24,481	12,209	19,456	10,694	11,594	12,504	11,597
10	20	11,754	11,471	11,613	14,236	11,077	12,657	21,379	22,363	12,683	18,808	10,446	10,915	10,756	10,706
5	20	10,834	9,972	10,403	11,141	9,655	10,398	18,941	20,496	11,494	16,977	8,974	9,859	9,166	9,333
1	20	7,284	6,657	6,971	6,690	6,249	6,470	14,423	15,941	9,046	13,137	5,989	6,458	5,771	6,073
0.5	20	6,214	5,593	5,904	5,250	5,109	5,180	12,609	14,006	8,026	11,547	4,947	5,249	4,594	4,930
0.1	20	4,469	3,843	4,156	3,157	3,281	3,219	9,176	10,264	6,132	8,524	3,072	3,379	2,770	3,074
25	30	7,368	8,453	7,911	6,020	5,516	5,768	23,084	16,170	11,468	16,907	5,612	7,025	6,580	6,406
10	30	6,571	7,684	7,128	5,561	5,665	5,613	19,680	14,470	10,519	14,890	5,349	6,729	5,626	5,901
5	30	5,199	6,313	5,756	4,484	4,789	4,637	16,181	12,636	9,505	12,774	4,360	5,496	4,448	4,768
1	30	2,976	3,538	3,257	2,741	2,674	2,708	10,327	8,562	6,888	8,592	2,425	3,119	2,526	2,690
0.5	30	2,238	2,625	2,432	2,080	2,113	2,097	8,241	7,147	5,644	7,011	1,792	2,279	1,821	1,964
0.1	30	1,309	1,585	1,447	1,337	1,317	1,327	5,404	4,727	4,002	4,711	1,005	1,352	1,093	1,150
25	35	4,205	5,028	4,617	4,221	4,035	4,128	10,768	11,569	6,601	9,646	3,667	4,152	3,850	3,890
10	35	4,572	4,370	4,471	3,637	4,049	3,843	10,519	11,328	7,755	9,867	3,419	3,994	3,390	3,601
5	35	3,247	3,365	3,306	2,830	3,264	3,047	9,921	9,939	6,197	8,686	2,627	3,098	2,678	2,801
1	35	1,766	1,847	1,807	1,611	1,876	1,744	6,011	6,135	4,008	5,385	1,429	1,673	1,433	1,512
0.5	35	1,290	1,322	1,306	1,257	1,369	1,313	4,756	4,925	3,251	4,311	987	1,180	1,069	1,079
0.1	35	759	801	780	809	852	831	2,921	3,177	2,073	2,724	601	730	660	664

Table 5-1: Continued.

		Compressive Dynamic Modulus (Mpa)											
		Mix ID			Mix ID			Mix ID			Mix ID		
Freq. (Hz)	Temp. ^{0}C	0212-A	0212-C	Average	0712-B	0712-D	Average	0609-B	0609-C	Average	1012-B	1012-C	Average
25	10	14,486	14,157	14,322	15,597	16,299	15,948	13,889	15,664	14,777	14,850	16,320	15,585
10	10	14,474	14,039	14,257	13,410	15,489	14,450	13,871	15,326	14,599	14,333	16,000	15,167
5	10	13,060	12,867	12,964	12,050	13,934	12,992	12,344	14,185	13,265	13,121	14,590	13,856
1	10	9,976	9,486	9,731	8,993	10,383	9,688	9,248	10,767	10,008	10,534	10,975	10,755
0.5	10	8,721	8,263	8,492	7,793	9,064	8,429	8,021	9,506	8,764	9,381	9,665	9,523
0.1	10	6,455	6,059	6,257	5,592	6,637	6,115	5,880	6,988	6,434	7,126	7,045	7,086
25	20	7,956	12,868	10,412	8,262	9,059	8,661	9,292	9,517	9,405	10,871	9,747	10,309
10	20	7,567	10,975	9,271	7,652	8,523	8,088	8,368	8,242	8,305	9,639	8,882	9,261
5	20	6,442	9,238	7,840	6,716	7,267	6,992	7,300	7,216	7,258	8,402	7,982	8,192
1	20	4,160	5,861	5,011	4,551	4,869	4,710	4,650	4,817	4,734	5,577	5,270	5,424
0.5	20	3,334	4,792	4,063	3,747	3,995	3,871	3,706	3,936	3,821	4,605	4,382	4,494
0.1	20	2,144	2,955	2,550	2,584	2,701	2,643	2,243	2,471	2,357	2,845	2,974	2,910
25	30	5,094	5,365	5,230	5,493	6,035	5,764	4,989	5,339	5,164	7,083	6,130	6,607
10	30	4,622	4,657	4,640	4,818	5,160	4,989	3,862	4,638	4,250	6,775	4,776	5,776
5	30	3,642	3,663	3,653	4,107	4,163	4,135	3,079	3,662	3,371	5,972	3,810	4,891
1	30	2,125	2,132	2,129	2,477	2,555	2,516	1,662	2,020	1,841	3,320	2,173	2,747
0.5	30	1,552	1,542	1,547	1,911	1,917	1,914	1,268	1,553	1,411	2,458	1,647	2,053
0.1	30	993	977	985	1,249	1,254	1,252	738	942	840	1,478	973	1,226
25	35	3,173	3,079	3,126	3,853	3,379	3,616	3,210	2,888	3,049	4,617	3,971	4,294
10	35	2,881	2,792	2,837	3,401	3,221	3,311	2,280	2,892	2,586	4,246	3,495	3,871
5	35	2,262	2,170	2,216	2,648	2,348	2,498	1,714	2,403	2,059	3,302	2,717	3,010
1	35	1,285	1,214	1,250	1,608	1,391	1,500	895	1,295	1,095	1,819	1,469	1,644
0.5	35	917	856	887	1,229	1,040	1,135	646	910	778	1,314	1,053	1,184
0.1	35	622	566	594	817	676	747	383	538	461	778	627	703

Figure 5-1, 5-2, 5,3 and 5-4 show the variation of compression dynamic modulus with change in loading frequency for all mixes at temperatures 10°C, 20°C, 30°C, and 35°C. The figures indicate that the dynamic modulus curve of mix 1037 is higher than all other mixes. This is because the mix contains highest aggregate size (NMA of 37.5 mm) and stiffer binder (PG 70). All other mixes have nominal maximum aggregate sizes ranging from 9.5 to 25mm and lower binder grade (PG 64). The combined relationship of average CDMs, frequency and temperature for individual mixes are given in Appendix A.

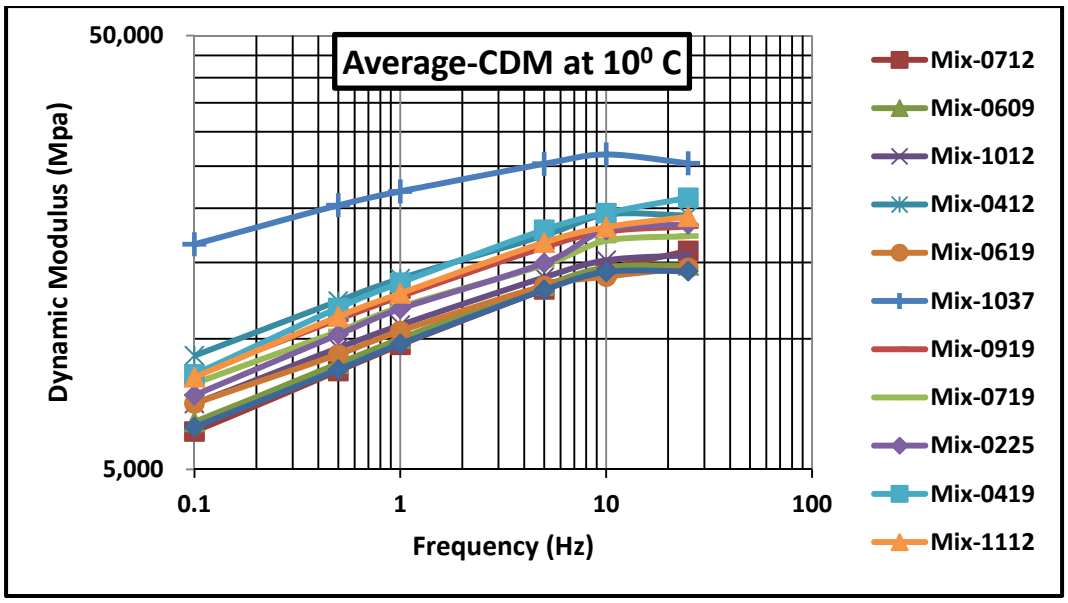

Figure 5-1 Compressive Dynamic Modulus vs Frequency at 10° C

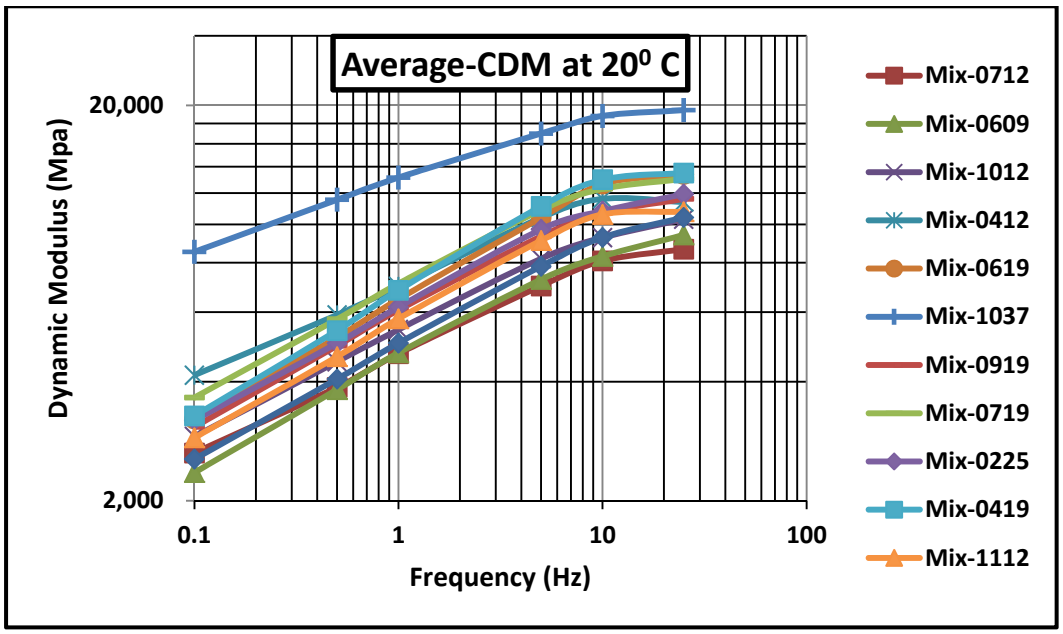

Figure 5-2 Compressive Dynamic Modulus vs Frequency at 20° C

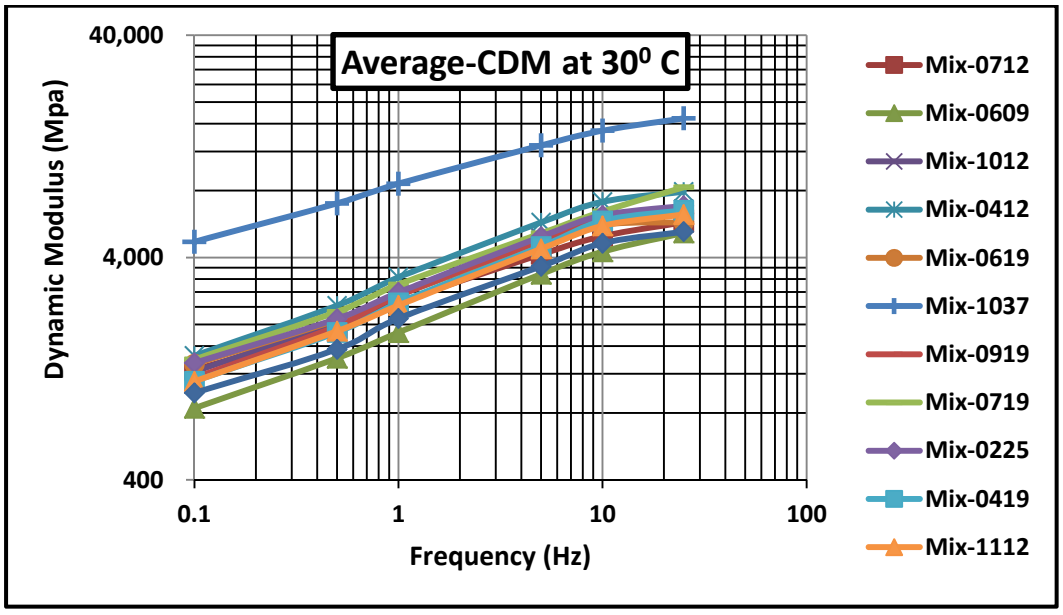

Figure 5-3 Compressive Dynamic Modulus vs Frequency at 30° C

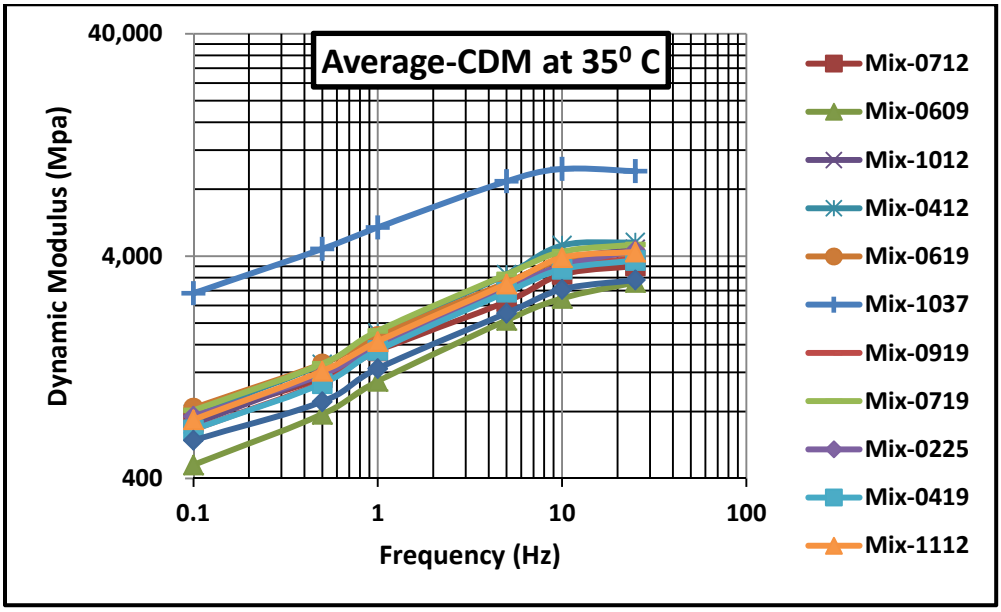

Figure 5-4 Compressive Dynamic Modulus vs Frequency at 35° C

5.1.2 Tensile Dynamic Modulus Perpendicular to Compaction (TDM ⊥)

The tensile dynamic modulus perpendicular to compaction (TDM⊥) for the tests performed at temperatures 10° C to 35° C and four load frequencies varying from 1Hz to 25Hz are given in Table 5-2.

Table 5-2 Tensile Dynamic Moduli Perpendicular to compaction

		Tensile Dynamic Modulus - Perpendicular to compression (Mpa)								
		Sample ID			**Sample ID**			**Sample ID**		
T ⁰C	**F Hz**	**0212B**	**0212C**	**Average**	**0225C**	**0225D**	**Average**	**0412C**	**0412D**	**Average**
10	25	12,229	19,133	**15,681**	16,651	20,343	**18,497**	19,415	21,451	**20,433**
	10	12,090	17,044	**14,567**	16,330	14,051	**15,191**	15,991	19,346	**17,668**
	5	9,955	10,925	**10,440**	15,756	14,025	**14,891**	14,051	18,754	**16,403**
	1	7,680	7,811	**7,746**	13,517	12,911	**13,214**	11,134	14,231	**12,683**

Table 5-2 Continued

		Sample ID			Sample ID			Sample ID		
T ^{0}C	**F Hz**	**0212B**	**0212C**	**Average**	**0225C**	**0225D**	**Average**	**0412C**	**0412D**	**Average**
20	25	6,158	7,815	**6,986**	11,090	14,219	**12,654**	12,877	13,918	**13,397**
	10	5,709	6,383	**6,046**	10,716	10,732	**10,724**	10,363	11,822	**11,093**
	5	4,550	5,508	**5,029**	9,813	10,297	**10,055**	8,980	10,279	**9,630**
	1	2,687	3,568	**3,127**	7,973	10,493	**9,233**	5,536	6,969	**6,252**
30	25	4,143	5,511	**4,827**	13,968	8,882	**11,425**	6,768	8,908	**7,838**
	10	3,021	3,838	**3,430**	8,521	6,477	**7,499**	4,925	6,196	**5,561**
	5	2,046	2,983	**2,515**	7,305	6,163	**6,734**	3,503	5,900	**4,702**
	1	861	1,347	**1,104**	4,488	4,048	**4,268**	1,915	3,117	**2,516**
35	25	2,376	2,808	**2,592**	7,752	6,310	**7,031**	5,379	6,729	**6,054**
	10	1,504	2,029	**1,766**	7,931	4,687	**6,309**	3,349	5,033	**4,191**
	5	1,010	1,362	**1,186**	7,334	3,765	**5,549**	2,090	3,567	**2,828**
	1	365	583	**474**	3,125	2,305	**2,715**	1,051	1,804	**1,428**
		Sample ID			**Sample ID**			**Sample ID**		
T ^{0}C	**F (Hz)**	**0419A**	**0419D**	**Average**		**0609C**	**Average**	**0619B**	**0619D**	**Average**
10	25	15,258	17,159	**16,208**		16,879	**16,879**	16,481	24,042	**20,262**
	10	13,549	16,314	**14,931**		15,095	**15,095**	15,985	22,500	**19,242**
	5	10,940	15,163	**13,051**		12,402	**12,402**	13,570	19,411	**16,490**
	1	10,500	10,262	**10,381**		9,780	**9,780**	11,572	14,022	**12,797**
20	25	9,118	11,833	**10,475**		12,186	**12,186**	9,702	12,118	**10,910**
	10	**SAMPLE FAILED**	9,906	**9,906**		10,234	**10,234**	8,337	11,352	**9,845**
	5		6,037	**6,037**		8,624	**8,624**	7,446	9,834	**8,640**
	1		3,768	**3,768**		5,011	**5,011**	4,804	6,561	**5,683**
30	25		4,309	**4,309**		10,478	**10,478**	6,829	7,183	**7,006**
	10		3,081	**3,081**		6,958	**6,958**	5,396	5,478	**5,437**
	5		2,270	**2,270**		2,506	**2,506**	3,407	4,159	**3,783**
	1		1,081	**1,081**		1,227	**1,227**	2,240	2,499	**2,369**
35	25		2,816	**2,816**		3,173	**3,173**	9,375	5,660	**7,517**
	10		1,928	**1,928**		2,381	**2,381**	5,027	4,283	**4,655**
	5		1,241	**1,241**		1,419	**1,419**	2,359	3,707	**3,033**
	1		569	**569**		617	**617**	1,352	1,820	**1,586**

Table 5-2 Continued

		Tensile Dynamic Modulus - Perpendicular to compression (Mpa)								
		Sample ID			Sample ID			Sample ID		
T ^{0}C	F Hz	0712B	0712D	Average	0719A	0719B	Average	0919A	0919B	Average
10	25	17,697	12,512	**15,105**	18,851	16,019	**17,435**	18,371	19,073	**18,722**
	10	16,205	11,917	**14,061**	18,294	14,891	**16,592**	17,761	18,544	**18,153**
	5	13,790	9,622	**11,706**	17,483	13,519	**15,501**	15,591	16,490	**16,041**
	1	10,766	7,216	**8,991**	13,937	10,833	**12,385**	13,280	12,493	**12,887**
20	25	10,818	7,838	**9,328**	16,895	10,500	**13,697**	34,118	14,402	**24,260**
	10	8,475	6,785	**7,630**	16,703	10,004	**13,353**	33,382	13,759	**23,571**
	5	6,893	4,588	**5,741**	13,588	8,773	**11,180**	12,467	11,018	**11,742**
	1	4,616	2,863	**3,739**	8,467	5,296	**6,882**	8,542	6,188	**7,365**
30	25	6,222	3,963	**5,092**	11,909	9,304	**10,607**	6,865	6,263	**6,564**
	10	4,809	2,902	**3,856**	8,963	7,401	**8,182**	5,912	4,855	**5,384**
	5	2,979	2,215	**2,597**	5,226	3,108	**4,167**	3,517	3,596	**3,556**
	1	1,733	1,174	**1,454**	2,416	1,976	**2,196**	1,702	1,587	**1,644**
35	25	3,513	2,936	**3,225**	8,303	4,571	**6,437**	6,418	5,329	**5,874**
	10	2,558	2,208	**2,383**	6,036	3,308	**4,672**	3,618	3,418	**3,518**
	5	1,811	1,533	**1,672**	2,654	2,886	**2,770**	2,223	2,232	**2,228**
	1	934	729	**831**	1,382	1,598	**1,490**	780	891	**836**
		Sample ID		Sample ID						
T ^{0}C	F Hz	1012B	Average	1037A		Average				
10	25	14,762	**14,762**	26,975		**26,975**				
	10	13,694	**13,694**	23,045		**23,045**				
	5	12,464	**12,464**	21,120		**21,120**				
	1	10,492	**10,492**	18,672		**18,672**				
20	25	10,063	**10,063**	13,108		**13,108**				
	10	9,182	**9,182**	10,785		**10,785**				
	5	7,353	**7,353**	9,647		**9,647**				
	1	4,638	**4,638**	7,447		**7,447**				
30	25	6,460	**6,460**	10,595		**10,595**				
	10	5,001	**5,001**	10,984		**10,984**				
	5	3,213	**3,213**	9,524		**9,524**				
	1	1,722	**1,722**	6,115		**6,115**				
35	25	5,063	**5,063**	14,855		**14,855**				
	10	3,415	**3,415**	16,526		**16,526**				
	5	2,088	**2,088**	7,077		**7,077**				
	1	927	**927**	3,143		**3,143**				

Figures 5-5 , 5-6, 5-7, and 5-8 show the variation of Tensile Dynamic Modulus with frequency at several temperatures for HMA samples extracted perpendicular to compaction.

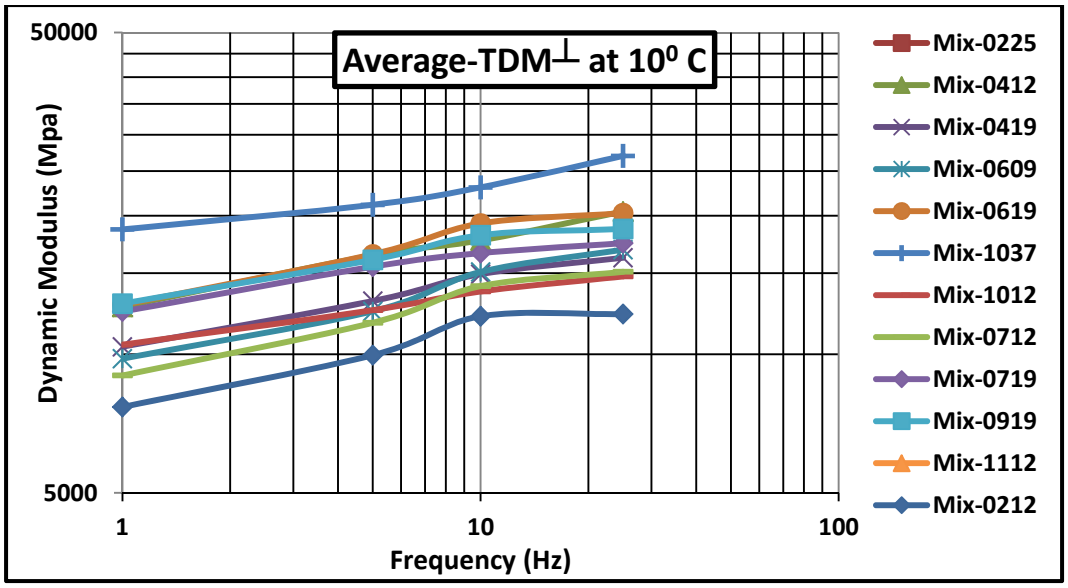

Figure 5-5 Tensile Dynamic Modulus (TDM⊥) vs Frequency at 10° C

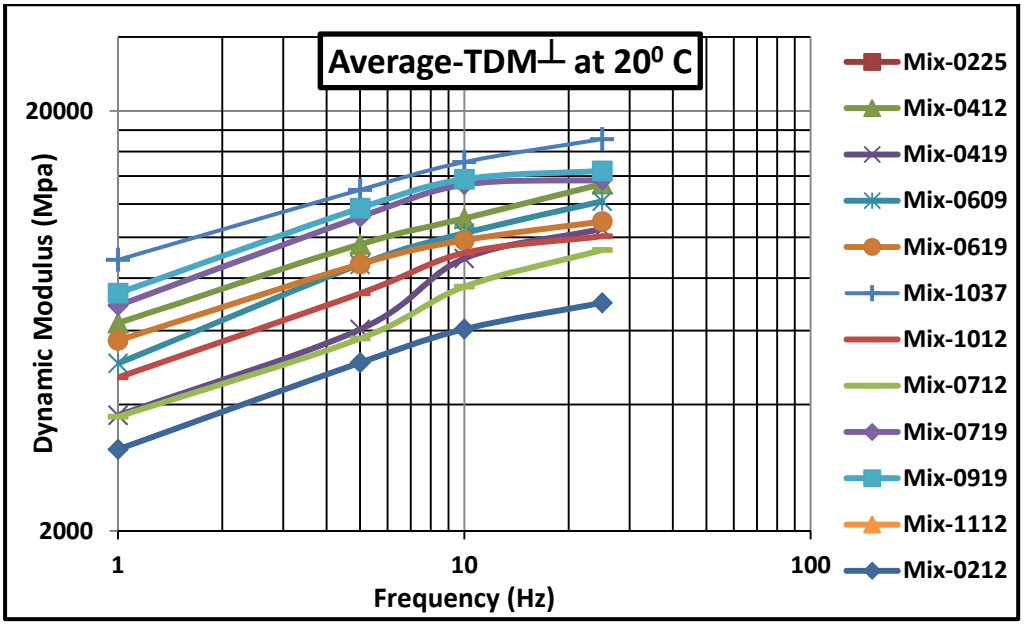

Figure 5-6 Tensile Dynamic Modulus (TDM⊥) vs Frequency at 20° C

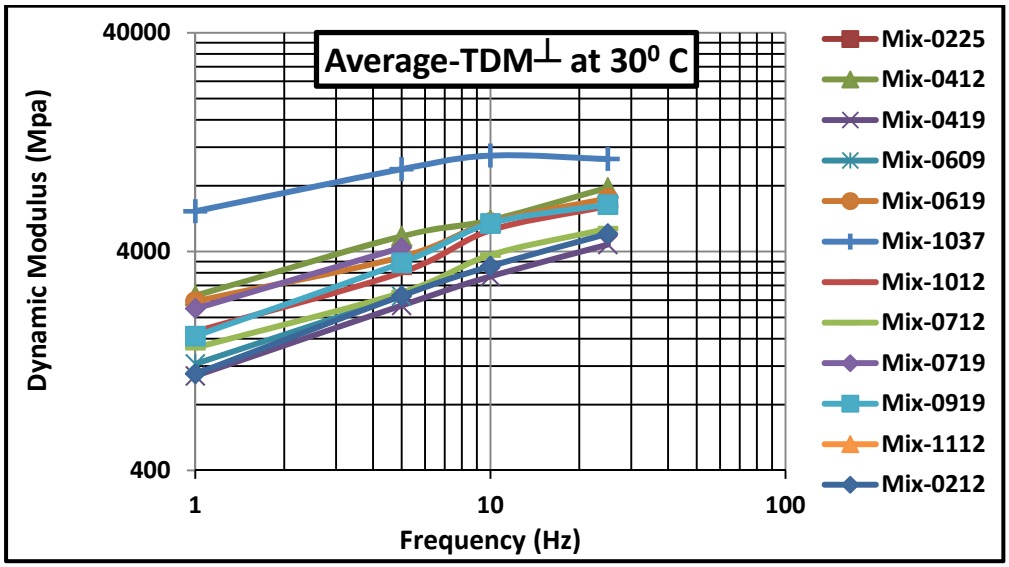

Figure 5-7 Tensile Dynamic Modulus (TDM⊥) vs Frequency at 30° C

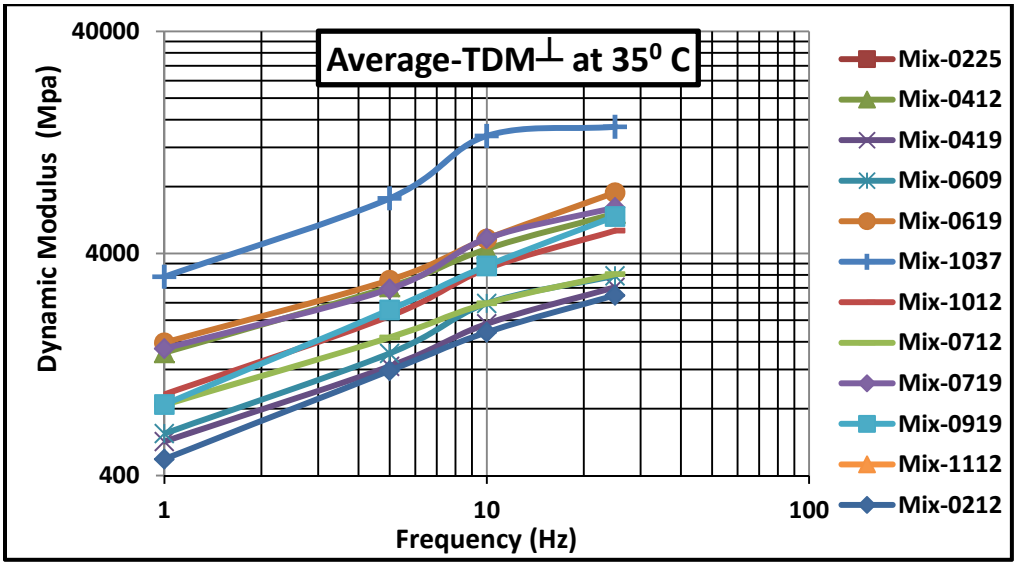

Figure 5-8 Tensile Dynamic Modulus (TDM⊥) vs Frequency at 35° C

5.1.3 Tensile Dynamic Modulus Parallel to Compaction (TDM II)

In this section, the results of the tensile dynamic modulus parallel to compaction (TDMII) are presented. The results are for the tests performed at temperatures 10°C to 35°C and frequencies varying from 1Hz to 25Hz, as shown in Table 5-3. Because of difficulties associated with axial tensile testing, such as test set up, and sample preparation, a few of the mixes did not exhibit good results at low temperatures and high frequency.

Table 5-3 Tensile Dynamic Moduli Parallel to compaction

		Tensile Dynamic Modulus II (Mpa)								
		Mix ID			Mix ID			Mix ID		
Freq. (Hz)	Temp. ^{0}C	0212B	0212C	Average	0225C	0225D	Average	0412C	0412D	Average
25	10	14,449	NA	14,449	13,700	17,643	15,672	18,635	18,972	18,803
10	10	11,709	NA	11,709	15,103	13,531	14,317	16,070	18,424	17,247
5	10	10,480	9,154	9,817	13,995	13,398	13,697	15,613	17,307	16,460
1	10	8,548	6,317	7,432	12,559	11,529	12,044	14,272	15,656	14,964
25	20	NA	NA	NA	NA	10,857	10,857	13,907	16,526	15,217
10	20	7,609	10,896	9,253	10,027	8,805	9,416	11,371	15,076	13,223
5	20	6,621	8,129	7,375	8,659	9,495	9,077	9,746	12,368	11,057
1	20	4,441	6,145	5,293	6,018	6,802	6,410	6,084	9,361	7,723
25	30	7,671	4,211	5,941	11,875	7,579	9,727	8,063	7,060	7,562
10	30	4,368	3,871	4,119	7,168	5,958	6,563	4,712	5,947	5,329
5	30	3,229	2,512	2,871	5,845	5,250	5,548	3,891	5,245	4,568
1	30	1,193	1,943	1,568	2,880	2,729	2,804	2,224	3,920	3,072
25	35	3,565	2,978	3,272	8,419	5,052	6,736	5,946	5,943	5,945
10	35	2,285	2,621	2,453	6,587	4,016	5,301	2,962	4,176	3,569
5	35	2,032	1,871	1,951	5,301	3,105	4,203	2,017	3,242	2,630
1	35	286	911	599	1,883	1,664	1,774	1,494	1,532	1,513
Freq. (Hz)	Temp. ^{0}C		0419D	Average	0609B	0609C	Average	0619B	0619D	Average
25	10		NA	NA	NA	NA	NA	NA	NA	NA
10	10		18,612	18,612	NA	NA	NA	13,640	NA	13,640
5	10		17,176	17,176	NA	NA	NA	13,337	NA	13,337
1	10		13,403	13,403	NA	NA	NA	11,193	NA	11,193
25	20		16,597	16,597	10,953	12,090	11,521	12,056	13,801	12,929
10	20		15,635	15,635	9,223	9,984	9,603	10,901	11,830	11,365
5	20		12,580	12,580	7,743	8,068	7,906	9,918	9,773	9,846
1	20		7,112	7,112	5,085	6,290	5,687	6,580	6,307	6,443
25	30		6,888	6,888	8,072	6,657	7,364	7,584	7,939	7,761
10	30		5,808	5,808	7,228	4,944	6,086	6,782	6,330	6,556
5	30		4,453	4,453	5,164	4,163	4,663	4,332	5,511	4,921
1	30		2,411	2,411	2,247	2,356	2,301	3,060	3,490	3,275
25	35		5,334	5,334	7,061	4,544	5,803	7,958	5,863	6,910
10	35		4,208	4,208	5,827	3,346	4,586	5,309	4,715	5,012
5	35		3,175	3,175	3,832	2,561	3,196	2,463	3,803	3,133
1	35		1,403	1,403	1,330	1,285	1,308	1,641	2,118	1,879

Table 5-3 Continued

		Tensile Dynamic Modulus II (Mpa)								
		Mix ID				Mix ID		Mix ID		
Freq. (Hz)	Temp. ^{0}C	1037A	1037D	Average		1012B	Average	0712B	0712D	Average
25	10	21,246	24,632	22,939		16,929	16,929	NA	15,073	15,073
10	10	16,049	23,933	19,991		15,856	15,856	16,201	14,479	15,340
5	10	14,761	21,898	18,329		15,790	15,790	14,429	13,369	13,899
1	10	14,198	18,745	16,471		14,200	14,200	11,981	10,938	11,460
25	20	13,484	22,433	17,959		13,495	13,495	NA	11,110	11,110
10	20	12,030	16,500	14,265		12,228	12,228	10,191	9,810	10,001
5	20	11,445	15,331	13,388		10,753	10,753	9,338	9,056	9,197
1	20	9,278	16,975	13,127		7,872	7,872	7,456	6,733	7,094
25	30		14,083	14,083		11,193	11,193	5,446	6,986	6,216
10	30	10,254	12,686	11,470		10,649	10,649	4,496	7,426	5,961
5	30	8,838	10,817	9,828		8,995	8,995	3,790	4,436	4,113
1	30	5,563	7,881	6,722		5,723	5,723	1,889	3,049	2,469
25	35	8,573	13,545	11,059		7,016	7,016	4,990	5,124	5,057
10	35	7,891	12,532	10,212		5,830	5,830	3,619	4,496	4,057
5	35	7,348	10,368	8,858		4,228	4,228	2,572	3,233	2,902
1	35	5,337	6,209	5,773		2,127	2,127	1,689	1,525	1,607
Freq. (Hz)	Temp. ^{0}C	0719A	0719B	Average	0919A	0919B	Average	1112B	1112D	Average
25	10	NA	NA	NA	18,663	N/A	18,663	NA	NA	NA
10	10	NA	14,324	14,324	15,141	16,898	16,020	NA	NA	NA
5	10	NA	13,846	13,846	14,160	16,502	15,331	NA	NA	NA
1	10	NA	13,433	13,433	12,444	14,887	13,665	NA	NA	NA
25	20	13,820	15,138	14,479	8,030	12,158	10,094	16,962	11,987	14,474
10	20	12,128	11,577	11,852	7,192	10,940	9,066	17,466	11,468	14,467
5	20	10,957	10,244	10,600	6,779	9,932	8,356	15,109	10,301	12,705
1	20	8,175	7,248	7,712	5,506	6,999	6,253	8,562	7,574	8,068
25	30	NA	9,734	9,734	7,707	7,790	7,748	8,853	8,157	8,505
10	30	6,274	6,230	6,252	5,866	7,359	6,613	6,414	7,336	6,875
5	30	4,824	5,368	5,096	5,529	6,512	6,020	4,231	6,351	5,291
1	30	2,734	3,258	2,996	3,270	3,348	3,309	2,742	3,709	3,226
25	35	3,595	6,957	5,276	4,789	7,013	5,901	5,777	5,772	5,775
10	35	3,387	4,894	4,141	4,045	5,232	4,638	4,714	4,894	4,804
5	35	2,518	4,355	3,437	3,389	3,792	3,591	2,974	4,077	3,525
1	35	1,385	2,081	1,733	1,653	2,269	1,961	1,683	2,137	1,910

The relationship between frequency and dynamic moduli parallel to compaction at temperatures 10°C, 20°C, 30°C, and 35°C are graphically presented in Figures 5-9, 5-10, 5-11 and 5-12. As was for the previous dynamic modulus tests the dynamic modulus iss increasing with frequency. Nevertheless, a few mixes did not follow this trend (e.g. Mix-1037 at 20°C). A thoroughly check on the calculations involved was performed and no error was detected. Therefore, this research concluded that the errors may be caused by sample preparation or setting up the samples during testing as mentioned earlier.

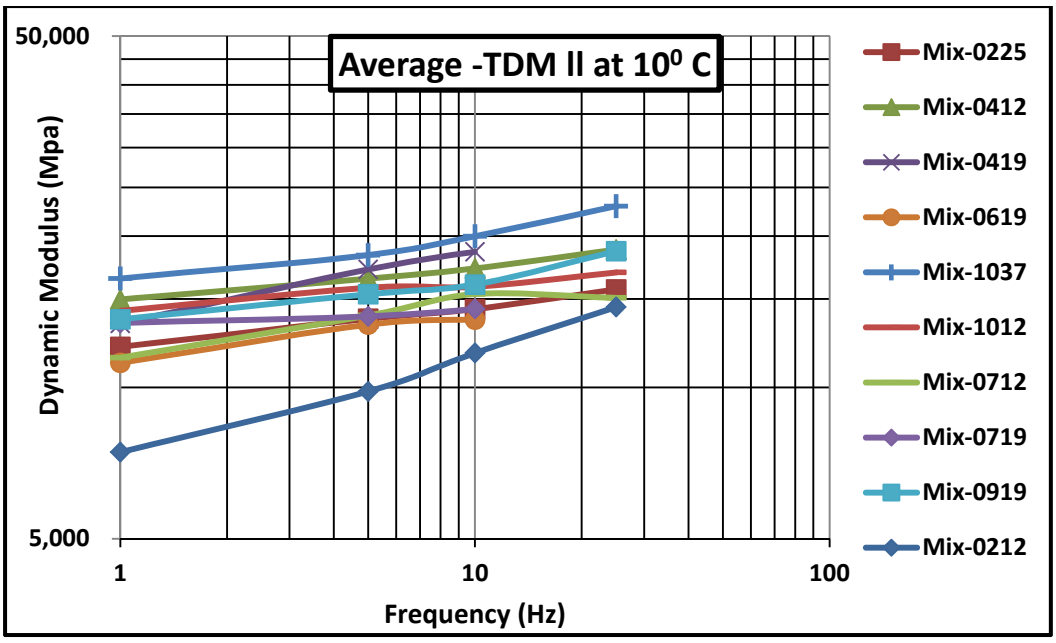

Figure 5-9 Tensile Dynamic Modulus (TDMll) vs Frequency at 10° C

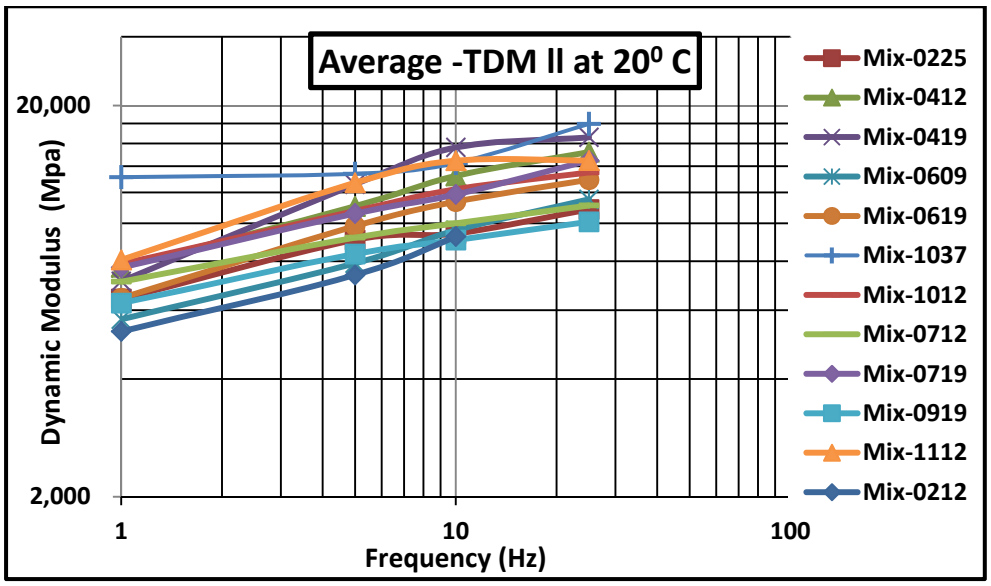

Figure 5-10 Tensile Dynamic Modulus (TDMll) vs Frequency at 20^{o} C

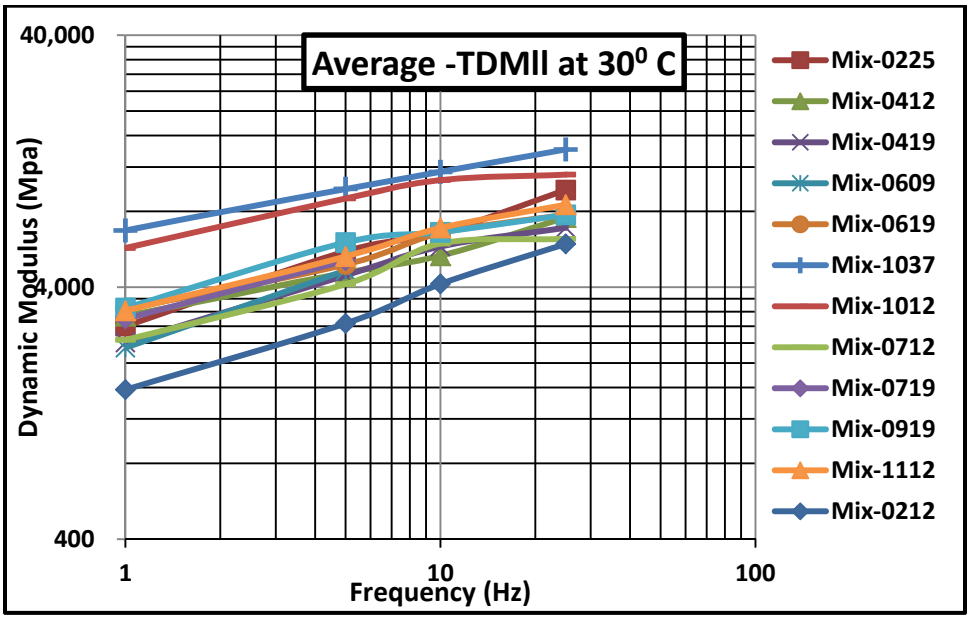

Figure 5-11 Tensile Dynamic Modulus (TDMll) vs Frequency at 30^{o} C

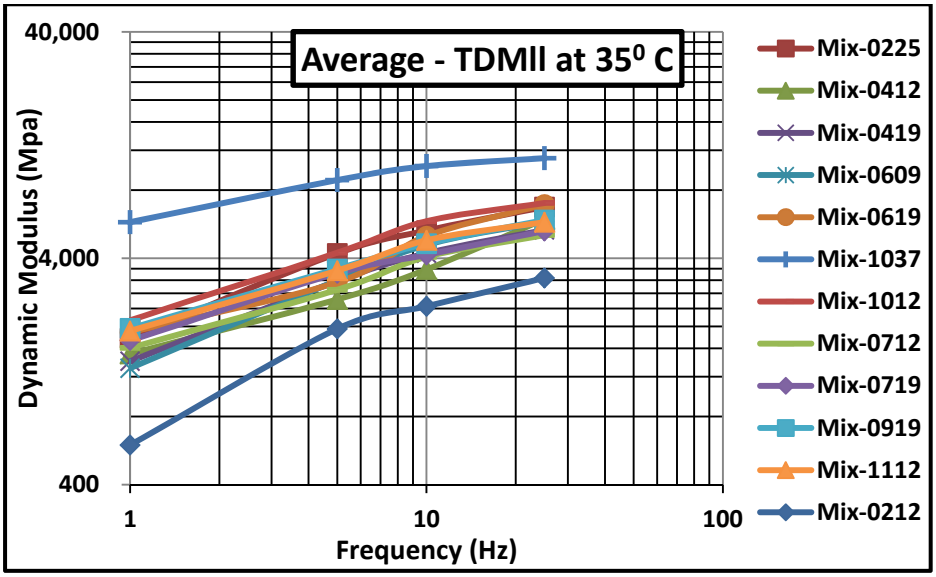

Figure 5-12 Tensile Dynamic Modulus (TDMll) vs Frequency at 35^{o} C

5.2 Determination of the relationship between Compressive and Tensile dynamic moduli of HMA

The Compression Dynamic Modulus (CDM) was compared with HMA Tensile Dynamic Modulus parallel to compaction (TDM$_{||}$) and Tensile Dynamic Modulus perpendicular to compaction (TDM$^{\perp}$). The data were compared and evaluated at each temperature level and for all temperatures combined. The first comparison aimed at determining relationship between the compressive and tensile behavior of HMA at each temperature; many previous researchers have used this approach to compare compression and tensile properties of HMA. Nevertheless, as will see later, this research found poor correlation between

compression and tension values especially at low temperatures. The second approach aimed at obtaining a single relationship that simplifies the determination of TDM from known CDM or vice versa.

5.2.1 Comparison: CDM versus TDM $^{\perp}$

In this section, the CDM was plotted against TDM $^{\perp}$ at temperatures 10^{o} C, 20^{o} C, 30^{o}C and 35^{o}C. The best-fit curves and their coefficient of determination (R^2) were computed for three different trend line equations (y = ax, y=ax+b, and y = ax^b). Of the three equations, the power equation (y = ax^b) produced the strongest R^2 at each temperature level. The power equation and R^2 at each temperature group are presented in Table 5-4. The results for the other equations are given in Appendix A.

Table 5-4 Statistical models relating TDM$^{\perp}$ and CDM at different temperatures

Temp. ^{o}C	Statistical Model	R²	Se
10	$TDM^{10\perp} = 2.6360 \times (CDM)^{0.8965}$	0.69	2222
20	$TDM^{20\perp} = 3.1978 \times (CDM)^{0.8566}$	0.60	2012
30	$TDM^{\perp 30} = 0.0754 \times (CDM)^{1.2791}$	0.82	1664
35	$TDM^{\perp 35} = 0.0099 \times (CDM)^{1.5519}$	0.89	1200

Based on this approach, the research concluded that strong correlation between CDM and TDM$^{\perp}$ exists at higher temperatures, whereas at low temperatures the correlation is not as strong.

As shown in Figure 5-13, the coefficient of determination (R^2) increased to 0.9071 when the results for all temperatures were combined. Based on this approach, the TDM may be determined using the following statistical model.

$$TDM^{\perp} = 0.2246 \times (CDM)^{1.1529} \quad \text{.....5-1}$$

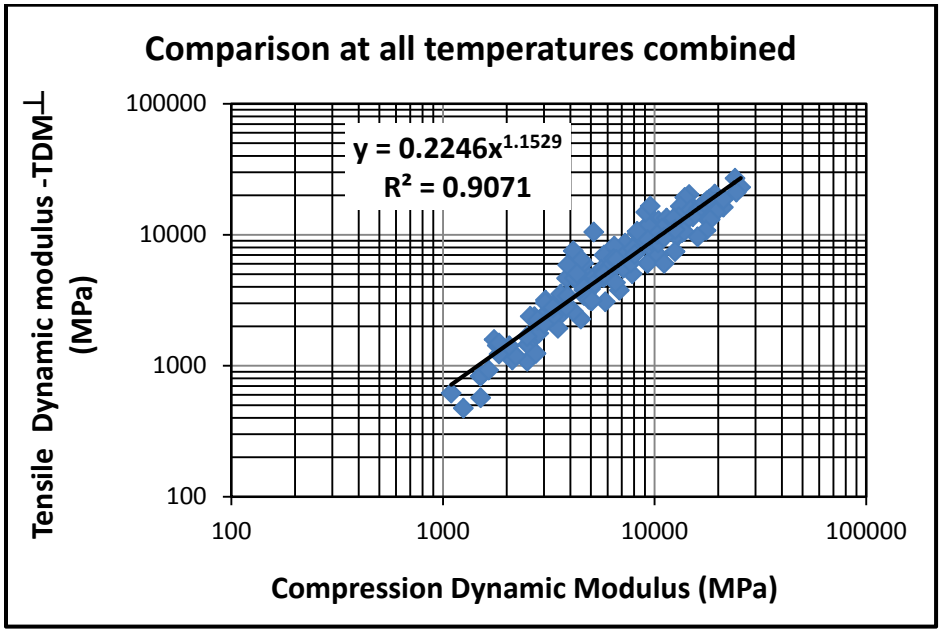

Figure 5-13 $TDM^{\perp}$ versusCDM for all temperatures combined

Table 5-5 shows the calculated Tensile Dynamic Moduli (TDM-calc) derived from the existing Compression Dynamic Moduli (CDM) using the equation 5-1. Measured TDM and CDM are also included in the table for comparison.

Table 5-5 Measured and Calculated Tensile Dynamic Modulus ($TDM^{\perp}$)

Measured		Calculated		Measured		Calculated	
CDM (Mpa)	$TDM^{\perp}$ (Mpa)	$TDM^{\perp}$ (Mpa)	CDM/TDM	CDM (Mpa)	$TDM^{\perp}$ (Mpa)	$TDM^{\perp}$ (Mpa)	CDM/TDM
25,540	23,045	27,070	0.9	6,992	5,741	6,079	1.2
24,366	21,120	25,640	1.0	6,971	6,252	6,058	1.2
24,036	26,975	25,241	1.0	6,818	3,768	5,905	1.2
21,193	18,672	21,831	1.0	6,607	6,460	5,694	1.2
21,140	16,208	21,768	1.0	6,539	4,309	5,627	1.2
19,494	14,931	19,825	1.0	6,470	5,683	5,559	1.2
19,338	17,668	19,643	1.0	6,448	8,182	5,537	1.2
19,242	20,433	19,530	1.0	6,406	6,564	5,495	1.2
18,345	13,108	18,485	1.0	6,073	7,365	5,167	1.2
18,158	18,722	18,268	1.0	5,901	5,384	5,000	1.2
17,844	13,051	17,904	1.0	5,848	3,081	4,948	1.2
17,668	18,153	17,701	1.0	5,776	5,001	4,877	1.2
17,523	10,785	17,533	1.0	5,768	7,006	4,870	1.2
17,311	16,403	17,289	1.0	5,764	5,092	4,866	1.2
17,244	17,435	17,211	1.0	5,756	4,702	4,858	1.2
16,829	16,592	16,735	1.0	5,613	5,437	4,719	1.2
16,262	16,041	16,087	1.0	5,424	4,638	4,536	1.2
15,995	9,647	15,783	1.0	5,230	4,827	4,349	1.2
15,948	15,105	15,729	1.0	5,164	10,478	4,287	1.2
15,585	14,762	15,317	1.0	5,140	4,167	4,263	1.2
15,167	13,694	14,844	1.0	5,072	3,143	4,198	1.2

Table 5-5 continued.

Measured		Calculated		Measured		Calculated	
CDM (Mpa)	TDM$^{\perp}$ (Mpa)	TDM$^{\perp}$ (Mpa)	CDM/TDM	CDM (Mpa)	TDM$^{\perp}$ (Mpa)	TDM$^{\perp}$ (Mpa)	CDM/TDM
14,795	15,501	14,425	1.0	5,011	3,127	4,140	1.2
14,777	16,879	14,405	1.0	4,989	3,856	4,120	1.2
14,599	15,095	14,205	1.0	4,891	3,213	4,026	1.2
14,575	20,262	14,178	1.0	4,768	3,556	3,910	1.2
14,450	14,061	14,038	1.0	4,734	5,011	3,877	1.2
14,322	15,681	13,895	1.0	4,710	3,739	3,855	1.2
14,257	14,567	13,822	1.0	4,640	3,430	3,789	1.2
13,909	19,242	13,434	1.0	4,637	3,783	3,786	1.2
13,856	12,464	13,375	1.0	4,617	6,054	3,767	1.2
13,819	10,595	13,334	1.0	4,506	6,437	3,663	1.2
13,768	12,683	13,277	1.0	4,484	2,270	3,643	1.2
13,493	10,475	12,972	1.0	4,471	4,191	3,630	1.2
13,468	10,381	12,944	1.0	4,294	5,063	3,465	1.2
13,375	10,910	12,841	1.0	4,250	6,958	3,424	1.2
13,265	12,402	12,719	1.0	4,187	4,672	3,366	1.2
13,238	16,490	12,689	1.0	4,135	2,597	3,318	1.2
13,037	13,697	12,467	1.0	4,128	7,517	3,311	1.2
12,992	11,706	12,418	1.0	3,890	5,874	3,092	1.3
12,984	9,906	12,409	1.0	3,871	3,415	3,074	1.3
12,964	10,440	12,387	1.0	3,843	4,655	3,049	1.3
12,657	9,845	12,049	1.1	3,827	2,816	3,035	1.3
12,528	12,887	11,909	1.1	3,653	2,515	2,876	1.3
12,495	10,984	11,872	1.1	3,616	3,225	2,842	1.3
12,494	7,447	11,871	1.1	3,601	3,518	2,829	1.3
12,300	13,353	11,658	1.1	3,493	1,928	2,731	1.3
11,842	12,385	11,159	1.1	3,371	2,506	2,621	1.3
11,613	11,093	10,911	1.1	3,311	2,383	2,568	1.3
11,395	13,397	10,675	1.1	3,310	2,770	2,567	1.3

Table 5-5 continued.

Measured		Calculated		Measured		Calculated	
CDM (Mpa)	TDM$^{\perp}$ (Mpa)	TDM$^{\perp}$ (Mpa)	CDM/TDM	CDM (Mpa)	TDM$^{\perp}$ (Mpa)	TDM$^{\perp}$ (Mpa)	CDM/TDM
11,114	6,037	10,372	1.1	3,306	2,828	2,563	1.3
11,071	9,524	10,326	1.1	3,257	2,516	2,520	1.3
10,876	11,180	10,117	1.1	3,126	2,592	2,403	1.3
10,755	10,492	9,987	1.1	3,049	3,173	2,335	1.3
10,419	12,797	9,629	1.1	3,047	3,033	2,333	1.3
10,412	6,986	9,621	1.1	3,025	2,196	2,314	1.3
10,403	9,630	9,612	1.1	3,010	2,088	2,300	1.3
10,398	8,640	9,606	1.1	2,837	1,766	2,148	1.3
10,309	10,063	9,511	1.1	2,801	2,228	2,117	1.3
10,008	9,780	9,191	1.1	2,756	1,241	2,078	1.3
9,731	7,746	8,899	1.1	2,747	1,722	2,070	1.3
9,688	8,991	8,854	1.1	2,708	2,369	2,036	1.3
9,542	16,526	8,700	1.1	2,690	1,644	2,021	1.3
9,405	12,186	8,556	1.1	2,586	2,381	1,931	1.3
9,333	11,742	8,481	1.1	2,516	1,454	1,871	1.3
9,271	6,046	8,416	1.1	2,504	1,081	1,860	1.3
9,261	9,182	8,405	1.1	2,498	1,672	1,856	1.3
9,085	14,855	8,222	1.1	2,216	1,186	1,616	1.4
8,661	9,328	7,780	1.1	2,129	1,104	1,543	1.4
8,305	10,234	7,413	1.1	2,059	1,419	1,485	1.4
8,280	10,607	7,388	1.1	1,843	1,490	1,306	1.4
8,192	7,353	7,297	1.1	1,841	1,227	1,305	1.4
8,088	7,630	7,190	1.1	1,807	1,428	1,277	1.4
8,068	7,077	7,170	1.1	1,744	1,586	1,226	1.4
7,911	7,838	7,009	1.1	1,644	927	1,146	1.4
7,840	5,029	6,937	1.1	1,512	836	1,040	1.5
7,725	6,115	6,820	1.1	1,508	569	1,037	1.5
7,258	8,624	6,347	1.1	1,500	831	1,030	1.5
7,128	5,561	6,215	1.1	1,250	474	835	1.5
7,085	6,882	6,173	1.1	1,095	617	717	1.5

Figure 5-6 shows the comparison between measured and computed tensile dynamic modulus perpendicular to the direction of compaction. As can be seen, the data are well distributed around the line of equality with a slight under-prediction of the computed tensile dynamic modulus (y = 0.985x). With coefficient of determination (R^2) of 0.863 and relative accuracy (se/sy) of 0.373, the correlation between the measured and computed TDM$^{\perp}$ proved to be good.

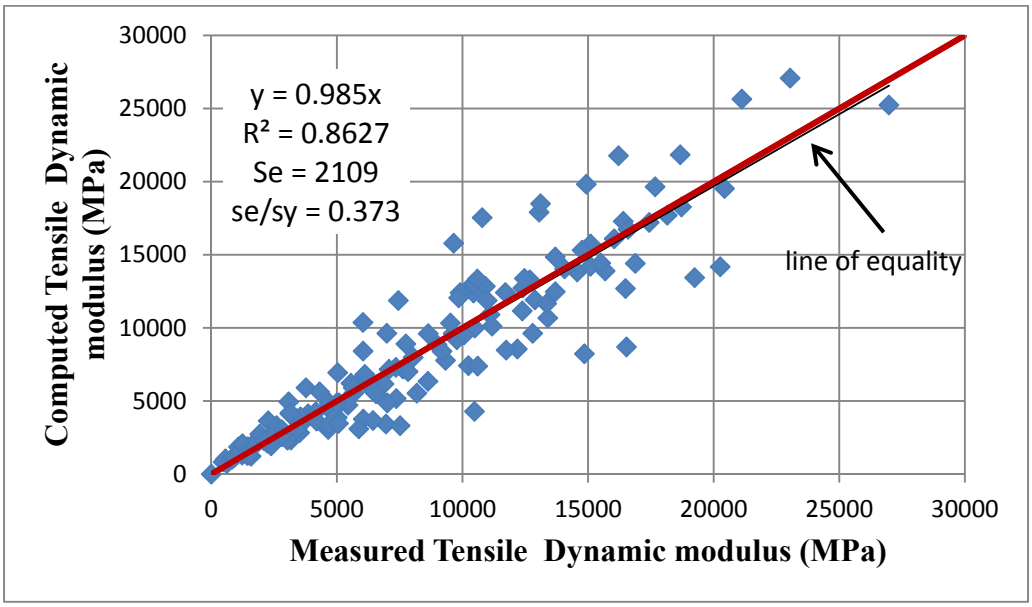

Figure 5-14 Comparison between Measured and Compute TDM$^{\perp}$

With the application of the spread sheet "solver" to optimize coefficients, this research introduced temperature (temp) parameter in the all combined relationship between TDM$^{\perp}$ and CDM as shown in equation 5-2.

$$TDM^{\perp} = 3.56975 \times (CDM^{0.8904}) * (TEMP^{-0.10458}) \quad \text{5-2}$$

Based on the equation 5-2 the correlation between TDM$\perp$ measured and TDM$\perp$ computed reduced to 0.82.

5.2.2 Comparison: CDM versus TDM ||

In this section, the relationship between CDM and TDM || was determined through statistical comparison of the dynamic moduli at temperatures 10^{o} C, 20^{o} C, 30^{o}C and 35^{o}C. The CDM was plotted against TDM || and then trend lines their coefficient of determination (R^2) were computed for three different models (y = ax, y=ax+b, and $y = ax^b$). Of the three equations, the power equation ($y = ax^b$) produced the strongest R^2 at each temperature level. The power equation and R^2 at each temperature group are presented in Table 5-6. The results for the other equations are given in Appendix B.

Table 5-6 Statistical models relating TDM || and CDM at different temperatures

Temp. ^{o}C	Statistical Model	R^2	Se
10	$TDM\| = 15.761 \times (CDM)^{0.7097}$	0.69	1,513
20	$TDM\| = 5.1072 \times (CDM)^{0.8325}$	0.73	1,603
30	$TDM\| = 1.7449 \times (CDM)^{0.9478}$	0.77	1,473
35	$TDM\| = 0.3962 \times (CDM)^{1.1368}$	0.84	1,033

Based on the R^2 displayed in Table 5-6, it is fair to conclude that the correlation strength between TDM || and CDM increases with temperature (from moderate to good).

As was for TDM$^{\perp}$, a better correlation was obtained when the second approach was used. Figure 5-15 shows relationship between TDM|| and CDM for all temperatures combined. The obtained coefficient of correlation (R^2) increased to 0.916.

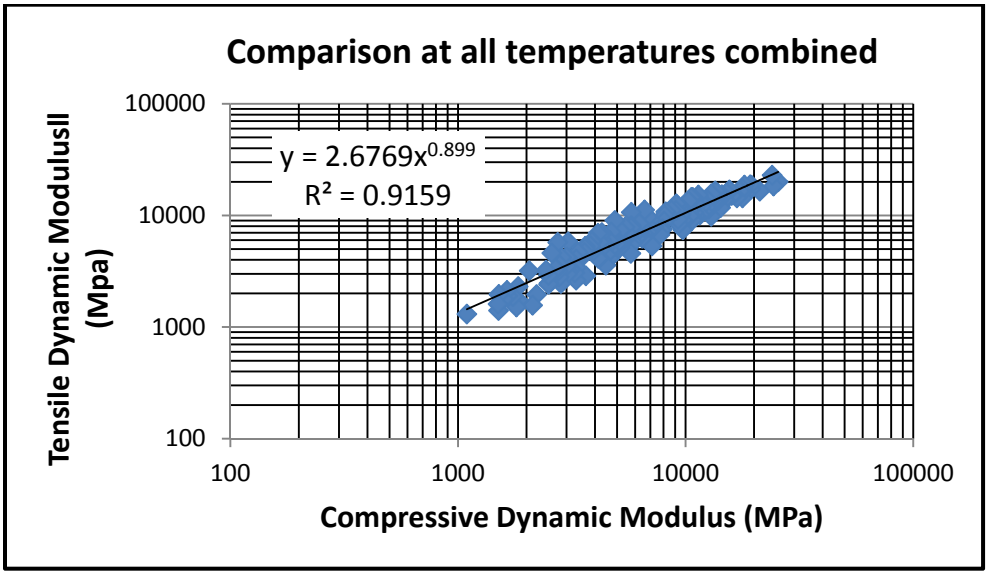

Figure 5-15 Comparisons of TDM|| and CDM for all temperatures combined.

The relationship between TDM|| and CDM at all temperature combines is:

$TDM_{||} = 2.6769 \times (CDM)^{0.899}$ 5-3

TDM|| = Tensile Dynamic Modulus Parallel to Compaction

CDM = Compressive Dynamic Modulus

Table 5-7 shows the calculated Tensile Dynamic Moduli (TDM||-calc) derived from the existing Compression Dynamic Moduli (CDM) using the

equation 5-3. Measured TDM|| , CDM and the ratio of CDM to TDM||-calc are also included in the table for comparison. From the table we can see the ratio CDM to TDM||-calc is 1.0 at high dynamic modulus (lower temperatures: 10^{o}C and 20^{o}C) and reduces to 0.8 at lower dynamic modulus (higher temperature: 35). For intermediate dynamic modulus, the ratio of CDM to TDM||-calc was 0.9. Tensile dynamic modulus is greater than compressive dynamic modulus especially at higher temperatures. This behavior could be associated with difficulties in setting up the tensile dynamic modulus test since in this test, the specimen and the loading ram are connected together.

Table 5-7 Measured and Calculated Tensile Dynamic Modulus (TDM ll)

Measured		Calculated	CDM/TDMll	Measured		Calculated	CDM/TDMll
CDM (Mpa)	TDMll (Mpa)	TDMll (Mpa)		CDM (Mpa)	TDMll (Mpa)	TDMll (Mpa)	
25,540	19,991	24,531	1.0	12,657	11,365	13,050	1.0
24,366	18,329	23,515	1.0	12,528	13,665	12,931	1.0
24,036	22,939	23,229	1.0	12,495	11,470	12,900	1.0
21,193	16,471	20,743	1.0	12,300	11,852	12,719	1.0
19,494	18,612	19,242	1.0	11,932	10,857	12,376	1.0
19,338	17,247	19,104	1.0	11,842	13,433	12,292	1.0
19,242	18,803	19,018	1.0	11,722	12,044	12,180	1.0
18,364	15,672	18,236	1.0	11,613	13,223	12,078	1.0
18,158	18,663	18,053	1.0	11,597	10,094	12,064	1.0
17,844	17,176	17,771	1.0	11,395	15,217	11,874	1.0
17,807	14,317	17,738	1.0	11,114	12,580	11,611	1.0
17,668	16,020	17,614	1.0	11,071	9,828	11,570	1.0

Table 5-7 Continued

Measured		Calculated	CDM/TDMll	Measured		Calculated	CDM/TDMll
CDM (Mpa)	TDMll (Mpa)	TDMll (Mpa)		CDM (Mpa)	TDMll (Mpa)	TDMll (Mpa)	
17,311	16,460	17,294	1.0	10,876	10,600	11,387	1.0
16,829	14,324	16,860	1.0	10,810	9,416	11,325	1.0
16,262	15,331	16,348	1.0	10,765	14,474	11,282	1.0
15,948	15,073	16,064	1.0	10,755	14,200	11,273	1.0
15,585	16,929	15,735	1.0	10,706	9,066	11,227	1.0
15,167	15,856	15,355	1.0	10,603	14,467	11,129	1.0
14,953	13,697	15,160	1.0	10,419	11,193	10,956	1.0
14,795	13,846	15,016	1.0	10,403	11,057	10,941	1.0
14,450	15,340	14,701	1.0	10,398	9,846	10,936	1.0
14,322	14,449	14,584	1.0	10,309	13,495	10,852	0.9
14,257	11,709	14,524	1.0	9,731	7,432	10,304	0.9
13,909	13,640	14,205	1.0	9,720	9,077	10,293	0.9
13,856	15,790	14,156	1.0	9,688	11,460	10,263	0.9
13,819	14,083	14,123	1.0	9,542	10,212	10,123	0.9
13,768	14,964	14,076	1.0	9,405	11,521	9,992	0.9
13,493	16,597	13,822	1.0	9,333	8,356	9,924	0.9
13,468	13,403	13,800	1.0	9,271	9,253	9,865	0.9
13,375	12,929	13,714	1.0	9,261	12,228	9,855	0.9
13,238	13,337	13,587	1.0	9,107	12,705	9,707	0.9
13,037	14,479	13,402	1.0	9,085	11,059	9,686	0.9
12,992	13,899	13,361	1.0	8,661	11,110	9,279	0.9
12,984	15,635	13,353	1.0	8,305	9,603	8,935	0.9
12,964	9,817	13,334	1.0	8,280	9,734	8,911	0.9
8,192	10,753	8,826	0.9	5,072	5,773	5,735	0.9
8,088	10,001	8,725	0.9	5,011	5,293	5,673	0.9
8,068	8,858	8,706	0.9	4,989	5,961	5,651	0.9
7,911	7,562	8,553	0.9	4,963	5,548	5,625	0.9
7,840	7,375	8,484	0.9	4,891	8,995	5,551	0.9
7,725	6,722	8,372	0.9	4,768	6,020	5,426	0.9
7,258	7,906	7,916	0.9	4,734	5,687	5,390	0.9
7,128	5,329	7,788	0.9	4,710	7,094	5,366	0.9
7,085	7,712	7,746	0.9	4,640	4,119	5,294	0.9
6,992	9,197	7,654	0.9	4,637	4,921	5,291	0.9
6,971	7,723	7,634	0.9	4,617	5,945	5,270	0.9
6,834	9,727	7,499	0.9	4,506	5,276	5,157	0.9
6,818	7,112	7,483	0.9	4,484	4,453	5,134	0.9
6,607	11,193	7,274	0.9	4,471	3,569	5,121	0.9
6,539	6,888	7,207	0.9	4,379	5,291	5,026	0.9
6,470	6,443	7,138	0.9	4,294	7,016	4,938	0.9

Table 5-7 Continued

Measured		Calculated	CDM/TDMll	Measured		Calculated	CDM/TDMll
CDM (Mpa)	TDMll (Mpa)	TDMll (Mpa)		CDM (Mpa)	TDMll (Mpa)	TDMll (Mpa)	
6,448	6,252	7,117	0.9	4,250	6,086	4,893	0.9
6,406	7,748	7,075	0.9	4,245	6,736	4,887	0.9
6,253	8,505	6,923	0.9	4,187	4,141	4,828	0.9
6,191	6,563	6,862	0.9	4,181	5,775	4,821	0.9
6,180	6,410	6,851	0.9	4,135	4,113	4,774	0.9
6,073	6,253	6,744	0.9	4,128	6,910	4,766	0.9
5,901	6,613	6,572	0.9	3,940	4,804	4,571	0.9
5,848	5,808	6,519	0.9	3,890	5,901	4,518	0.9
5,776	10,649	6,446	0.9	3,871	5,830	4,498	0.9
5,774	8,068	6,444	0.9	3,843	5,012	4,469	0.9
5,768	7,761	6,439	0.9	3,827	5,334	4,453	0.9
5,764	5,446	6,435	0.9	3,653	2,871	4,270	0.9
5,756	4,568	6,427	0.9	3,628	5,301	4,244	0.9
5,613	6,556	6,283	0.9	3,616	5,057	4,231	0.9
5,555	6,875	6,224	0.9	3,601	4,638	4,216	0.9
5,424	7,872	6,092	0.9	3,493	4,208	4,102	0.9
5,230	5,941	5,896	0.9	3,371	4,663	3,972	0.8
5,164	7,364	5,829	0.9	3,311	4,057	3,909	0.8
5,140	5,096	5,804	0.9	3,310	3,437	3,908	0.8
3,306	2,630	3,904	0.8	2,504	2,411	3,040	0.8
3,257	3,072	3,852	0.8	2,498	2,902	3,034	0.8
3,126	3,272	3,712	0.8	2,437	3,226	2,968	0.8
3,049	5,803	3,630	0.8	2,216	1,951	2,725	0.8
3,047	3,133	3,628	0.8	2,129	1,568	2,628	0.8
3,025	2,996	3,604	0.8	2,059	3,196	2,550	0.8
3,010	4,228	3,588	0.8	1,843	1,733	2,308	0.8
3,002	3,525	3,579	0.8	1,841	2,301	2,306	0.8
2,852	4,203	3,418	0.8	1,807	1,513	2,267	0.8
2,837	2,453	3,402	0.8	1,744	1,879	2,196	0.8
2,801	3,591	3,363	0.8	1,653	1,910	2,093	0.8
2,787	2,804	3,348	0.8	1,644	2,127	2,083	0.8
2,756	3,175	3,315	0.8	1,590	1,774	2,022	0.8
2,747	5,723	3,304	0.8	1,512	1,961	1,932	0.8
2,708	3,275	3,262	0.8	1,508	1,403	1,927	0.8
2,690	3,309	3,243	0.8	1,500	1,607	1,918	0.8
2,586	4,586	3,130	0.8	1,095	1,308	1,446	0.8
2,516	2,469	3,054	0.8				

The accuracy of the model for determining TDM|| from CDM was statistically evaluated using coefficient of determination (R^2), relative accuracy (se/sy) and line of equality as shown in Figure 5-12. The Figure 5-16 shows computed TDM|| plotted against measured TDM||. The data are equally distributed on both side of the line of equality, showing no bias (y = 0.9968x). Good correlation between measured and computed TDM||, with an R^2 of 0.91 was observed.

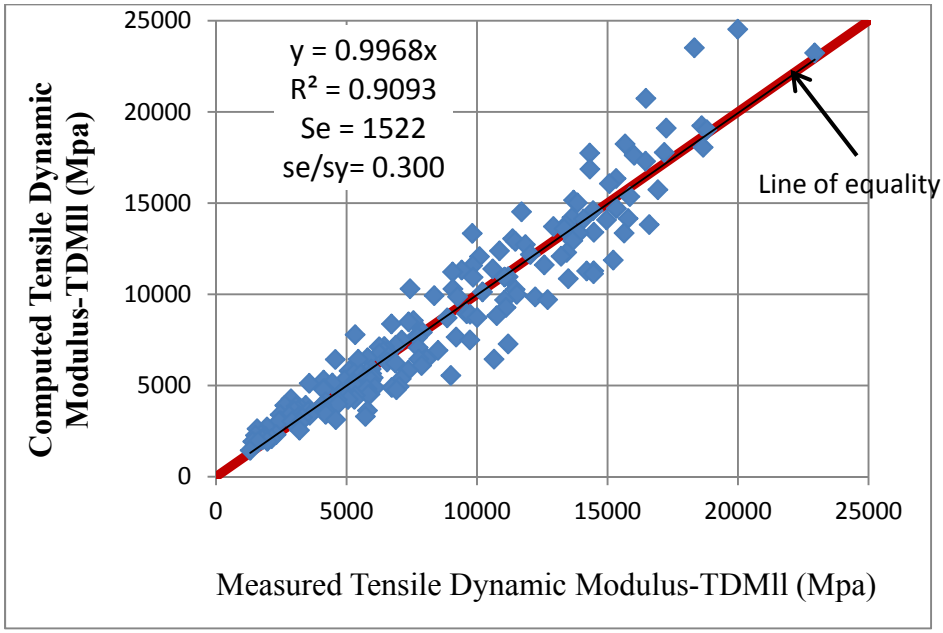

Figure 5-16 Comparison between Measured and Compute TDM||

The temperature was included as an independent variable in the relationship between TDM|| and CDM. After optimization of coefficients using solver, the following equation was obtained:

$$TDM|| = 1.07896 \times CDM^{0.94378} \times TEMP^{0.1876} \quad \text{.....5-4}$$

Based on this equation, the correlation between TDM|| measured and TDM|| computed reduced to 0.817.

Chapter 6

Finite element modeling

6.1 Introduction

This research used the generalized finite element program (Abaqus) for computing the strain responses at the bottom of perpetual pavement HMA layers. The program has an extensive material library that can be used to model most engineering materials including hot mix asphalt (HMA). Abaqus allows the combination of constitutive models to characterize complex materials such as HMA.

6.2 Model Geometry

A 312-inch long x 82.5-inch wide x 120-inch deep Finite Element structure was built to model section 1 of the Kansas Perpetual Pavement on US75 Highway. The dimension of the model were selected to accommodate both the steering and rear axle loads of the test truck with negligible edge effects (Figure 6-1).

Due to symmetry of the geometry and the loading applied by the truck, only one-half of the pavement structure was modeled. The Mesh of the model geometry is shown in Figure 6-2.

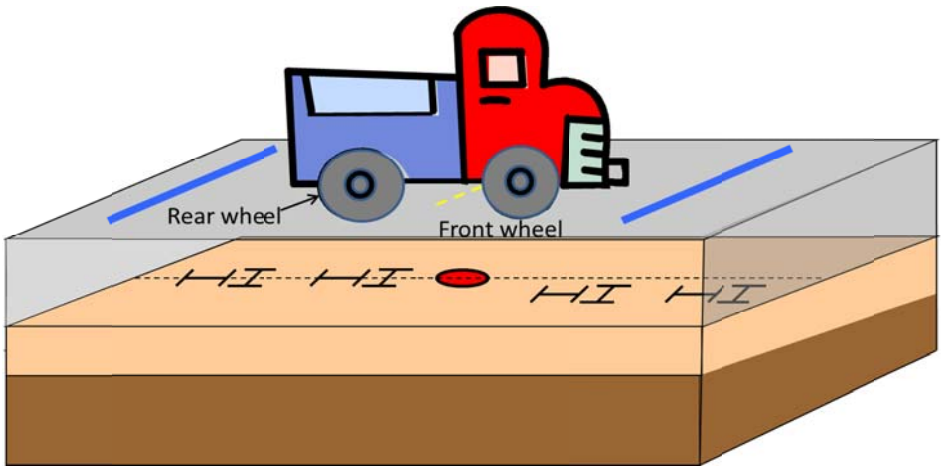

Figure 6-1 Schematic drawing showing a truck passing over an instrumented pavement section.

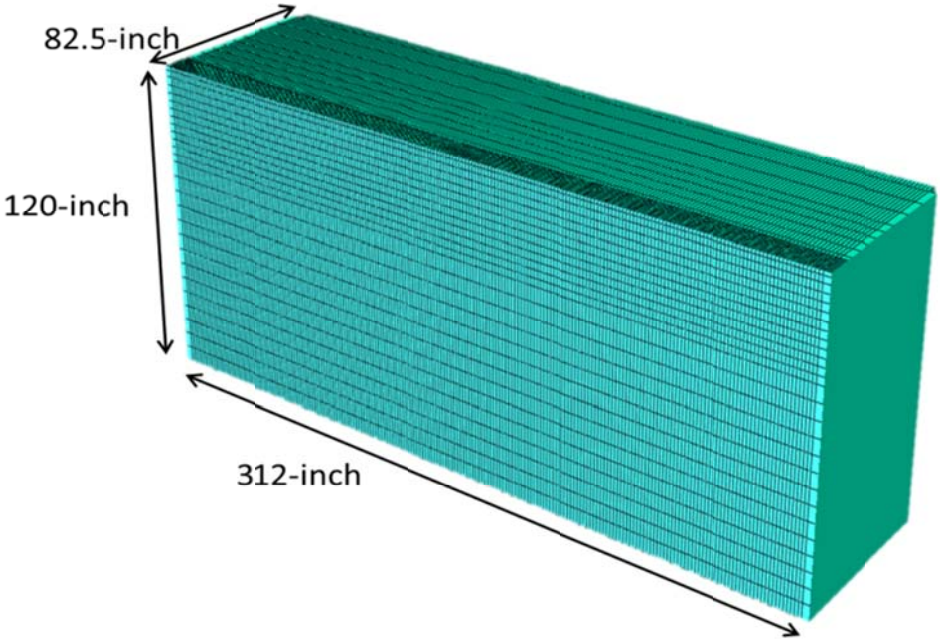

Figure 6-2 Finite Element geometry model

Table 6-1 shows the thicknesses of five structural layers of the perpetual pavement used in the geometry model. As seen in the table, the bottom layer is infinite. However, in the geometry model, a deep layer (> 100 inches) fixed at the bottom was used.

Table 6-1 Structural layers used in the Finite Element geometry model

Layer	Thickness (inch)	Material	Mix Code
Surface	1.6	HMA SM 9.5A: PG 70-28	S
Binder	2.4	HMA SM 19A: PG 70-28	M
Base	9	HMA SM 19A: PG 70-22	1
Sub-base	6	Lime Treated Soil	
Sub-grade	101 (infinite)	Clayey Soil	

6.3 Material characterization

The lime-treated subbase and subgrade soil layers were characterized by Elastic moduli derived from the resilient modulus tests reported in Chapter 3. The HMA materials were characterized by Prony series, compressive and tensile dynamic moduli. However, this research did not have laboratory determined tensile dynamic modulus for the materials used for the pavement; instead, the research computed tensile modulus for each HMA layer using compressive-to-tensile dynamic modulus relationship derived in the lab for New York mixes, as shown in Chapter 5. The compressive dynamic moduli used were extracted from the master curves at 20^0C constructed based on dynamic modulus tests results

reported in Chapter 3 (Figure 6-3, 6-4 and 6-5). The master curves at reference temperature of 20^0C were selected to reflect the pavement temperature during the field-testing. In order to determine the compressive dynamic modulus that represents the HMA pavement layer during field-testing, a vehicle speed of 20 mph was used. In the laboratory, this speed is equivalent to 10 Hz (0.1sec).

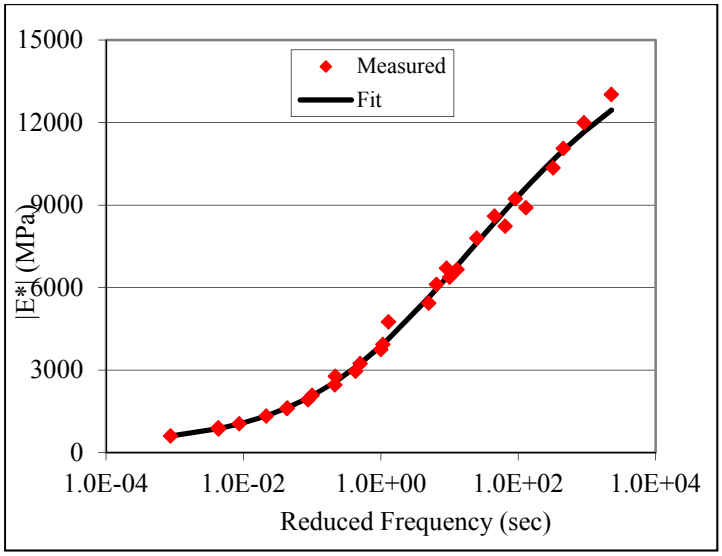

Figure 6-3 Dynamic Modulus Master Curve – Mix S

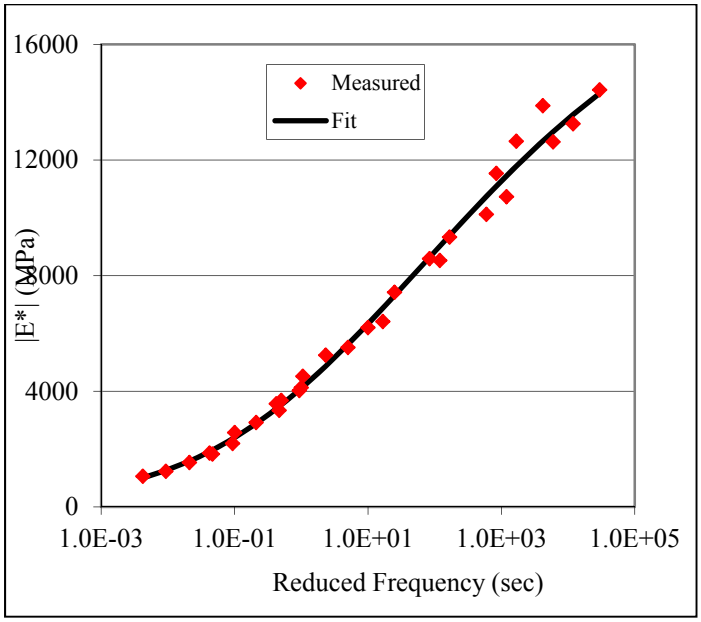

Figure 6-4 Dynamic Modulus Master Curve – Mix M

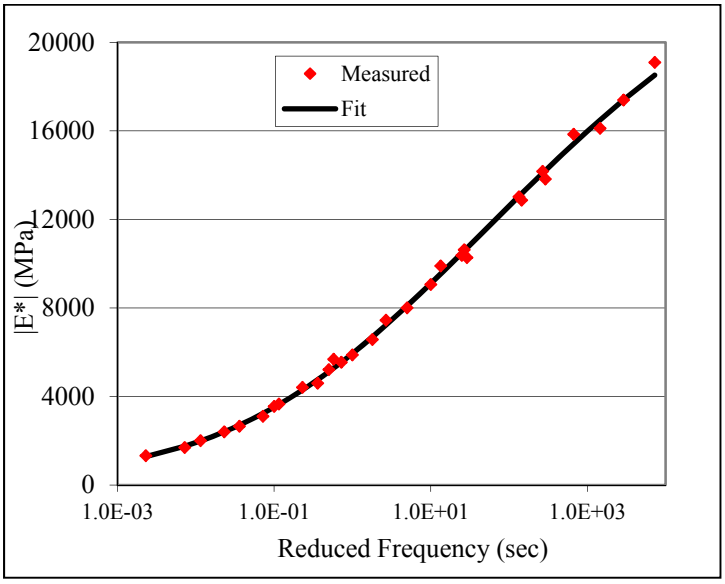

Figure 6-5 Dynamic Modulus Master Curve – Mix 1

The HMA layers Compressive and tensile dynamic moduli together with elastic resilient moduli for sub-grade and sub-base layers are shown in Table 6-2.

Table 6-2 Layers moduli used in the FE model analysis

	Compressive-DM psi (Mpa)	Tensile-DM psi (Mpa)	Resilience Modulus psi (Mpa)
Surface (Mix S)	297,617 (2052)	214,535 (1479)	N/A
Binder (Mix M)	372,529 (2569)	277,914 (1916)	N/A
Base (Mix 1)	514,811 (3550)	403,530 (2782)	N/A
Subbase	N/A	N/A	50,038 (345)
Subgrade	N/A	N/A	15,000 (103)

To implement both compressive and tensile dynamic modulus of the HMA layers, a visco-hyperelastic constitutive model was used. Abaqus/CAE uses a combination of viscoelastic Prony series and hyper-elastic model to represent the visco-hyperelastic model.

6.3.1 Prony series

Abaqus program has two options of implementing Prony series to define the viscoelastic time dependent properties of materials: time domain viscoelasticity and frequency domain viscoelasticity. The time domain option was used in the FE analysis to define the viscoelastic time dependent behavior of the asphalt mixes.

Three prony series input parameters are needed for time domain viscoelasticity. These parameters are the dimensionless shear relaxation modulus (g_i), the dimensionless bulk relaxation modulus (k_i), and the reduced relaxation time (τ_i). The parameters are defined as:

$$g_i = \frac{G_i}{G_0} \quad \text{----------} \quad (6\text{-}1)$$

Where,

g_i = dimensionless shear relaxation modulus at time i

G_i = shear relaxation modulus at time i

G_0 = initial shear relaxation modulus

$$k_i = \frac{K_i}{K_0} \quad \text{----------} \quad (6\text{-}2)$$

Where,

k_i = dimensionless bulk relaxation modulus at time i

K_i = bulk relaxation modulus at time i

K_0 = initial bulk relaxation modulus

The prony series parameters were calculated by developing a Microsoft Excel spreadsheet to fit curves representing Equations 6-3 and 6-4 to the computed shear stress ($G_R(t)$) and bulk stress ($K_R(t)$) relaxation moduli data.

$$G_R(t) = G_0\left(1 - \sum_{i=1}^{N} g_i^P \left(1 - e^{-t/\tau_i}\right)\right) \quad \text{----------(6-3)}$$

$$K_R(t) = K_0\left(1 - \sum_{i=1}^{N} k_i^P \left(1 - e^{-t/\tau_i}\right)\right) \quad \text{----------(6-4)}$$

Where,

G_0 , K_0= Instantaneous shear and bulk relaxation modulus

g_i^P , k_i^P =Prony series coefficients

t =Time, sec

τ_i = Relaxation or reduced time, sec

Table 6-3 presents the calculated Prony series parameters for the asphalt concrete mixes used in this research.

Table 6-3 Prony Series Parameters

	gi	ki	τi
Mix S	0.308954	0.38104	0.001
	0.103362	0.119207	0.01
	0.213567	0.151703	0.1
	0.155012	0.160324	1
	0.127155	0.117885	10
Mix M	0.677686	0.59063	0.001
	0	0	0.01
	0.104582	0.164675	0.1
	0.073812	0.082773	1
	0.074241	0.093324	10
Mix 1	0.432905	0.479071	0.001
	0.04744	0.044055	0.01
	0.183055	0.181144	0.1
	0.115363	0.107065	1
	0.119419	0.106327	10

6.2.2 Hyper-elastic model

Through Abaqus Hyper-elastic material tab, users can input nominal strains and stresses to characterize stiffness of materials. Therefore, in the material tab, stress-strain data points were inputted in ascending order from negative to positive to represent a stress-strain curve which has the desired slopes, corresponding to the desired Compressive and Tensile moduli. Thereafter the material model was evaluated using the Abaqus built-in calibration subroutine.

Abaqus version 6.12-2 has a built-in calibration subroutine to compare stress-strain test data with the behavior predicted by different hyper-elastic material formulations known as strain energy potentials. The subroutine uses a single element geometry model to find hyper-elastic strain energy potential that can develop a stress-strain curve that best fit the test data. Abaqus material library has the following strain energy potential forms.

- Arruda-Boyce,
- Marlow form,
- Mooney-Rivlin,
- Neo-Hookean,
- Ogden,
- polynomial,

- reduced polynomial,
- Yeoh,
- and Van der Waals

Out of the energy potential forms mentioned, only the Ogden strain energy potential was found suitable for characterizing the stiffness of HMA based on Compressive and Tensile moduli. The rest of the strain energy potentials computed best curves relatively far from the test data. In ABAQUS, the form of Ogden strain energy potential is:.

$$U = \sum_{i=1}^{N} \frac{2\mu_i}{\alpha_i^2}\left(\bar{\lambda}_1^{\alpha_i} + \bar{\lambda}_2^{\alpha_i} + \bar{\lambda}_3^{\alpha_i}\right) + \sum_{i=1}^{N} \frac{1}{D_i}(J^{el} - 1)^{2i} \text{ ----------} (6\text{-}5)$$

Where

$\bar{\lambda}_i$=Deviatoric principal stretches

J^{el}=Elastic volume ratio

μ_i,α_i, and D_i = temperature-dependent material constants. While μ_i and α_i describe the shear behavior of material, D_i term represents the compressibility of the material. However, unless volumetric test data are available, D_i is assumed to be zero and at this point the material is fully incompressible.

N= Strain energy potential level (order of the polynomial). During evaluation of the hyper-elastic constitutive model, the model prediction was checked for N levels ranging from one to six.

Figure 6-6, 6-7 and 6-8 show the behavior predicted by the Ogden-Hyper-elastic constitutive model for the Perpetual Pavement base, binder and surface course HMA materials. As the figures show, the difference between predicted and experimental data curve is minimal.

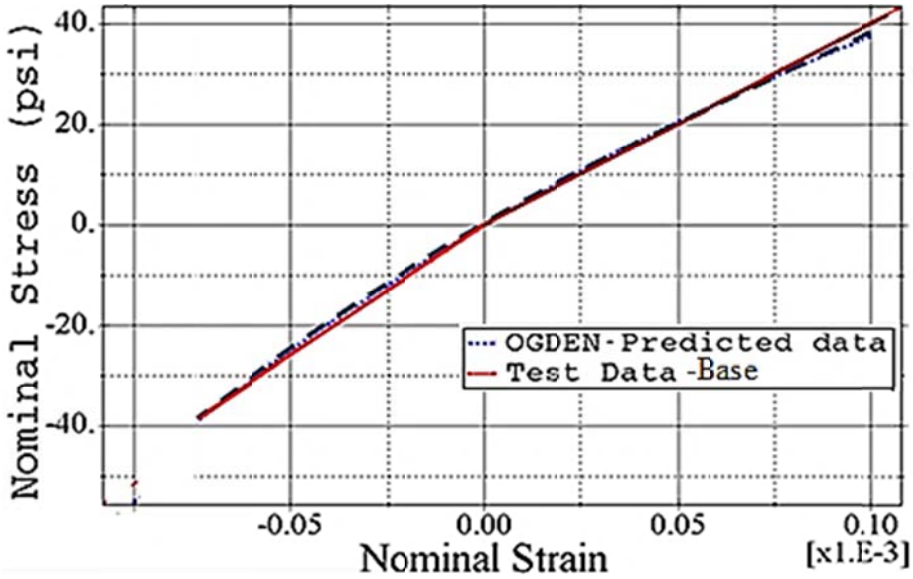

Figure 6-6 Comparison of FE model (Ogden) with experimental data for HMA Base layer

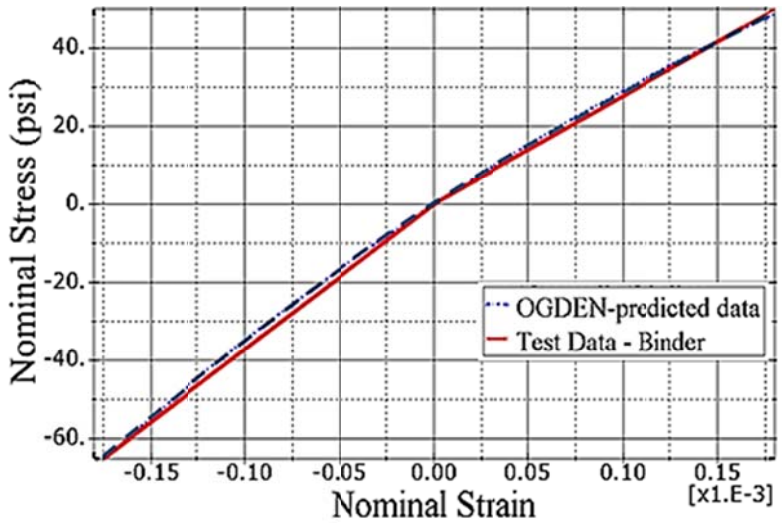

Figure 6-7 Comparison of FE model (Ogden) with experimental data for HMA Binder layer

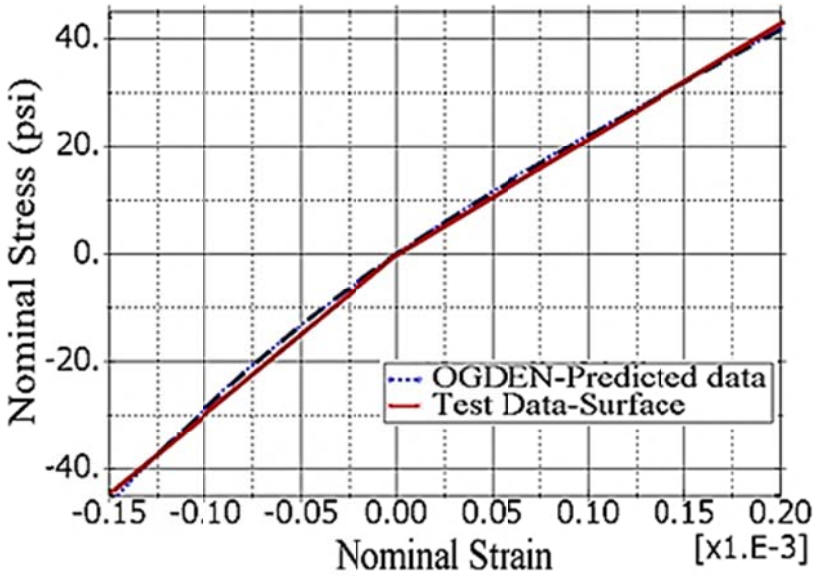

Figure 6-8 Comparison of FE model (Ogden) with experimental data for HMA Surface layer.

6.2.3 Testing the visco-hyperelastic model for HMA materials

Before adopting the selected model for modeling the pavement structure, it was tested on HMA solid cylinder (6" diameter x 15" deep). For simplicity, the research used 3-inch x 15-inch axisymmetric mesh, comprised of 500, 0.3-inch x 0.3-inch linear quadrilateral elements of type CAX4R (Figure 6-9).

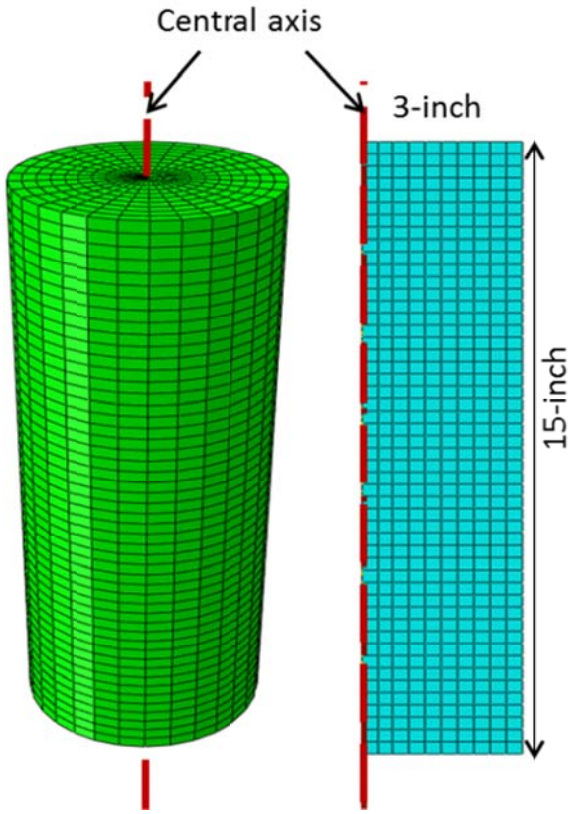

Figure 6-9 Axisymetry mesh used for testing the visco-hyperelastic material model

The objective was to validate the use of hyperelastic models for HMA material characterization by comparing with linear-viscoelastic model, which is commonly used for the characterization HMA materials. Under pure tension, the FE analysis results based on three different models were compared: linear viscoelastic, linear visco-hyperelastic and non-linear visco-hyperelastic. Abaqus implements the three models as follows.

- *Linear viscoelastic*

In this case, Abaqus software typically allows the user to insert the Prony series and initial elastic modulus (E_0). The parameters define materials time dependence and stiffness respectively. During analysis, Abaqus automatically picks the same Prony series and modulus at the beginning of every time increment and use the information to characterize the material. The Prony series, modulus and loads used in this model are shown in Table 6-4.

Table 6-4 Material parameters used in the FE-linear viscoelastic model

Prony series			Modulus (psi)	Creep load (psi)
gi	ki	τi		
0.4329	0.47907	0.001	514,811	150
0.04744	0.04406	0.01		
0.18305	0.18114	0.1		
0.11536	0.10706	1		
0.11942	0.10633	10		
0	0	100		

- *Linear Visco-Hyperelastic*

As for the linear viscoelastic material model, the inputs for this model were Prony series and modulus. The modulus was derived from a set of linear stress-strain data points shown in Table 6-5 below.

Table 6-5 Stress-Strain data used in the FE-linear visco-hyperelastic model

Stress (psi)	Strains	Modulus (psi)		Stress (psi)	Strains	Modulus (psi)
-80	-0.0001554	514,811		1	1.94E-06	514,811
-77	-0.00015	514,811		4	7.77E-06	514,811
-74	-0.000144	514,811		7	1.36E-05	514,811
-71	-0.000138	514,811		10	1.94E-05	514,811
-68	-0.000132	514,811		13	2.53E-05	514,811
-65	-0.000126	514,811		16	3.11E-05	514,811
-62	-0.00012	514,811		19	3.69E-05	514,811
-59	-0.000115	514,811		22	4.27E-05	514,811
-56	-0.000109	514,811		25	4.86E-05	514,811
-53	-0.000103	514,811		28	5.44E-05	514,811
-50	-9.71E-05	514,811		31	6.02E-05	514,811
-47	-9.13E-05	514,811		34	6.6E-05	514,811
-44	-8.55E-05	514,811		37	7.19E-05	514,811
-41	-7.96E-05	514,811		40	7.77E-05	514,811
-38	-7.38E-05	514,811		43	8.35E-05	514,811
-35	-6.8E-05	514,811		46	8.94E-05	514,811
-32	-6.22E-05	514,811		49	9.52E-05	514,811
-29	-5.63E-05	514,811		52	0.000101	514,811
-26	-5.05E-05	514,811		55	0.000107	514,811
-23	-4.47E-05	514,811		58	0.000113	514,811
-20	-3.88E-05	514,811		61	0.000118	514,811
-17	-3.3E-05	514,811		64	0.000124	514,811
-14	-2.72E-05	514,811		67	0.00013	514,811
-11	-2.14E-05	514,811		70	0.000136	514,811
-8	-1.55E-05	514,811		73	0.000142	514,811
-5	-9.71E-06	514,811		76	0.000148	514,811
-2	-3.88E-06	514,811		79	0.000153	514,811
				82	0.000159	514,811

- *Non-linear Visco-Hyperelastic*

The inputs for this model were inserted into the program the same way as was for linear visco-hyperelastic. However, the set of stress-strain data points for characterization of compressive and tensile behavior were different. In the compression zone, the stress-strain data points represented a modulus of 514,811 psi. In the tension zone, the points represented a modulus of 403,530 psi. The set of stress-strain data points used this case are shown in Table 6-6.

Table 6-6 Stress-Strain data used in the FE non-linear visco-hyperelastic model

Compressive Modulus				Tensile Modulus		
Stress (psi)	Strains	Modulus (psi)		Stress (psi)	Strains	Modulus (psi)
-80	-1.55E-04	514,811		1	2.48E-06	403,530
-77	-1.50E-04	514,811		4	9.91E-06	403,530
-74	-1.44E-04	514,811		7	1.73E-05	403,530
-71	-1.38E-04	514,811		10	2.48E-05	403,530
-68	-1.32E-04	514,811		13	3.22E-05	403,530
-65	-1.26E-04	514,811		16	3.97E-05	403,530
-62	-1.20E-04	514,811		19	4.71E-05	403,530
-59	-1.15E-04	514,811		22	5.45E-05	403,530
-56	-1.09E-04	514,811		25	6.20E-05	403,530
-53	-1.03E-04	514,811		28	6.94E-05	403,530
-50	-9.71E-05	514,811		31	7.68E-05	403,530
-47	-9.13E-05	514,811		34	8.43E-05	403,530
-44	-8.55E-05	514,811		37	9.17E-05	403,530
-41	-7.96E-05	514,811		40	9.91E-05	403,530

Table 6-6 continued

Compressive Modulus				Tensile Modulus		
Stress (psi)	Strains	Modulus (psi)		Stress (psi)	Strains	Modulus (psi)
-38	-7.38E-05	514,811		43	1.07E-04	403,530
-35	-6.80E-05	514,811		46	1.14E-04	403,530
-32	-6.22E-05	514,811		49	1.21E-04	403,530
-29	-5.63E-05	514,811		52	1.29E-04	403,530
-26	-5.05E-05	514,811		55	1.36E-04	403,530
-23	-4.47E-05	514,811		58	1.44E-04	403,530
-20	-3.88E-05	514,811		61	1.51E-04	403,530
-17	-3.30E-05	514,811		64	1.59E-04	403,530
-14	-2.72E-05	514,811		67	1.66E-04	403,530
-11	-2.14E-05	514,811		70	1.73E-04	403,530
-8	-1.55E-05	514,811		73	1.81E-04	403,530
-5	-9.71E-06	514,811		76	1.88E-04	403,530
-2	-3.88E-06	514,811		79	1.96E-04	403,530

6.2.4 Comparison of the viscoelastic and visco-hyperelastic models

Figure 6-10 shows strain development history at the mid-point of the HMA cylinder based on the finite element analysis. The maximum tensile strains for the linear viscoelastic (LVE) and linear visco-hyperelastic (LVHE) were 92.64, 95.68, micro-strains respectively. The results are relatively close.

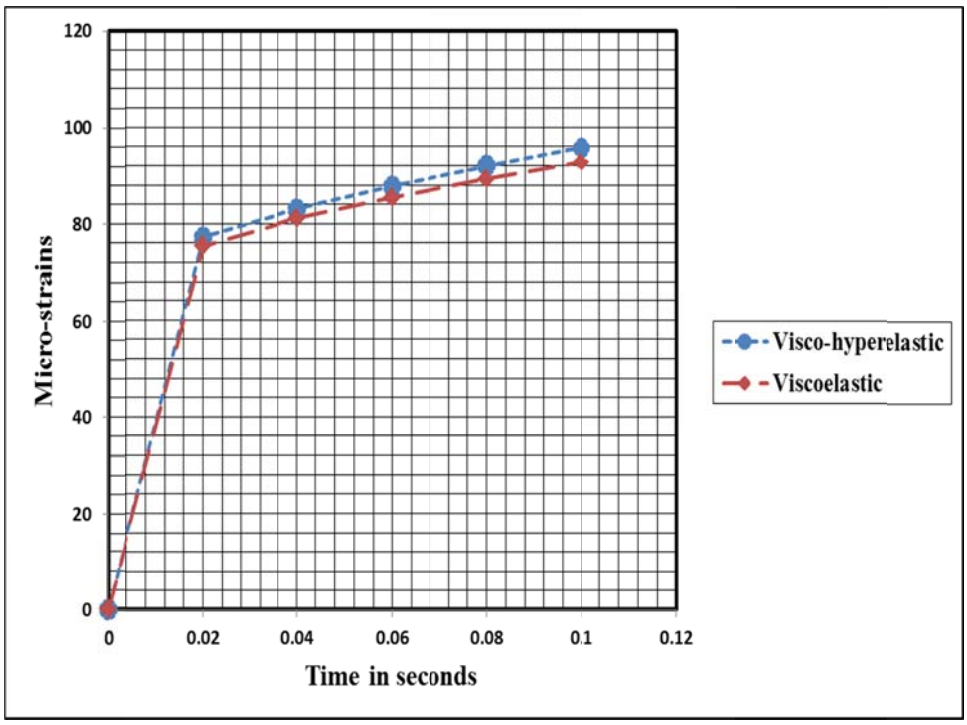

Figure 6-10 HMA cylinder strain development history

6.3 Element Type and size

Typically 3D Finite element pavement models perform well with 3D eight node solid brick elements. However, the accuracy of the Fine element analysis depends on the size and aspect ratio of the elements. The element size may vary depends upon the geometry dimension, contact restrictions, load magnitude, analysis type (static or dynamic), capacity of the computer and computational time. When there is no computational time constraint, it is typical to adopt a fine

mesh (small element size). Fine mesh (small elements size) offer more accurate results than coarser mesh (large elements).

Abaqus requires that the aspect ratio (ratio between the longest and shortest edge of an element), to be less than 10 for accurate results. However, an aspect ratio of less or equal to 4 is recommended for areas around wheel path (loaded areas) (Hibbitt, Karlsson and Sorensen. 2012).

In order to achieve optimum accuracy without increasing the computational cost, a biased mesh was used. Small elements were used in the HMA layer along the wheel path where high stress-strain gradients occur, and increasingly large element size were used far away from the loading path.

A convergence test was performed using a static load to determine the optimal number of elements needed. After convergence test, it was determined that 1.0 x 1.5-inches elements were suitable for the area around the wheel path. 1.5 x 6-inch and 1.5 x 11-inches element sizes were used toward the far ends. All elements used in the model were type C3D8R except for the sides away from the symmetry plane of the model where infinite element type CIN3D8R were used (Figure 6-11).

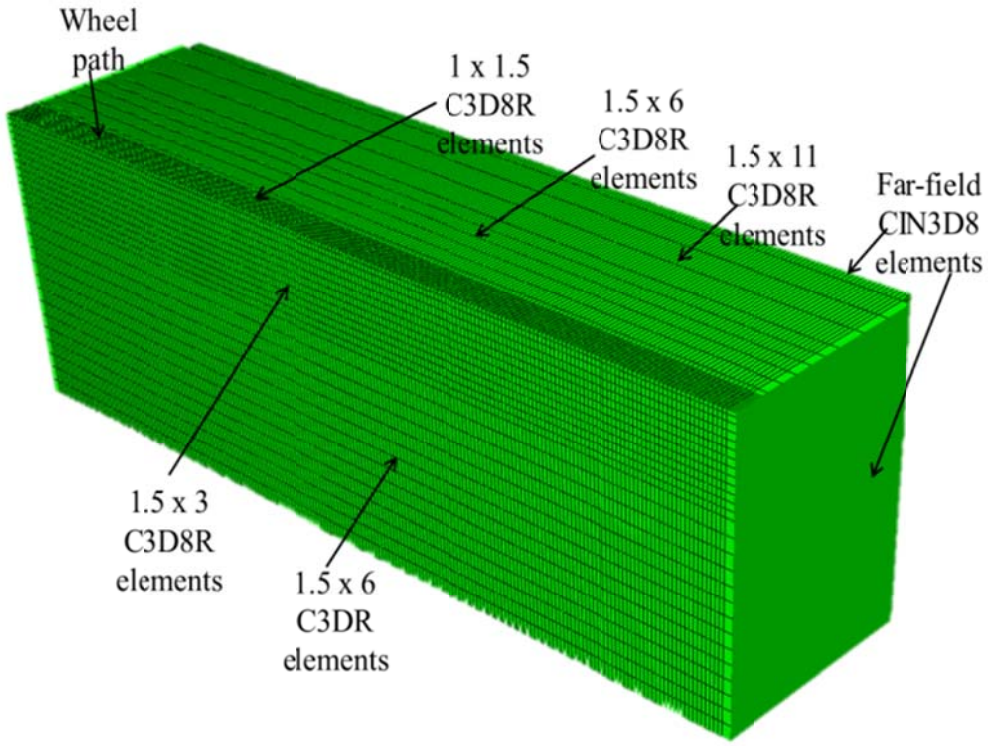

Figure 6-11 Element type and size

The C3D8R element is a solid eight-node linear brick element with reduced integration. Due to reduced integration, the element offers relatively low computational cost. However, because its integration point is located at the middle of the element, small elements are usually required for accurate results (Figure 6-12a). A special case of the C3D8R elements is CIN3D8. The CIN3D8 elements have five finite solid faces and one infinite face (Figure 6-12b). Finite element programs use CIN3D8 elements to represent far-field regions of continuous structures such as pavements. Abaqus/CAE does not support infinite

elements in its current setting. However these elements were included in the input file using a text editor.

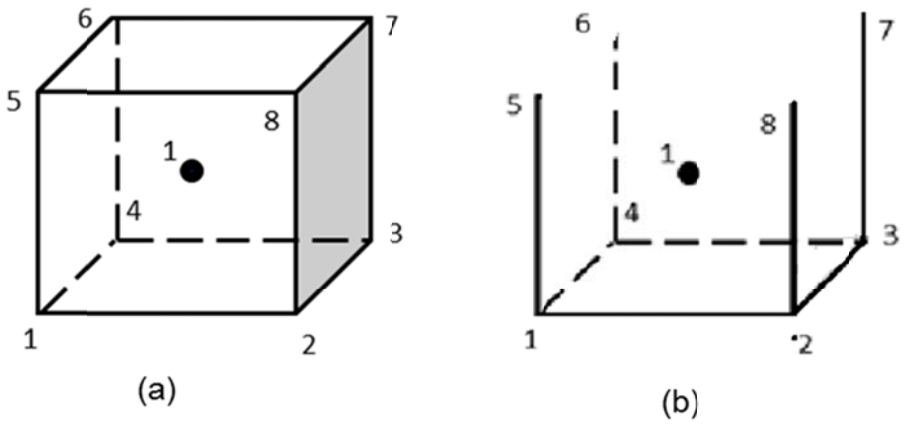

Figure 6-12: Type of elements used (a) C3D8R finite element (b) CIN3D8 Infinite element

6.4 Boundary Conditions

In this research, three different types of boundary conditions were employed to represent the pavement end supports.

i. *Infinite boundaries*: this type of boundary was assigned to three vertical sides far from the loading area (Figure 6-13). The boundaries allow reduction of elements that would have been used to extend the model far from the dynamical loaded area. They do so by offering a smooth decay of stresses to the far ends of the geometry model.

ii. *Z-Asymmetry:* in order to take advantage of symmetry of the geometry and loading only a half of the pavement structure was modeled. To do so, the horizontal movement of the nodes in the symmetry plane was restricted(Figure 6-13).

iii. *Fixed end*: The movement of the nodes at the bottom of the pavement structure (located 120-inches from the surface) was restricted in all directions. (Figure 6-13).

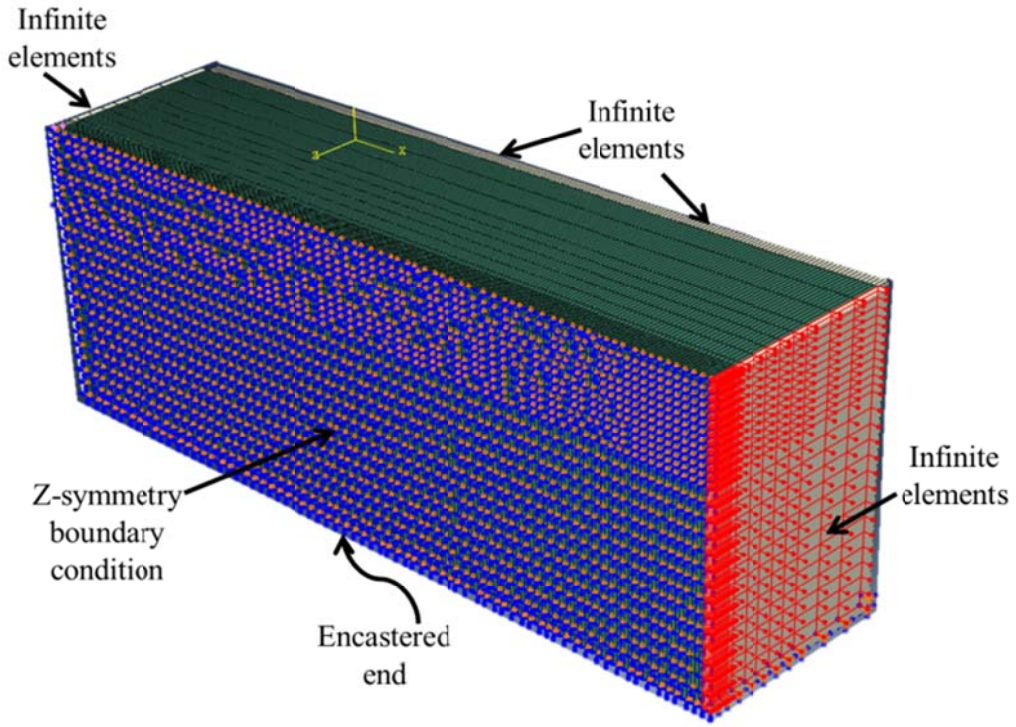

Figure 6-13 Boundary Conditions of the Model

6.5 Loading

6.5.1 Tire imprint

The tire imprint is the contact area between the tire and pavement surface. The size of tire imprint depends on contact pressure, which is more often assumed equal to the tire inflation pressure. In this case, the tire inflation pressure and wheel load are used to calculate the size of tire imprint. However, in this research the dimension of the tire imprints were measured in the US 75 Perpetual Pavement project every time when the pavement response measurements were conducted. The tire imprint dimensions used in this research are shown in Figure 6-14.

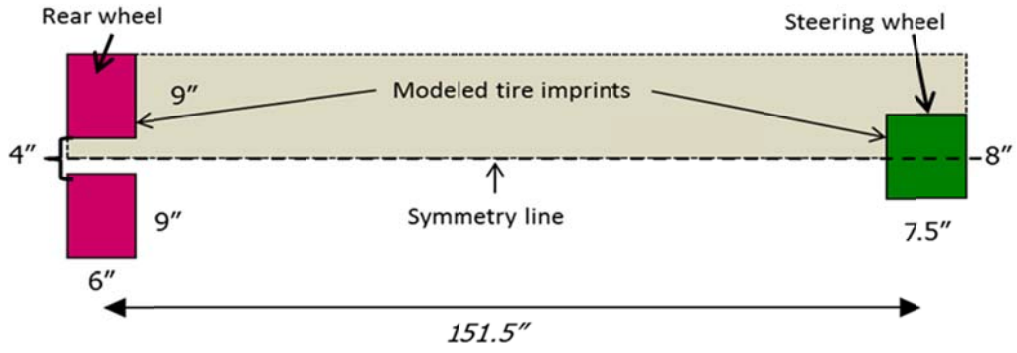

Figure 6-14 Tire Imprint dimensions

6.5.2 Surface partitions

There are two ways in which external loads may be applied to an Abaqus model: element loading or surface loading. Since the research used more than 400

surfaces to define the vehicle moving load, the surface loading procedure was selected to avoid redefining of the loaded surfaces when element size changes. The surfaces along which the truck tires passed were partitioned into small spaces multiple of both rear and steering tire imprints. In addition, a few more partition lines along the length were added to allow for repositioning of the wheels when necessary (Figure 6-15).

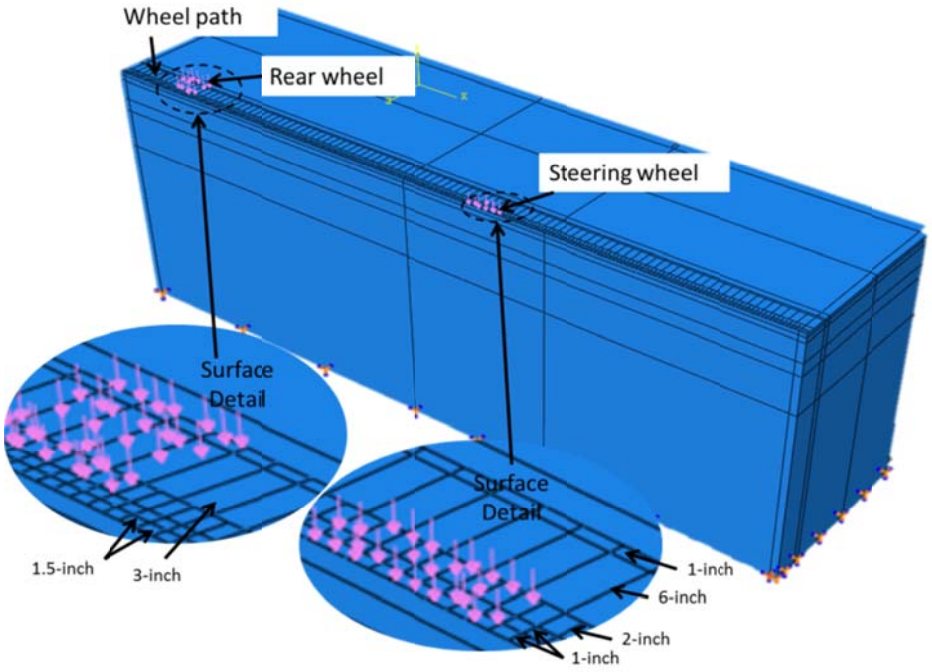

Figure 6-15 Wheel Path Surface Partition

6.5.3 Simulation of Moving Loads

In Abaqus finite element model, traffic loads may be applied statically or dynamically. In this research, dynamic moving wheel loads were modeled by

implementing the concept of step loading with trapezoidal loading amplitude. There are three main components of this concept: the entry surface segment (or element), the tire imprint segments and the leaving segment (element). When a vehicle approaches a given surface segment, the surface is loaded with amplitude that increases linearly from 0 to 1. Similarly, as the tire moves away from a given surface segment, the loading amplitude that simulates the decrease in loading from 1 to 0 is used. The surface segments within the tire imprint are loaded with constant loading amplitude of 1. Table 6-7 and Figure 6-16 show the transition of wheel load from step-1 to step-2, step-2 to step-3 and so on, along the wheel path.

Table 6-7 Wheel load transition parameters

	Step 1			**Step 2**			**Step 3**			**Step 4**		
Load position	Leave	Tire Imprint	Entry	Leave	Tire Imprint	entry	Leave	Tire Imprint	entry	Leave	Tire Imprint	entry
Surface	S1	S2	S3	S2	S3	S4	S3	S4	S5	S4	S5	S6
Aplitude	1 to 0	1 to 1	0 to 1	1 to 0	1 to 1	0 to 1	1 to 0	1 to 1	0 to 1	1 to 0	1 to 1	0 to 1

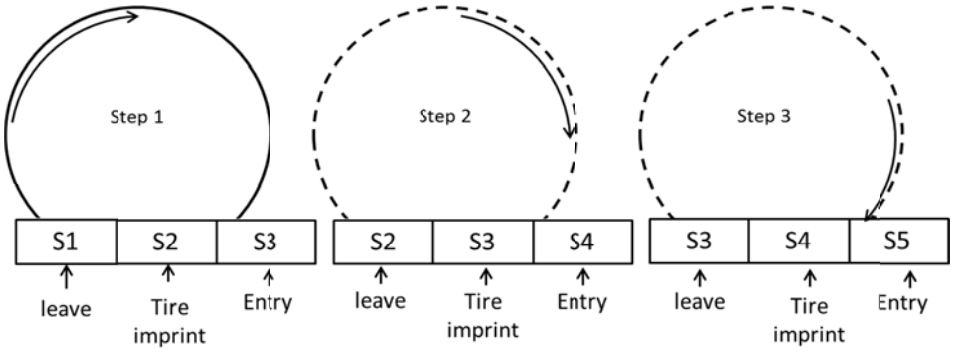

Figure 6-16 Schematic drawing of a moving tire based on the trapezoidal loading method.

The duration of each step or step time was calculated based on the speed of the vehicle and the length of the surface segment along the direction of the vehicle. At first, the speed was converted from miles per hour into inches per second. Then the size of each segment on the wheel path was divided by the speed in inches per second to obtain the time required for each step to move the load at the desired speed. In this model, the length of surface segment used to advance wheel load from one-step to the next was 3 inches. To model the load moving at 20 mph, which is equals to 352 inches per second, the 3 inches was divided by 352 inches per second, and a step time of 0.008523 seconds was obtained. The same was followed to obtain step time of 0.004262 and 0.002841 seconds for the 40 mph and 60 mph speeds respectively. Thereafter, loading amplitudes were created using the tabular option in ABAQUS. Tables 6-8 presents the tabular data used to create the loading amplitudes for 20 mph speed.

Table 6-8 Loading Amplitude Tabular Data for 20 mph

Entry surface segment		Within tire imprit		Leaving surface segement	
Step time (s)	Amplitude	Step time (s)	Amplitude	Step time (s)	Amplitude
0	1	0	1	0	0
0.008523	0	0.008523	1	0.008523	1

The total step time used in here was further divided into small segments (time increments) to allow for the solution to converge. Abaqus has two options

of implementing time increments: automatic or fixed by the user. Abaqus recommend the automatic method to avoid convergence problems. Table 6-9 shows load amplitude data with the sub-divided step time.

Table 6-9 Subdivided Loading Amplitude Tabular Data for 20 mph

Entry surface segment		Within tire imprit		Leaving surface segement	
Step time (s)	Amplitude	Step time (s)	Amplitude	Step time (s)	Amplitude
0.000E+00	0	0.000E+00	1	0.000E+00	1
4.262E-04	0.05	4.262E-04	1	4.262E-04	0.95
8.523E-04	0.1	8.523E-04	1	8.523E-04	0.9
1.278E-03	0.15	1.278E-03	1	1.278E-03	0.85
1.705E-03	0.2	1.705E-03	1	1.705E-03	0.8
2.131E-03	0.25	2.131E-03	1	2.131E-03	0.75
2.557E-03	0.3	2.557E-03	1	2.557E-03	0.7
2.983E-03	0.35	2.983E-03	1	2.983E-03	0.65
3.409E-03	0.4	3.409E-03	1	3.409E-03	0.6
3.835E-03	0.45	3.835E-03	1	3.835E-03	0.55
4.262E-03	0.5	4.262E-03	1	4.262E-03	0.5
4.688E-03	0.55	4.688E-03	1	4.688E-03	0.45
5.114E-03	0.6	5.114E-03	1	5.114E-03	0.4
5.540E-03	0.65	5.540E-03	1	5.540E-03	0.35
5.966E-03	0.7	5.966E-03	1	5.966E-03	0.3
6.392E-03	0.75	6.392E-03	1	6.392E-03	0.25
6.818E-03	0.8	6.818E-03	1	6.818E-03	0.2
7.245E-03	0.85	7.245E-03	1	7.245E-03	0.15
7.671E-03	0.9	7.671E-03	1	7.671E-03	0.1
8.097E-03	0.95	8.097E-03	1	8.097E-03	0.05
8.523E-03	1	8.523E-03	1	8.523E-03	0

6.6 The Results of the Finite Element Analysis

Figure 6-17 shows FE longitudinal and transverse strain evolution at the bottom of perpetual pavement HMA layers based on the visco-hyperelastic model at a truck speed 20 mph. The strain curves generated two major peaks during the loading history: The first peak was generated when the steering wheel passed direct over a given point. Similarly, the second peak was generated when the rear wheels passed the same point. In the longitudinal direction, the first and second peak strains were 18.9 and 32.8 micro-strains respectively. Likewise, on the transverse direction the first and second peak strains were 22.3 and 31.7 micro-strains respectively. In terms of the shape of the curve, the longitudinal strain history curve begins and ends with negative values to indicate that the pavement was in compression when the wheels were approaching and leaving a given element. The transverse strains were tensile throughout the duration of loading. Contour plots of the strains in the plane of symmetry are shown in Figure 6-18a-b. Blue color around point “A” shows existence of compressive longitudinal strains in the vicinity of that point (Figure 6-18a). Figure 6-18b, which represents transverse strains, shows no blue color at the same area, meaning transverse strains are always positive.

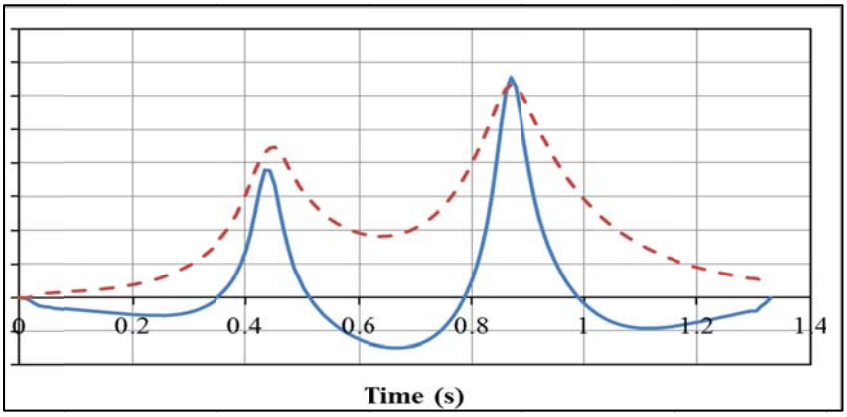

Figure 6-17 Computed strain development at the bottom of HMA layers based on the Visco-hyperelastic model.

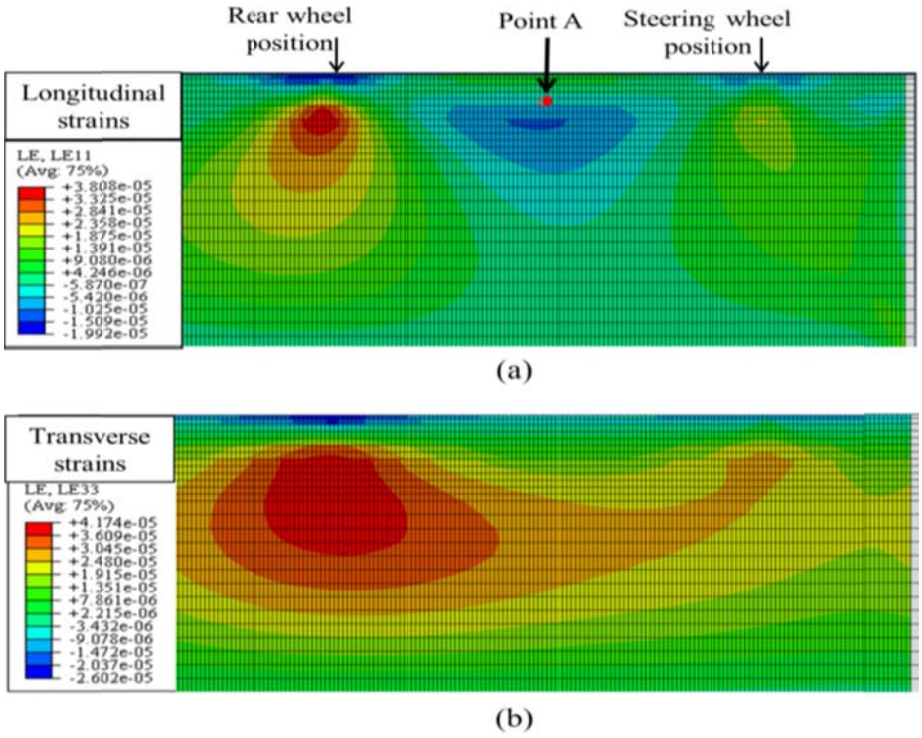

Figure 6-18 Contour plots of (a) Longitudinal strain (b) Transverse strains in the plane symmetry

For comparison, this research used FE linear viscoelastic model to compute the responses at the bottom of the Perpetual Pavement HMA layers. The model utilizes compressive dynamic modulus to characterize the stiffness of HMA layers. Figure 6-19 shows the strain development at the bottom of HMA layers based on the FE viscoelastic model. In the longitudinal direction, the peak strains corresponding to front and rear wheels were 16.5 and 30.96 micro-strains respectively. In the transverse direction the peak strains were 21.1 and 30.93 micro-strains respectively.

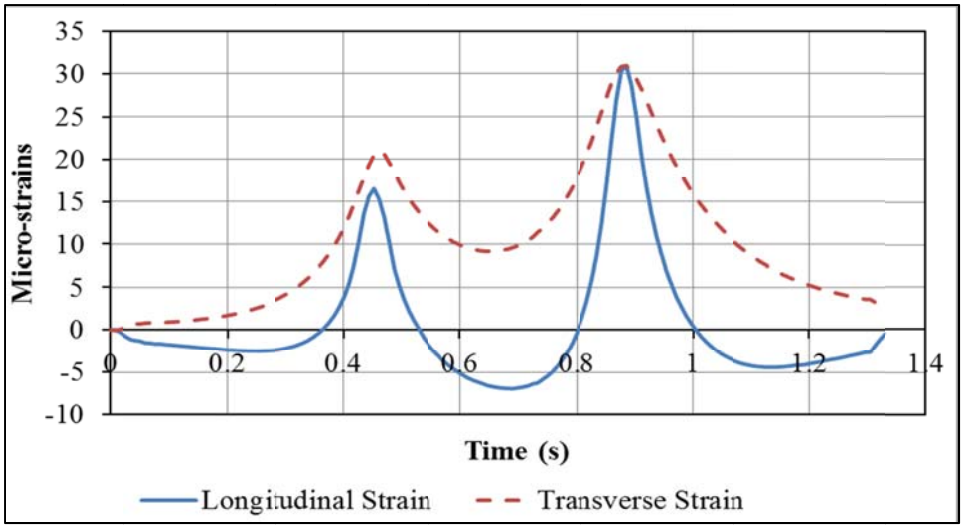

Figure 6-19 Computed strain development at the bottom of HMA layers based on the linear viscoelastic model.

6.7 Comparison of measured and computed strains based on viscoelastic and visco-hyper-elastic models

Figures 6-20, 6-21 and 6-22 show histograms that compares field-measured and FE computed strains at the bottom of Perpetual Pavement HMA layers for truck speeds of 20 mph, 40mph and 60mph. At a speed of 20 mph as shown in Figure 6-20, both viscoelastic and the enhanced visco-hyper-elastic models predicted the peak strains closer to the measured values, expect for transverse strains under the rear wheel. Both viscoelastic and the enhanced visco-hyper-elastic models could not accurately predict the transverse strains under the rear wheels. The difference could be due to a possibility that HMA is stiffer in longitudinal direction than in transverse direction, whereas in finite element modeling both transverse and longitudinal behaviors of HMA are considered the same.

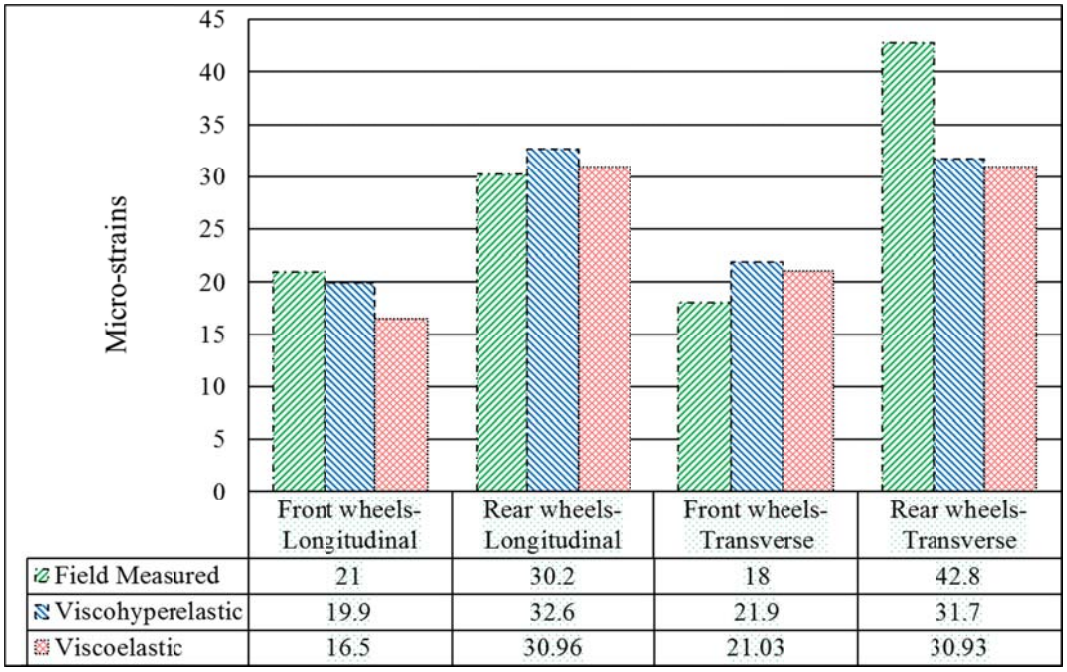

	Front wheels-Longitudinal	Rear wheels-Longitudinal	Front wheels-Transverse	Rear wheels-Transverse
Field Measured	21	30.2	18	42.8
Viscohyperelastic	19.9	32.6	21.9	31.7
Viscoelastic	16.5	30.96	21.03	30.93

Figure 6-20 Comparison of measured and FE analysis results at speed of 20 mph

At a speed of 40 mph and 60 mph as shown in Figure 6-21 and 6-22 respectively, both viscoelastic and the enhanced visco-hyper-elastic models predicted the peak longitudinal strains under the rear wheel closer to the measured values. However, on all other cases (longitudinal strains under the front wheels and transverse strains under front and rear wheels), the measured strains were 1.5 to 2 times of the computed strains. Both viscoelastic and the enhanced visco-hyper-elastic models showed less accurate values when strains were relatively small.

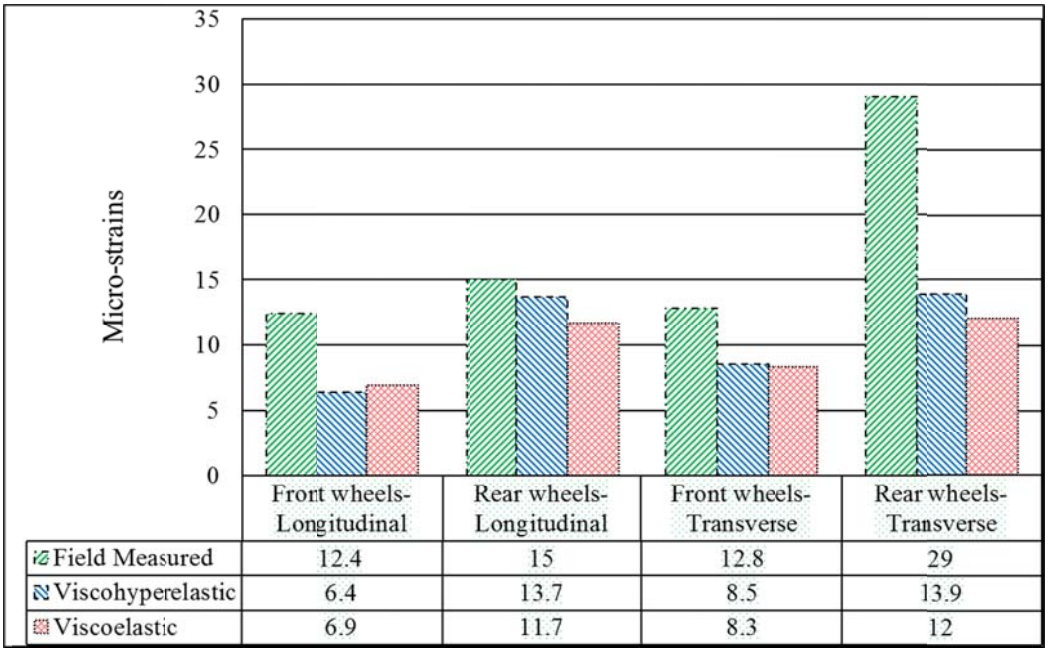

	Front wheels-Longitudinal	Rear wheels-Longitudinal	Front wheels-Transverse	Rear wheels-Transverse
Field Measured	12.4	15	12.8	29
Viscohyperelastic	6.4	13.7	8.5	13.9
Viscoelastic	6.9	11.7	8.3	12

Figure 6-21 Comparison of measured and FE analysis results at speed of 40 mph

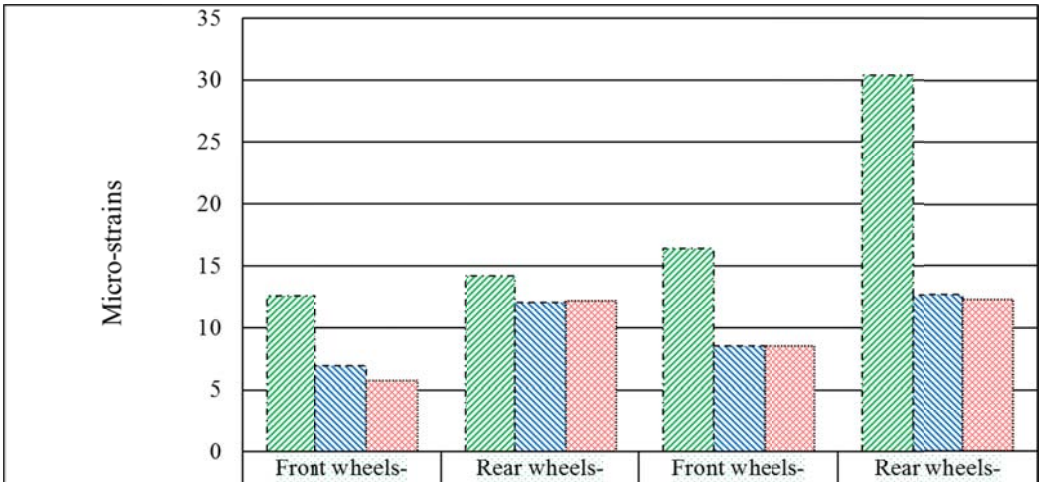

	Front wheels-Longitudinal	Rear wheels-Longitudinal	Front wheels-Transverse	Rear wheels-Transverse
Field Measured	12.6	14.2	16.4	30.4
Viscohyperelastic	6.9	12.1	8.5	12.7
Viscoelastic	5.7	12.2	8.5	12.3

Figure 6-22 Comparison of measured and FE analysis results at speed of 60 mph

Chapter 7

Summary, conclusions and recommendations

7.1 Summary

The first objective of this research was to investigate the relationship between Compressive and Tensile dynamic modulus of HMA through laboratory experiments. The Compressive and Tensile dynamic moduli (parallel and perpendicular to compaction) were determined in the laboratory using UTM 25 machine. The moduli were then compared to establish the best model that relates Compressive and Tensile dynamic moduli. A visco-hyper-elastic model that incorporates both Compressive and Tensile behavior of HMA was developed thereafter.

The visco-hyper-elastic model was used in Abaqus finite element program to estimate strain responses at the bottom of HMA layers of the Kansas US75 Perpetual Pavement sections. In addition, the strains computed by this model were compared to strains computed by a linear viscoelastic constitutive model to determine if improvement was made because of using both Compressive and Tensile Modulus in the model.

7.2 Conclusion

The major findings of this research are:

- The following relationship between Compressive Dynamic Modulus (CDM) and Tensile Dynamic Modulus parallel to compaction (TDMll) was found: $TDM|| = 2.6769 \times (CDM)^{0.899}$, where the moduli are measured in MPa.

- The research found the following relationship for the estimation of the Tensile Dynamic Modulus perpendicular to compaction ($TDM^{\perp}$):

  $TDM^{\perp} = 0.2246 \times (CDM)^{1.1529}$, where the moduli are measured in MPa.

- This research used 2-inch (dia.) x 3-inch (deep) and 4-inch (dia.) x 6-inch (deep) specimens to determine Tensile Dynamic Modulus perpendicular to compaction ($TDM^{\perp}$) and Tensile Dynamic Modulus parallel to compaction (TDMll) respectively. The research found that a tensile test on the small specimens was less expensive and relatively easy to perform. The test requires:

  - Less time in the environment chamber,
  - Less amount of glue which leads to lower costs

- Less applied load for testing. The relatively lower magnitude of applied load reduces errors associate with glues especially at higher temperatures.

- This research successively incorporated Compressive Dynamic Modulus and computed Tensile Dynamic Modulus (computed based on CDM to $TDM^{\perp}$ formulation) in an enhanced visco-hyper-elastic FE element model to compute tensile strains responses of HMA materials. The applicability of the model was verified using field measured strains from the Kansas US75 Perpetual pavement project.

- Both viscoelastic and the enhanced visco-hyper-elastic models predicted longitudinal strains closer to the measured values at speed of 20 mph. However, at higher speeds (40 mph and 60 mph), where the developed strains were relatively smaller, the predicted strains were 1/2 to 2/3 of the measured strains.

7.3 Recommendations

The major findings of this research are:

- Gyratory compacted specimens have the same Tensile Dynamic Modulus ($TDM^{\perp}$) in all directions perpendicular to compaction. Future studies

should investigate possible differences between Tensile Dynamic Modulus in the longitudinal and transverse directions by testing field cores instead.

- The statistical models that relates the CDM and TDM are limited to the following test conditions:
    - Loading frequency between 1Hz and 25Hz
    - Temperature between 10^{o}C and 35^{o}C

  More tests are required to improve the models beyond these conditions.
- Visco-hyperelastic material model that incorporated both the compressive and tensile behavior of HMA may be used to compute the response of asphalt pavements.
- The relationships developed in this research to compute the TDM from the CDM should be used when the TDM cannot be measured.

Appendix A

Comparison of Compressive and Tensile Dynamic Modulus Perpendicular to the Direction of Compaction

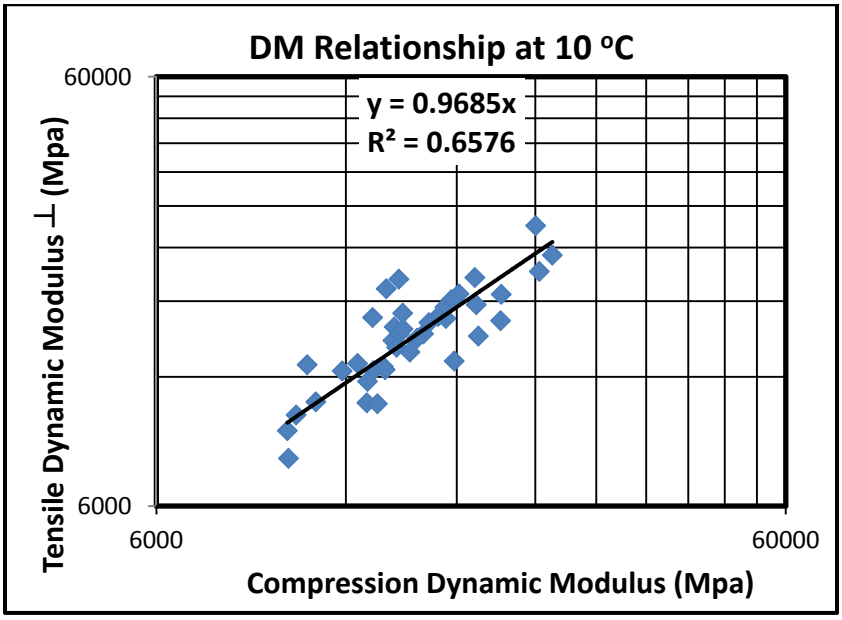

Figure A-1 CDM vs TDM ⊥ at 10°C: Best fit by y=ax model

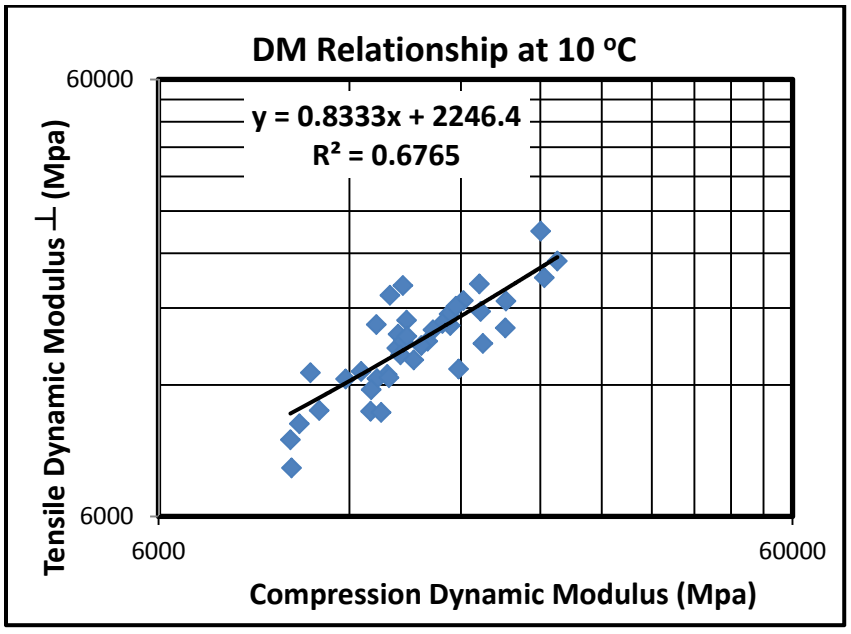

Figure A-2 CDM vs TDM ⊥ at 10°C: Best fit by y=ax + b model

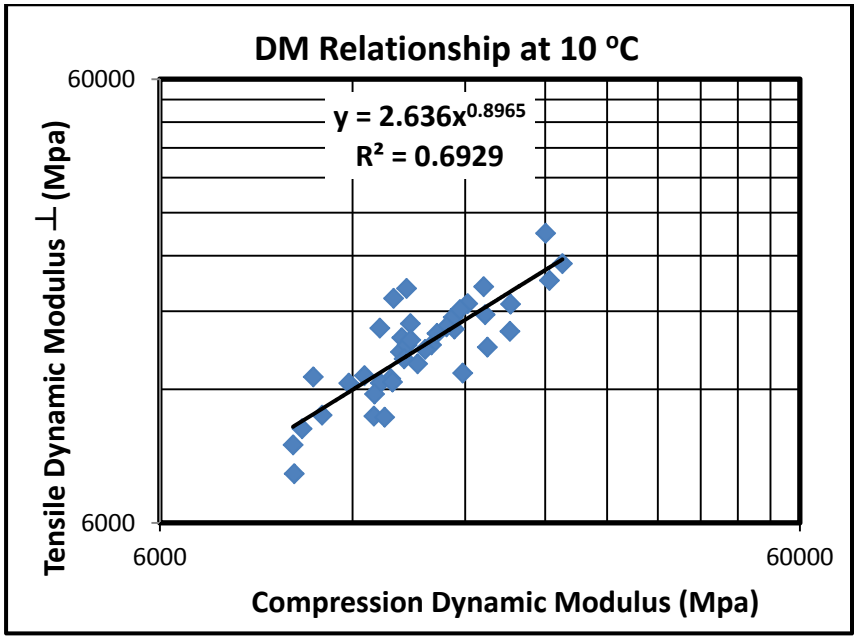

Figure A-3 CDM vs TDM ⊥ at 10°C: Best fit by $y=a.x^b$ model

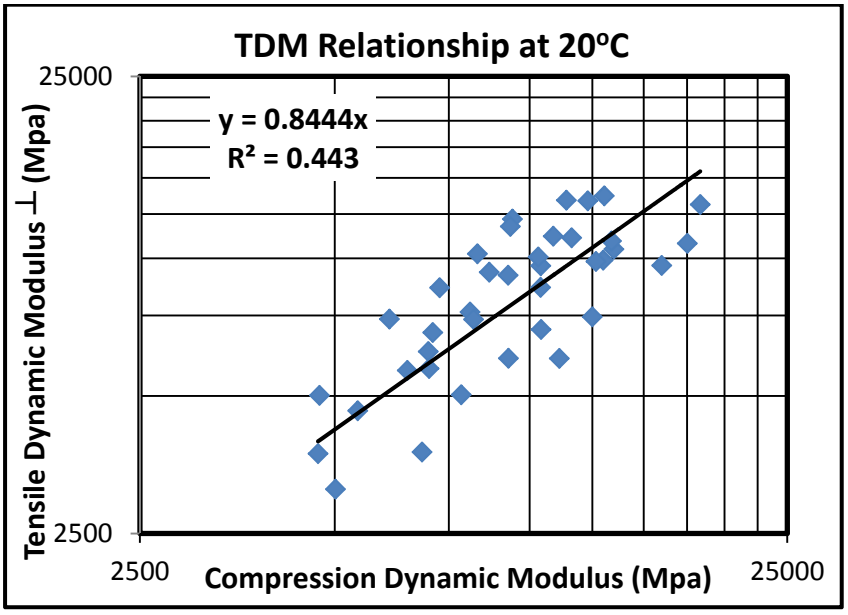

Figure A-4 CDM vs TDM ⊥ at 20°C: Best fit by y=ax model

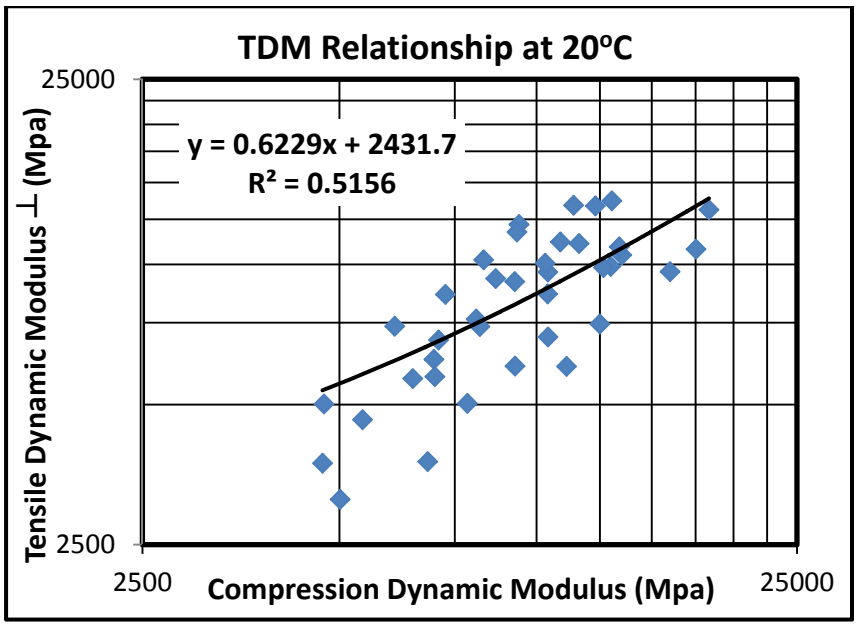

Figure A-5 CDM vs TDM ⊥ at 20°C: Best fit by y=a.x + b model

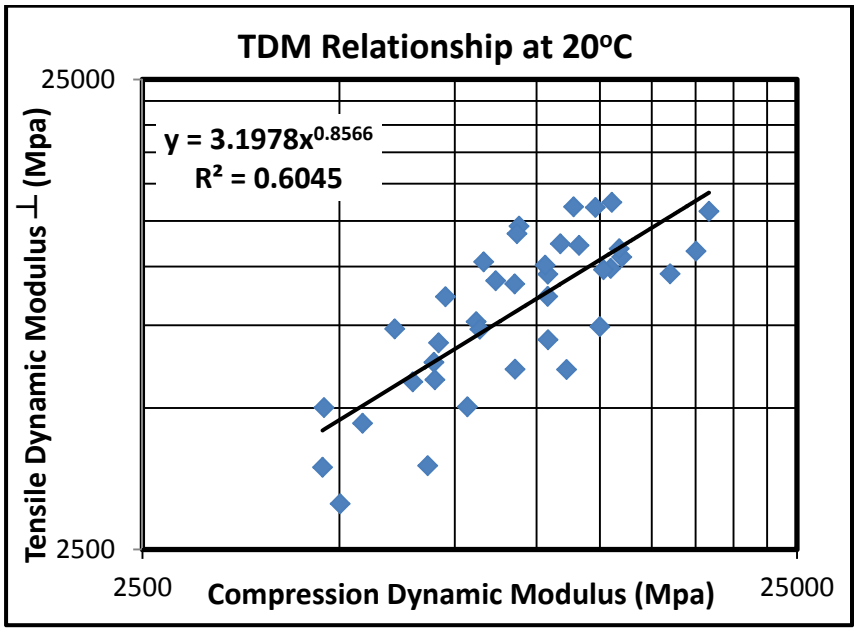

Figure A-6 CDM vs TDM ⊥ at 20°C: Best fit by $Y=a.x^b$ model

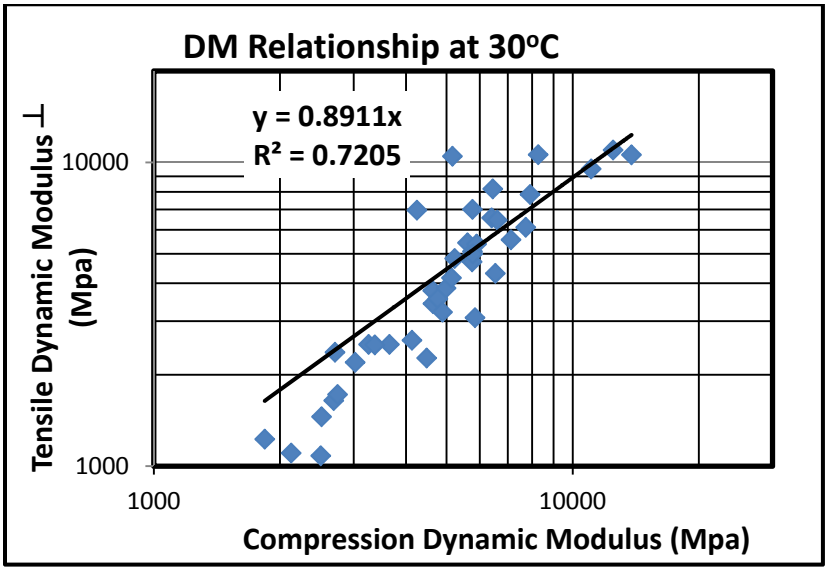

Figure A-7 CDM vs TDM ⊥ at 30°C: Best fit by y=ax model

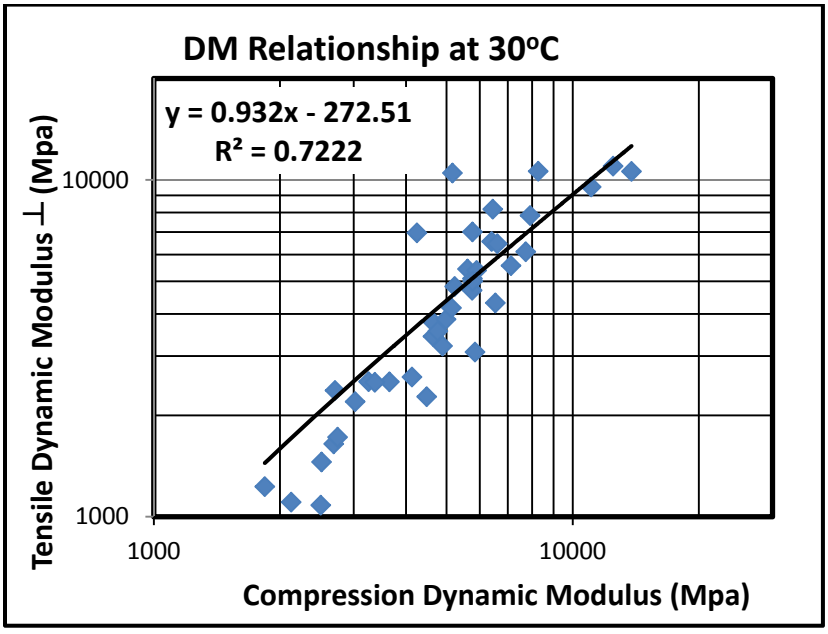

Figure A-8 CDM vs TDM ⊥ at 30°C: Best fit by y=a.x + b model

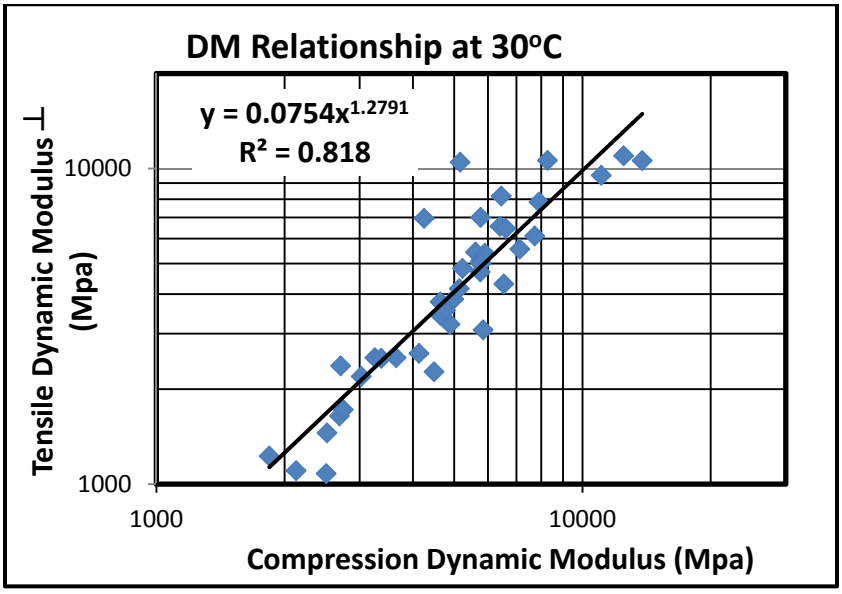

Figure A-9 CDM vs TDM ⊥ at 30°C: Best fit by $Y=a.x^b$ model

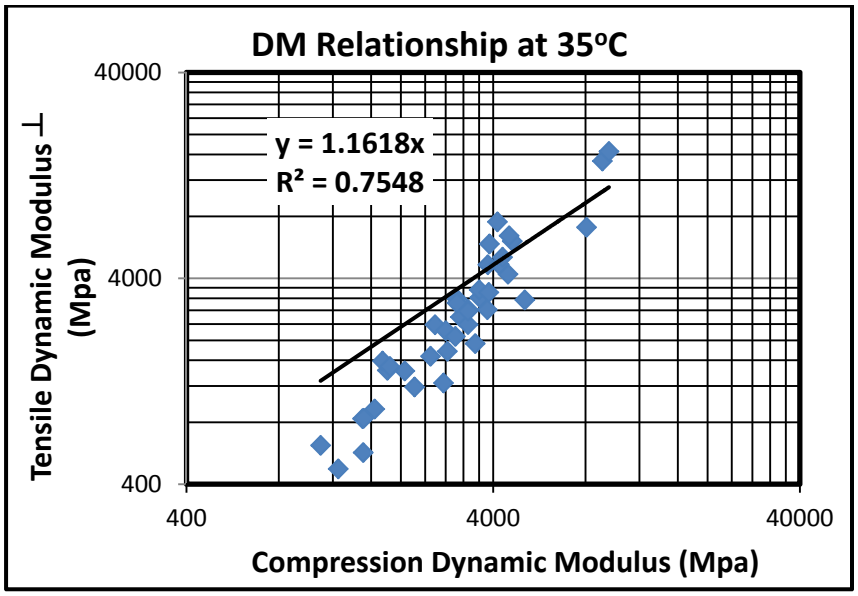

Figure A-10 CDM vs TDM ⊥ at 35°C: Best fit by y=ax model

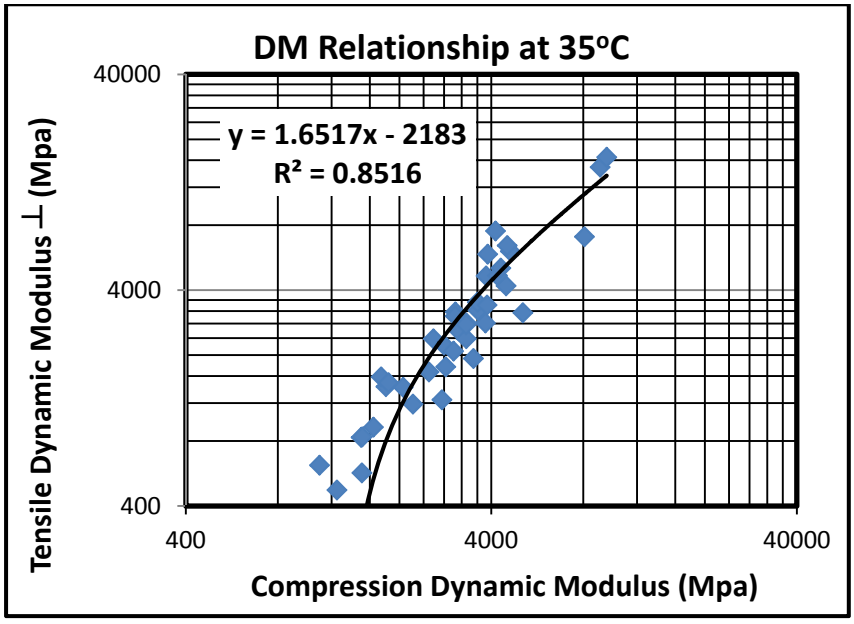

Figure A-11 CDM vs TDM ⊥ at 35°C: Best fit by y=a.x + b model

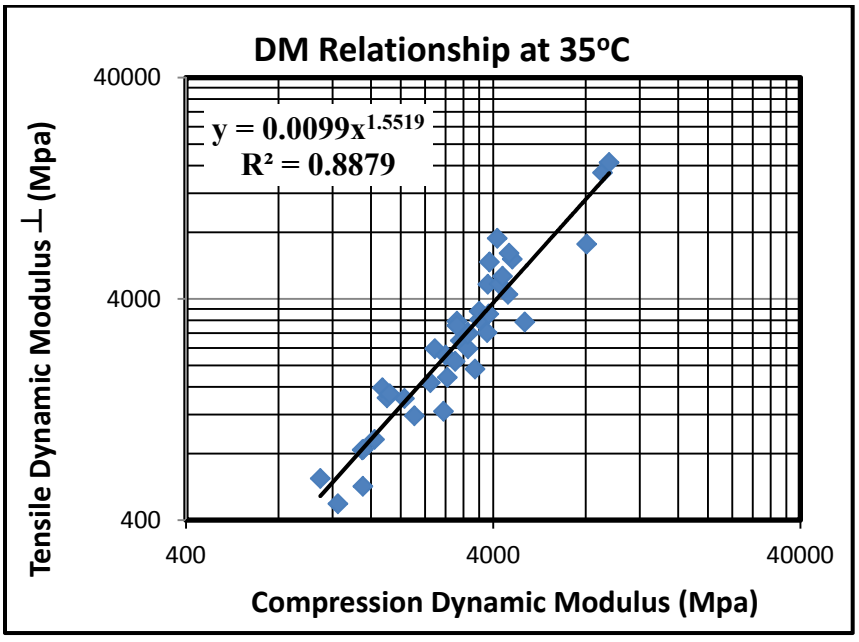

Figure A-12 CDM vs TDM ⊥ at 30°C: Best fit by $Y=a.x^b$ model

Appendix B

Comparison of Compressive and Tensile Dynamic Modulus Parallel to the Direction of Compaction

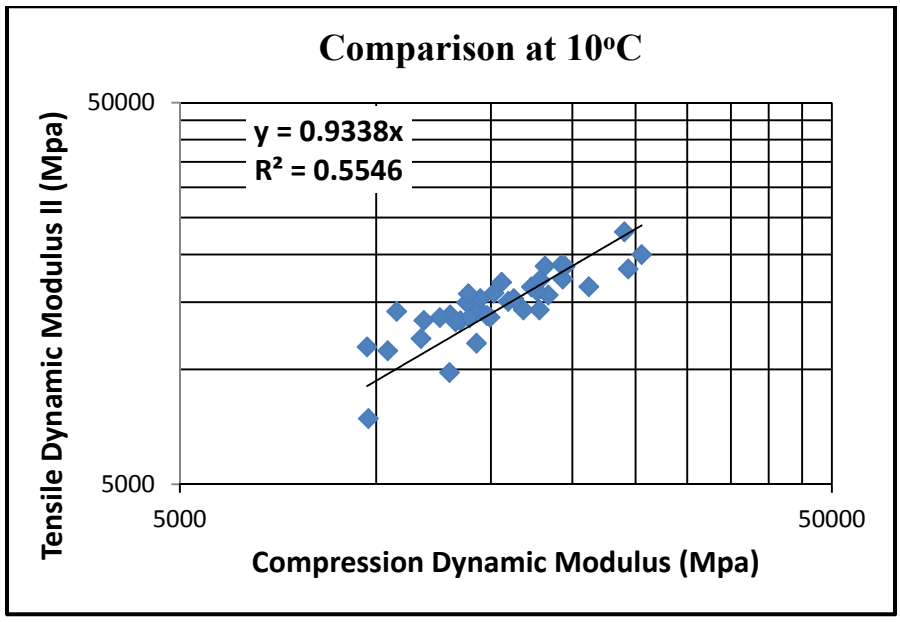

Figure B-1 CDM vs TDM ll at 10°C: Best fit by y=ax model

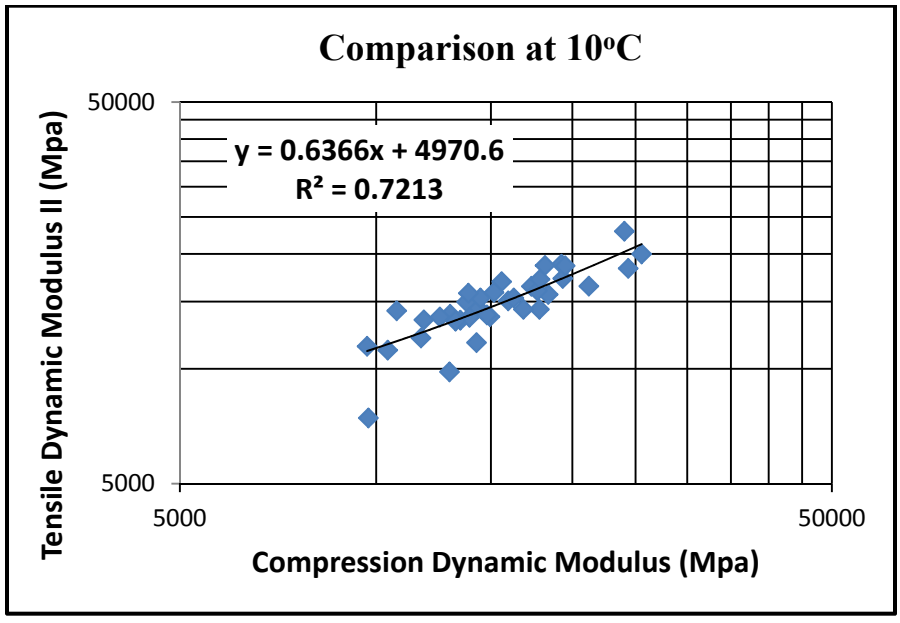

Figure B-2 CDM vs TDM ll at 10°C: Best fit by y=a.x + b model

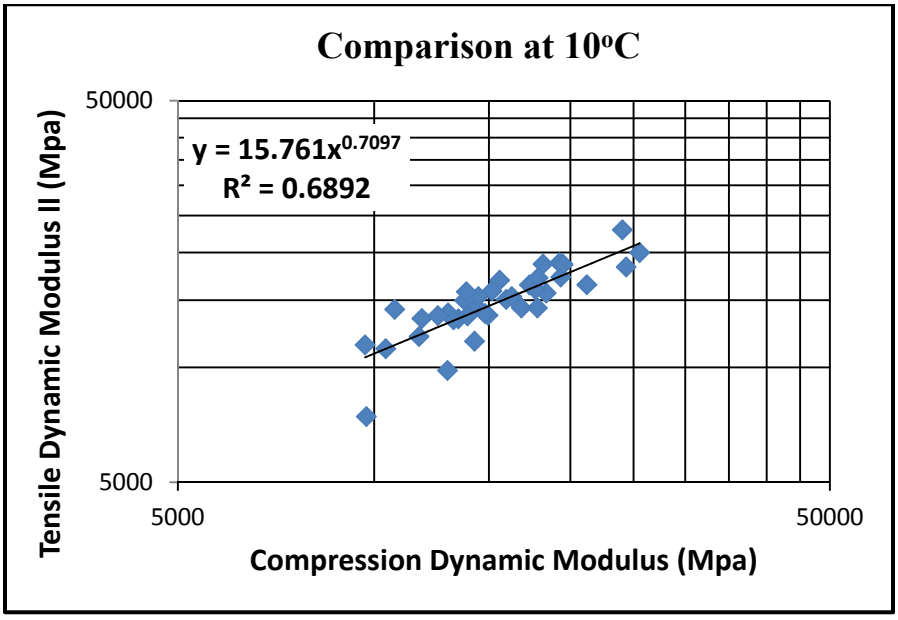

Figure B-3 CDM vs TDM ll at 10°C: Best fit by $Y=a.x^b$ model

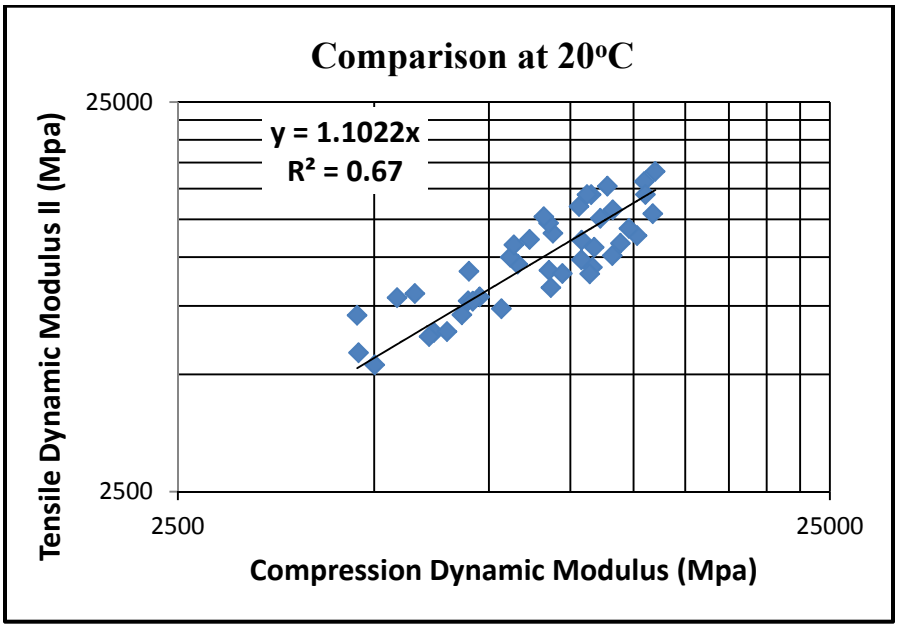

Figure B-4 CDM vs TDM ll at 20°C: Best fit by y=ax model

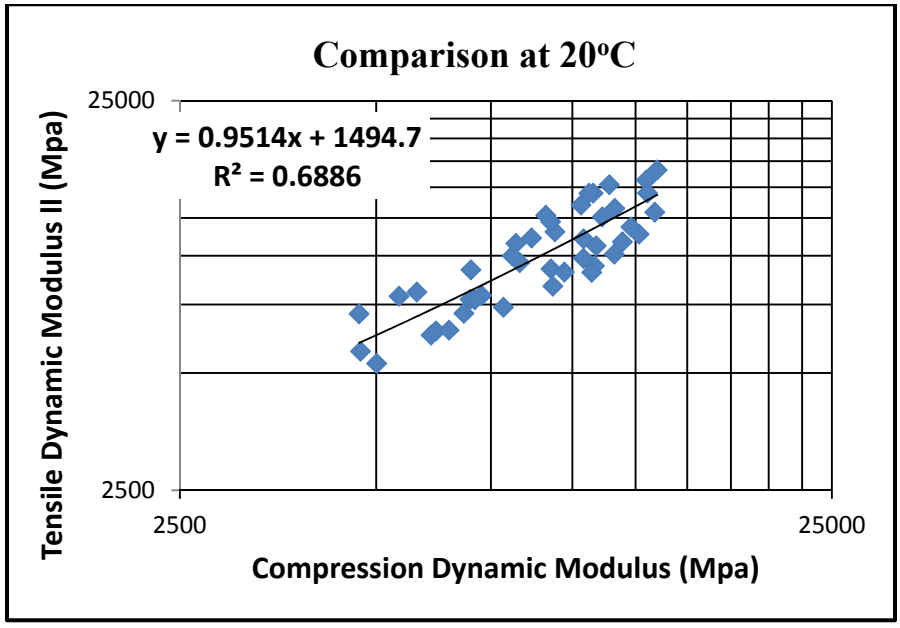

Figure B-5 CDM vs TDM ll at 20°C: Best fit by y=a.x + b model

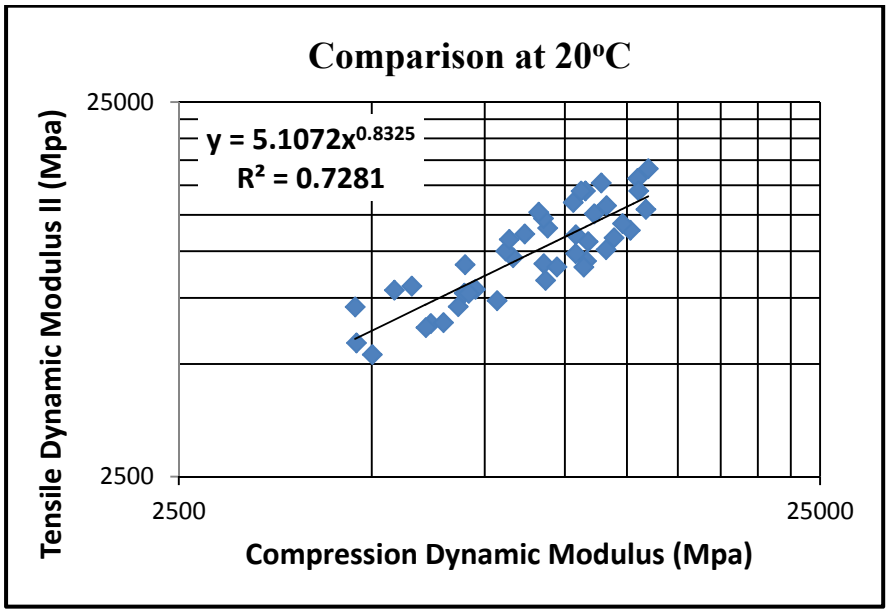

Figure B-6 CDM vs TDM ll at 20°C: Best fit by $Y=a.x^b$ model

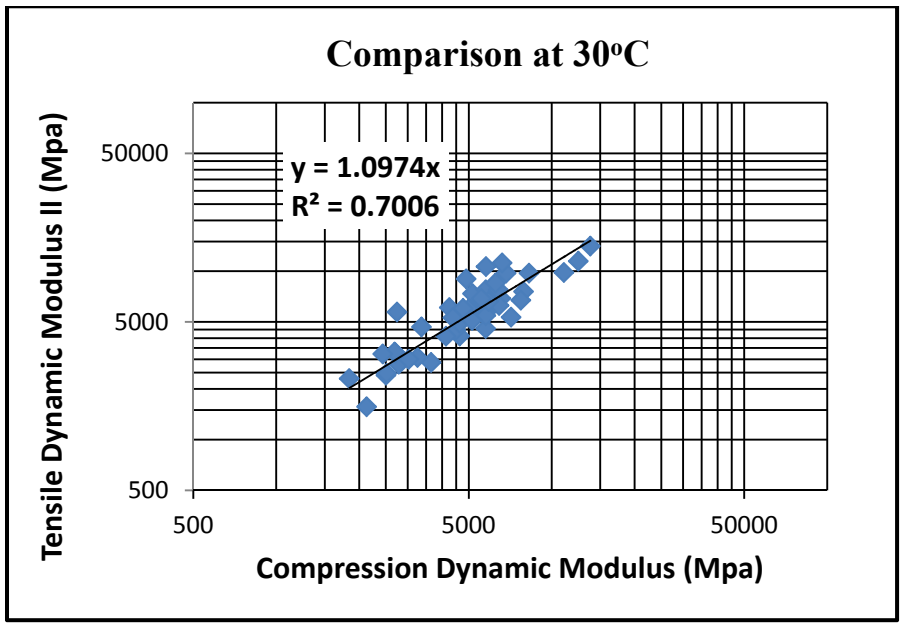

Figure B-7 CDM vs TDM ll at 30°C: Best fit by y=ax model

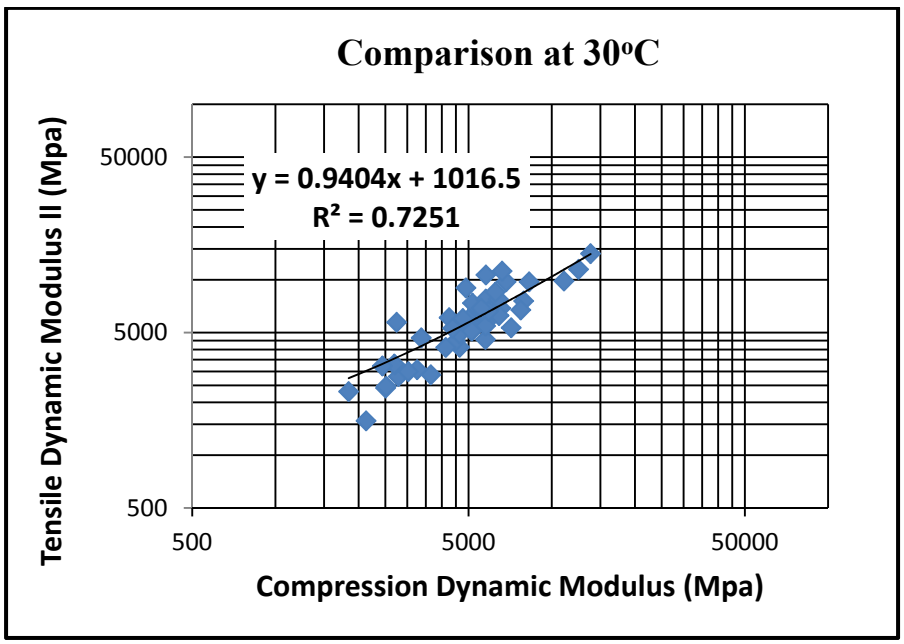

Figure B-8 CDM vs TDM ll at 30°C: Best fit by y=a.x + b model

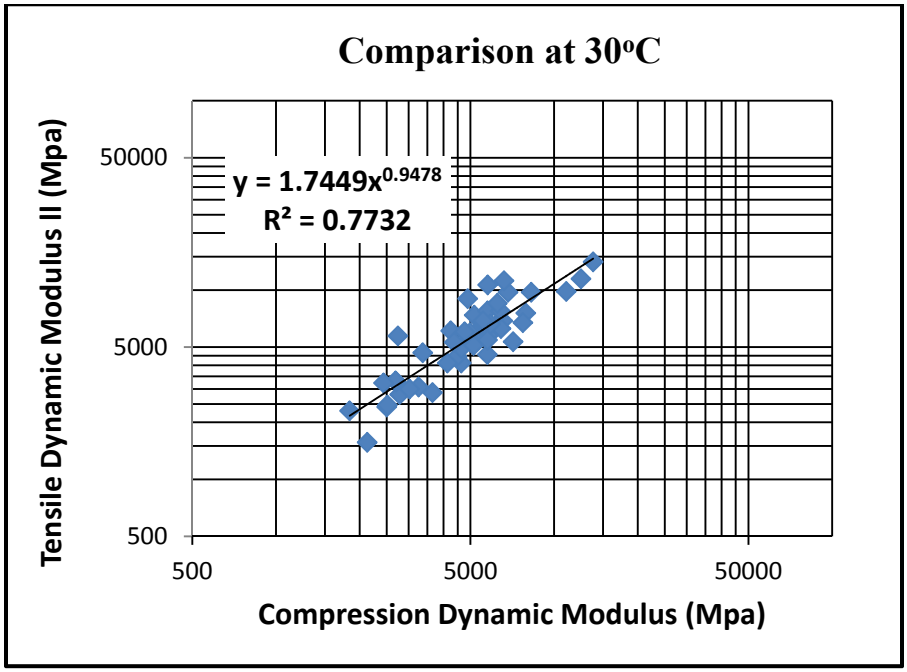

Figure B-9 CDM vs TDM ll at 30°C: Best fit by $y=a.x^b$ model

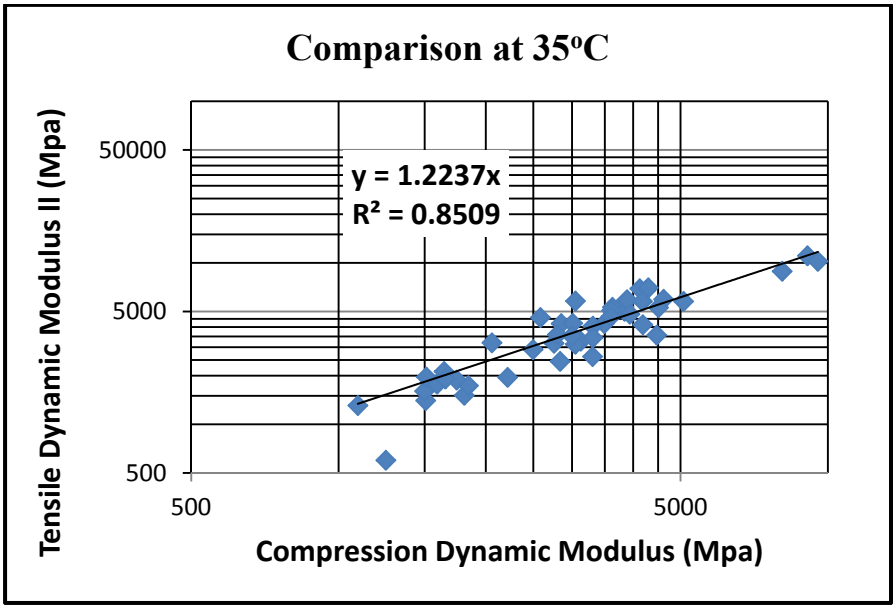

Figure B-10 CDM vs TDM ll at 35°C: Best fit by y=ax model

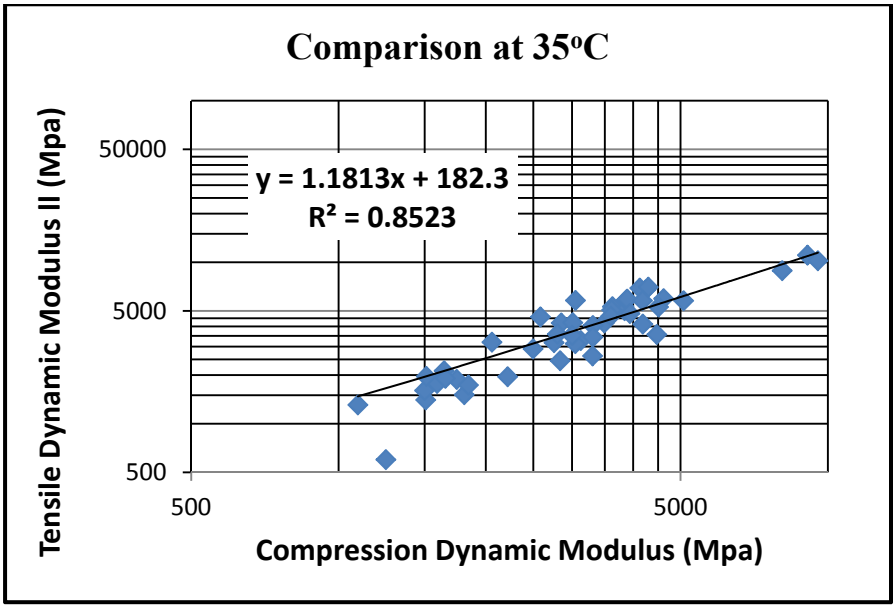

Figure B-11 CDM vs TDM ll at 30°C: Best fit by y=a.x + b model

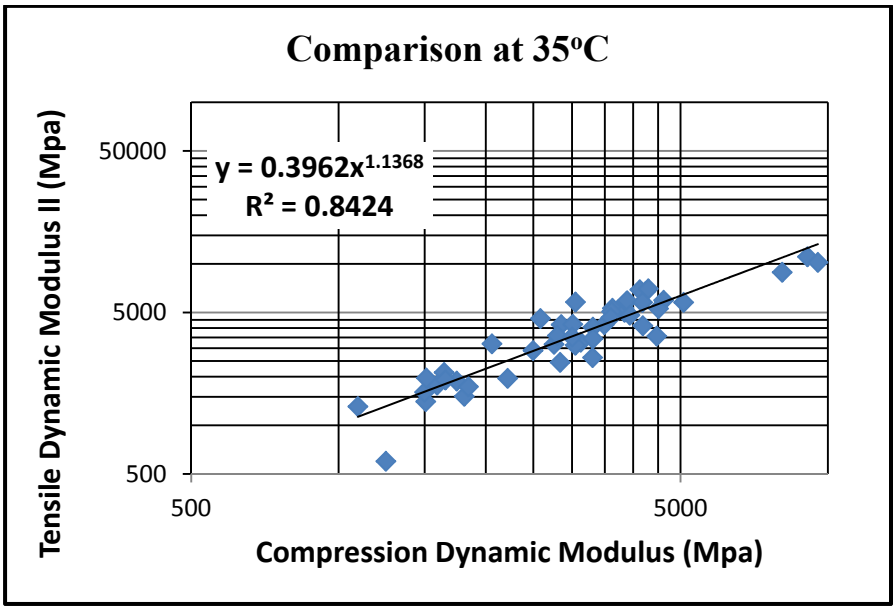

Figure B-12 CDM vs TDM ll at 35°C: Best fit by $y=a.x^b$ model

References

1. (http://www.betterroads.com/applications-innovations-10/) browsed sept 2014
2. AASHTO (1993). AASHTO Guide for Design of Pavement Structures, American Association of State Highway and Transportation Officials, Washington, D.C
3. AASHTO, (2004). Guide for mechanistic-empirical design of new and rehabilitated pavement structures. NCHRP project 1-37A final report. Washington, DC: American Association of State Highway and Transportation Officials.
4. APA. *Asphalt Pavement Alliance: Perpetual Pavements – A Synthesis,* 2010.
5. Asphalt Institute (AI).1996a. Performance Graded Asphalt. SP-1. Lexington, Kentucky
6. Asphalt Pavement Alliance (APA). *Perpetual pavement on I-40,* http://www.asphaltinstitute.org/wpcontent/uploads/Thickness_Mix/Perpetual_Pavement_I_40_Oklahoma_City.pdf (browsed July 2014)
7. Brown, E. R., Kandhal, P. S., and Zhang, J. N. (2001b). "Performance testing for hot mix asphalt." *Rep. No. 01-05, NCAT*

8. Burmister, D. M., 1943. “The theory of Stresses and Displacements in Layered Systemsand Application to the Design of Airport Runways,” Proceedings, Highway ResearchBoard, Vol. 23, pp 126-144).
9. Burmister, D. M., 1945. “ The General Theory of Stresses and Displacements in Layered Soil Systems,” *Journal of Applied Physics*, Vol. 16, pp 84-94, 126-127, 296-302)
10. Button J. W., 2001, *Perpetual Bituminous Pavements*. Transportation Research Circular No. 503. Transportation Research Board, National Research Council. Washington, D.C.
11. CAIT: Center for Advanced Infrastructure and Transportation, *Indirect tensile tester,* Rutger University of New Jersey. http://cait.rutgers.edu/prp/indirect-tensile-tester-idt browsed Dec. 2014
12. Chen. Y. G., 2009. *Viscoelastic Modeling of Flexible Pavement* [Dissertation], Akron: University of Akron.
13. Cho, Y. H., B. F. McCullough, and J. Weissmann, 1996. Considerations on Finite-Element Method Application in Pavement Structural Analysis. Transportation Research Record. 1539: 96-101
14. Chrishao Han. H., 1973. “Application of layered system analysis to the design of flexible pavements,”A thesis presented to the graduate faculty of Lehigh University

15. Christensen, D.W., and Bonaquist, R.F., 2004. Evaluation of indirect tensile test (IDT) procedures for low-temperature performance of hot mix asphalt. NCHRP Report 530.
16. Corte, J-F. 2001. Development and Uses of Hard-Grade Asphalt and of High-Modulus Asphalt Mixes in France. Transportation ResearchCircular No. 503. Perpetual Bituminous Pavements.Transportation Research Board. Washington, DC. pp. 12-31.
17. D'Angelo, J.A., J. Bukowski, T. Harman, and B. Lord (2004). The Federal Highway Administration's Long-Life Pavement Technology Program. *Proceedings*. Intl. Symp. on Design and Construction of Long Lasting Asphalt Pavements. National Center for Asphalt Technology. Auburn University, Alabama pp. 103-118.
18. El-Hakim, M., (2009). Instrumentation and Overall Evaluation of Perpetual and Conventional Flexible Pavement Designs, MASc Thesis, University of Waterloo, Waterloo, Ontario
19. Elseifi, M. A.; Al-Qadi, I. L.; Yoo, P. J. (2006). "Viscoelastic Modeling and Field Validation of Flexible Pavements," ASCE Journal of Engineering Mechanics, Vol. 132 No. 2, pp 172-178

20. FOSTER, C.R.,and R. G.AHLVlN, 1954. "Stresses and Deflections Induced by a Uniform Circular Load,"Proceedings, Highway Research Board ,Vol. 33, pp. 467-470.
21. Hargett, E.R., and Johnson, E.E., (1961) Strength properties of bituminous concrete tested in tension and compression. Highway research board 40, 430-440)
22. Hernandez Jaime A. (2010). Evaluation of the Response of Perpetual Pavement at Accelerated Pavement Loading Facility: Finite Element Analysis and Experimental Investigation, Russ College of Engineering and Technology of Ohio University.
23. Hornyak N. J. (2010). Perpetual Pavement Analysis for the Marquette Interchange Instrumentation Project, a dissertation presented to Marquette University, Wisconsin.
24. Huang Y. H. (2004). “Pavement Analysis and design”. Pearson Prentice Hall, NJ
25. Huang, Y. H. (1993). Pavement analysis and design, Prentice-Hall. Englewood Cliffs, N.J
26. HUANG, Y. H., 1967. "Stresses and Displacements in Viscoelastic Layered Systems Under Circular Loaded Areas, "Proceedings, 2nd

International Conference on the Structural Design of Asphalt Pavements,pp. 225-244.

27. Huber, G. 2000. Performance Survey on Open-Graded Friction Course Mixes. NCHRP Synthesis 284. Transportation Research Board,Washington, DC.
28. K. Su, R. Maekawa, Y. Hachiya, L. Sun, 2009. "A new rutting evaluation indicator for asphalt mixtures" Proceedings of the 8th International Conference (BCR2A'09), University of Illinois at Urbana - Champaign, Champaign, Illinois, USA)
29. Kallas, B.F., Dynamic modulus of asphalt concrete in tension and tension compression. Proceedings of the Association of Asphalt Paving Technologists. 39 (1970) 1-23
30. Kassem, Emad, Lubinda F. Walubita, Tom Scullion, Eyad A. Masad, and Andrew Winnett. 2008. *Evaluation of Full-Depth AsphaltPavement Construction Using X-Ray Computed Tomographand Ground Penetrating Radar*. Jn of Performance of ConstructedFacilities. American Society of Civil Engineers. Washington, D.C. pp. 408-416.
31. Kennedy, T.W., Haas, R., Smith, P., Kennepohl, G.A., Hignel, E.T., 1977. Engineering evaluation of sulfur-asphalt mixtures. Transportation Research Record 659. pg. 12-17

32. Kim, Y.R., Seao, Y., King, M., and Momen, M., 2004. Dynamic modulus testing of asphalt concrete in indirect tension mode. Transportation Research Record 1891. Pg. 163-173
33. Kim. Y. R., Ban. H., Im. S. 2010. Impact of Truck Loading on Design and Analysis of Asphaltic Pavement Structures. Phase II.
34. Liao, Y. (2007). Viscoelastic FE modeling of asphalt pavements and its applications to U.S. 30 perpetual pavement. Ph.D. Dissertation, Civil Engineering Department, Ohio University, Athens, OH.
35. Loulizi, A., Flintsch, G. W., Al-Qadi, I. L., and Mokarem, D., (2006). Comparing Resilient Modulus and Dynamic Modulus of Hot-Mix As phalt as Material Properties for Flexible Pavement Design Transportation Research Record, No. 1970, pp. 161–170
36. Lytton, R.L., Uzan, J., Fernando, E.G., Roque, R., Hiltunen, D., Stoffels, S.M., (1993). Development and Validation of Performance Prediction Models and Specifications for Asphalt Binders and Paving Mixes. Strategic Highway Research Program (SHRP-A-357). National Research Council. Washington, DC.
37. Missouri Asphalt Pavement Association (MAPA). *Perpetual Pavements,* http://www.moasphalt.org/facts/asphalt/perpetual.htm. Browsed Feb. 2012),

38. Molenaar, A., van de Ven, M., Liu, X., Scarpas, A., Medani, T., Scholten, E. (2008). Advanced Mechanical Testing of Polymer Modified Base Course Mixes. In: Proc., Asphalt – Road for Life, Copenhagen, pp. 842–853

39. Monosmith, C. L., and Secor, K. E. (1962).‘‘Viscoelastic behaviour of asphalt concrete pavements.’’Proc., 1st Int. Conf. on the Struct. Des. of Asphalt Pavements , Rd. Res. Lab., University of Michigan, Ann Arbor, Mich., 476–498

40. Myers, L., R. Roque, and B. Birgisson, 2001.”Use of Two-Dimensional Finite Element Analysis to Represent Bending Response of Asphalt Pavement Structures”.‖International Journal of Pavement Engineering. 2: 201 - 214.

41. Newcomb, D. E., Buncher, M. and Huddleston, I. J, (2001). “Concepts of Perpetual Pavements”, Transportation Research circular, Number 503, PP 4-11.

42. Newcomb, D.E. and K.R. Hansen. (2006). “Mix Type Selection for Perpetual Pavements. Proceedings”. International Conference on Perpetual Pavements. Ohio University, Columbus.CD-ROM.

43. Nunn, M., Brown, A., Weston, D. and Nicholls, J. C. (1997). Design of long-life flexible pavements for heavy traffic. Report No. 250, Transportation Research Laboratory, Berkshire, United Kingdom
44. Panneerselvam, Dinesh. 2005. "Mechanics of Asphalt Concrete: Analytical and Computational Studies." Electronic Thesis or Dissertation. Case Western Reserve University. https://etd.ohiolink.edu/
45. Park, D., Martin, A., and Masad, E. (2005). "Effects of Nonuniform Tire Contact Stresses on Pavement Response." *J. Transp. Eng.*, 131(11), 873–879.
46. Pavement interactive, 2008. "Flexible Pavement Response". http://www.pavementinteractive.org/article/flexible-pavement-response/. Browsed July 2014.
47. Pirabarooban, S., Zaman, M., Tarefder, R. A. (2003). " Evaluation of Rutting Potential in Asphalt Mixes Using Finite Element Modeling," The Transportation Factor 2003. Annual Conference and Exhibition of the Transportation Association of Canada
48. Portillo M. M (2008). Measured and theoretical response of perpetual pavement structures. MSc Thesis, University of Texas, Arlington

49. Powel, B. R., (2001) *As-Built Properties Of Experimental Sections On The 2000 NCAT Pavement Test Track.*Report No 01-02, National Center for Asphalt Technology, Auburn University.
50. Romanoschi, S., N. Dumitru, and O. Dumitru. "Resilient Modulus and the Fatigue Properties of Kansas Hot Mix Asphalt Mixes". Kansas Department of Transportation Report K-Tran:KSU 02-6. National Technical Information Service, Springfield, Va., 2006).
51. Sargand S., 2004. OHIO ASPHALT PROJECT ARTICLES, *ODOT tests the perpetual pavement concept*. http://www.flexiblepavements.org/sites/www.flexiblepavements.org/files/way30ppprojectarticle.pdf. (Browsed January 2013)
52. Sargand, S. M., Khoury, I. S., Romanello, M. T., and Figueroa, J. L. (2006). "Seasonal and Load Response Instrumentation of the Way-30 Perpetual Pavement," *InternationalConference on Perpetual Pavement (CDROM)*, Columbus, Ohio.
53. Shatnawi S.R., 1994. Fatigue performance of asphalt concrete mixes using a new repetitive direct tension test. California Department of Transportation.
54. Timm, D. and Young, J. (2004). The Effects of Load Spectra and Variability on Perpetual Pavement Design. International Symposium on

Design & Construction of Long Lasting Asphalt Pavements. Auburn, AL: International Society for Asphalt Pavements.

55. Timm, D.H. and D.E. Newcomb, 2006. Perpetual Pavement Design for Flexible Pavements in the U.S. International Journal of Pavement Engineering, Vol. 7, No. 2, pp. 111-119).
56. Von Quintus, H.L., Rauhut, J., and Kennedy T., 1982. Comparisons of asphalt concrete stiffness as measured by various testing techniques. Proceedings of the Association of Asphalt Paving Technologists. 51, pg. 35-49.
57. VonQuintus, H. (2001). Hot mix asphalt layer thickness design for longer life bituminous pavements. Transportation research circular.
58. Walubita L. F,Scullion T., 2010. Texas perpetual pavements – new design guidelines. TEXAS TRANSPORTATION INSTITUTE, Texas A&M University System, College Station, Texas.).
59. Wang H., Al-Qadi I., (2009) Combined effect of moving wheel loading and three-dimensional contact stresses on perpetual pavement responses. Transportation Research Record: Journal of the Transportation Research Board 2095(1): 53–61
60. Weissman, S., Harvey, J., Long, F., and Monismith, C. L. (1998). "*Material Modeling for Asphalt Mix and Pavement Analysis/Design*

Rutting and Fatigue Considerations," Proceedings of the First National Symposium on 3D Finite Element Modeling for Pavement Analysis & Design, pp 179-225, Charleston, West Virginia.)

61. West, R., and Timm D.H. (2012). *Phase IV NCAT Pavement Test Track Findings*. Report No 12-10, National Center for Asphalt Technology, Auburn University.
62. Willis, J. R., and Timm, D.H. (2009). Field-Based Strain Thresholds for Flexible Perpetual Pavement Design. Report No 09-09, National Center for Asphalt Technology, Auburn University.
63. Witczak, M. W., and Root, R. E. (1974). "Summary of complex modulus laboratory test procedures and results."*Fatigue and dynamic testing of bituminous mixtures, ASTM STP 561*, ASTM, Philadelphia, Pa., 67–94
64. Wu, H. (2011). Investigating properties of pavement materials utilizing loaded wheel tester (LWT). PhD dissertation, University of Tennessee, Knoxville, Tennessee, USA.
65. Yoder, E.J., and Witczak, M.W., 1975. "Principles of Pavement Design." J. Wiley and Sons, Inc., Second Edition
66. Yoo,P.J.,Al-Qadi,I.L.,Elseifi,M.A., and Janajreh,I.(2006). "Flexible pavement response to different loading amplitudes considering layer

interface condition and lateral shear forces," International Journal of Pavement Engineering, Vol. 7, No. 1, 73 - 86)

67. Mateos, A., Snyder, M. B. (2002). "Validation of Flexible pavement Structural Response Models with data from the Minnesota Road Research Project," Transportation Research Record, No. 1806, pp 19-29, Transportation Research Board, Washington D.C.
68. Wang H. (2011). "Analysis of tire-pavement interaction and pavement responses using a decoupled modeling approach," a dissertation presented to graduate college at University of Illinois at Urbana-Champaign.
69. King, M., Momen M., and Kim Y. R., (2005) "Typical Dynamic Moduli Values of Hot MixAsphalt in North Carolina and Their Prediction". Transportation Research Board, 84th Annual Meeting Compendium of Papers CD-ROM, Washington, D.C,
70. Kim Y. R., Momen. R., King. M., (2005). "Typical dynamic moduli for NorthCarolina asphalt concrete mixtures", Final report, North Carolina Department of Transportation.

Biographical information

Tito P. Nyamuhokya is originally from the United Republic of Tanzania. He received his Bachelors of Science degree in Civil Engineering from the University of Dar es Salaam, Tanzania in November, 2003. After graduation he worked with different civil engineering firms for a period of three years. In January of 2007 he started the Master of Science in civil engineering program at Kansas State University in the area of pavement and geotechnical engineering. In the month of August of the same year, he transferred to the University of Texas at Arlington to continue with his Master of Science in civil engineering, and graduated in August, 2009. Immediately after acquiring the Master's degree, he enrolled in a PhD program at the same University. In August 2015, he successfully completed the program requirements and was awarded a PhD in Civil engineering. Dr. Stefan Romanoschi, his supervising professor, guided him in both Masters and PhD programs. During his PhD program, he was privileged to teach Civil engineering materials laboratory for undergraduate and conduct researches related to geotechnical engineering, pavement and materials. His plans after graduating include getting a job in either higher education institutions or civil engineering firms to acquire more experience and knowledge, before establishing his own company.